Directionality of damage growth in fibre metal laminates and hybrid structures

Gupta, Mayank

DOI
10.4233/uuid:8cc4134d-1456-45ea-b9f0-b023f7d39630

Publication date
2017

Document Version
Final published version

Citation (APA)
Gupta, M. (2017). *Directionality of damage growth in fibre metal laminates and hybrid structures*. [Dissertation (TU Delft), Delft University of Technology]. https://doi.org/10.4233/uuid:8cc4134d-1456-45ea-b9f0-b023f7d39630

DIRECTIONALITY OF DAMAGE GROWTH IN FIBRE METAL LAMINATES AND HYBRID STRUCTURES

MAYANK GUPTA
Delft University of Technology

DIRECTIONALITY OF DAMAGE GROWTH IN FIBRE METAL LAMINATES AND HYBRID STRUCTURES

Directionality of damage growth in hybrid and FML structures

Proefschrift

ter verkrijging van de graad van doctor
aan de Technische Universiteit Delft,
op gezag van de Rector Magnificus prof.ir. K.C.A.M. Luyben;
voorzitter van het College voor Promoties,
in het openbaar te verdedigen op
vrijdag 12 Mei, 2017 om 15:00 uur

door

Mayank GUPTA

Ingeniero de Aeronauticos,
E.T.S.I.A., Universidad Polytecnico de Madrid, Madrid Spanje
geboren te Etah, India

Dit proefschrift is goedgekeurd door:

Promotor: Prof.dr. Rinze Benedictus
Copromotor: Dr. ir. R. C. Alderliesten

Samenstelling promotiecommissie:

Rector Magnificus,	Voorzitter
Prof. Rinze Benedictus,	Delft University of Technology, Promotor
Dr. ir. R C. Alderliesten,	Delft University of Technology, Copromotor

Onafhandelijke leden:

Prof. R. Curran,	Delft University of Technology, The Netherlands
Prof. I. M. Richardson,	Delft University of Technology, The Netherlands
Prof. dr. ir. T. Tinga,	Twente University of Technology, The Netherlands
Prof. Dr-Ing. P. Horst,	Braunschweig University of Technology, Germany
Dr. C. Walters,	TNO, Delft, The Netherlands

This research was carried out under project number M11.4.10407 in the framework of the Research Porgram of the Materials innovation institute M2i (www.m2i.nl).

Keywords: Fibre Metal Laminates, Glare, mixed-mode ratio, Stress intensity factor, *T*-stress, Crack paths, Fracture angle, Fatigue

Cover design by*:* ProefschriftMaken II www.proefschriftmaken.nl

Printing and layout by*:* ProefschriftMaken II www.proefschriftmaken.nl

ISBN: 978-94-6295-609-4

An electronic version of this dissertation is available at

http://repository.tudelft.nl/.

Dedicated to

The Outliers – who actually change the *status quo*

Summary

Fibre-metal laminates (FMLs) have been studied intensively for the past three decades because of their enhanced fatigue properties compared to monolithic metals. Most of these studies have focused on the fatigue damage under in-axis loading. These studies led to the application of FMLs in the aircraft structure in the early 21st century. However, the main application remains limited to the aircraft fuselage where the loading direction remains mostly constant. The few studies in the damage directionality of FMLs show that crack paths in FMLs under off-axis loading can undergo small deflections in biaxial GLAss REinforced aluminium (Glare) grades but show a significant amount of deflection in uniaxial Glare grades. In order to extend FML application to other parts of the aircraft structure where the loading direction is not constant or where uniaxial Glare is required – like aircraft wings - more understanding is required about the directionality of damage in FMLs under off-axis loading. To this effect the present research in damage directionality of FMLs under off-axis loading was undertaken.

The thesis begins with an introduction to the problem of damage directionality in FMLs under off-axis loading. The problem raises the scientific question, 'What mechanisms govern the crack path deflection in FMLs under off-axis loading'. Thereafter, a brief introduction to FMLs and these damage mechanisms are presented. Subsequently, various crack path theories used in monolithic metals are presented because from previous studies, it was concluded that the crack growth in metal governs the path taken by the damage.

It was concluded that although the specimen is under uniaxial loading, the off-axis fibres induce shear loading at the crack tip due to laminate orthotropy and a transverse fibre-bridging component. Hence, it was concluded that the mixed-mode theory using the Maximum Tangential Stress (MTS) is the most suitable theory for predicting crack paths. Because the previous research in FMLs was done using Stress Intensity Factors (SIFs), the mixed-mode approach using SIFs was deemed suitable to develop the analytical model. To verify the presence of mixed-mode loading– both tensile and shear loading – at the crack tip in FMLs under the application of uniaxial loading, Digital Image Correlation (DIC) was utilized. Additional to the DIC tests, more tests were performed under fatigue loading to observe the crack path behaviour in various Glare grades under a wider range of off-axis angles.

Thereafter, the analytical model was developed. To develop the analytical model, the previously developed fatigue model for in-axis loading was modified. The modification was necessary to include the effect of transverse fibre-bridging and laminate orthotropy, and the resulting mixed-mode ratio was used to predict the fracture angle. Finally, it is briefly shown that the model developed for fatigue will not work under quasi-static loading and using a non-linear plasticity based model would be a better approach.

In conclusion, the thesis showed that the crack paths in FMLs under fatigue loading deflect because of the presence of mixed-mode loading at the crack tip. The amount of deflection

depends on the mixed-mode ratio induced which, in turn depends on the Glare grade and the off-axis angle.

Samenvatting

De afgelopen drie decennia is er veel onderzoek gedaan naar vezel-metaallaminaten (VML's) vanwege hun verbeterde vermoeiingseigenschappen in vergelijking met monolithische metalen. De meeste van deze studies richtte zich op vermoeiingsschade onder belasting parallel aan de hoofdas. Deze studies hebben geleid tot toepassing van vezelmetaallaminaten in de vliegtuigconstructie in de 21e eeuw. De hoofdtoepassing blijft echter beperkt tot de vliegtuigromp, waar de belastingsrighting redelijk constant blijft. Deze beperkte toepassing komt voort uit het feit dat er maar weinig studies zijn geweest naar het richtingsgedrag van schade in VML's. Het kleine aantal studies dat er is geweest naar het richtingsgedrag van schade in VML's, laat zien dat scheurpaden in VML's onder belasting anders dan langs de hoofdas kan variëren van kleine afbuigingen in bi-axiale GLAss Reinforced aluminium (Glare) typen tot significante hoeveelheden afbuiging in het uni-axiaal Glare typen. Om de toepassing van VML's uit te breiden naar onderdelen van de vliegtuigconstructie waar de belastingsrichting niet constant is of waar uni-axiaal Glare is vereist (zoals vliegtuigvleugels), is er meer begrip nodig betreffende het richtingsgedrag van schade in VML's onder belasting niet in lijn met de hoofdas. Hiertoe is dit onderzoek over richtingsgedrag van schade in VML's onder belasting niet in lijn met de hoofdas ondernomen.

Het proefschrift begint met een introductie van het probleem van het richtingsgedrag van schade in VML's onder belasting niet in lijn met de hoofdas. Het probleem leidt tot de wetenschappelijke vraag: 'Welke mechanismen bepalen de afbuiging van het scheurpad in VML's onder belastingen niet in lijn met de hoofdas'. Daarna wordt een korte introductie gegeven van VML's en deze schademechanismen. Vervolgens worden verschillende theorieën betreffende scheurpaden in monolithische metalen gepresenteerd, omdat uit de vorige studies is geconcludeerd dat de scheurgroei in metaal het pad van de schade bepaalt.

Het is geconcludeerd dat hoewel het proefstuk onder uni-axiale belasting staat, de vezels niet in lijn met de hoofdas voor schuifbelasting aan de scheurtip zorgen door orthotropie van het laminaat en een transverse vezeloverbruggingcomponent. Daarom is er geconcludeerd dat theorie van gecombineerde (belastings-)modus gebruikmakend van de maximale tangentiële spanning (MTS) voor het voorspellen van scheurpaden de meest geschikte theorie is. Omdat voorgaand onderzoek naar VML's is gedaan gebruikmakend van spanningsintensiteitsfactoren (SIF's), werd de theorie van gecombineerde modi gebruikmakend van SIF's geschikt geacht om een analytisch model te ontwikkelen. Om de aanwezigheid van gecombineerde belastingsmodi (zowel trek- als schuifbelasting) aan de scheurpunt onder uni-axiale belasting te verifiëren, zijn er digitale beeldcorrelatietesten (DIC-testen) uitgevoerd. Naast deze DIC-testen zijn er meer testen uitgevoerd onder vermoeiingsbelasting om scheurpadgedrag te observeren in verschillende Glare typen onder een groter bereik van hoeken afwijkend van de hoofdas.

Daarna werd het analytisch model ontwikkeld. Om het analytische model te ontwikkelen is het in het verleden ontwikkelde vermoeiingsmodel voor belasting langs de hoofdas aangepast. De aanpassing was nodig om het effect van transverse vezeloverbrugging op te nemen, laminaatorthotropie en de resulterende verhouding van gecombineerde (belastings-)modi werd gebruikt om de breukhoek te voorspellen. Tenslotte, wordt er bondig aangetoond dat het model

ontwikkeld voor vermoeiing niet zal werken onder quasi-statische belasting en het gebruik van een model gebaseerd op niet-lineaire plasticiteit een betere aanpak zou zijn.

Samenvattend, heeft het proefschrift laten zien dat de scheurpaden in VML's onder vermoeiingsbelasting afbuigen door de aanwezigheid van gecombineerde belastingsmodi aan de scheurtip. De hoeveelheid afbuiging hangt af van de veroorzaakte verhouding van gecombineerde (belastings-) modi die op zijn beurt afhangt van het Glare-type en de hoek ten opzichte van de hoofdas.

Table of contents

List of Abbreviations:

A380 – Airbus A380
ARALL – Aramid reinforced aluminium layers
BL – Boundary layer
CLT – Classical laminate theory
CN – Centrally notched
CT – Compact tension
CTOD – Crack tip opening displacement
DCB – Double cantilever beam
DCDB – Double cleavage double drilled
DEC – Double edge-cracked
DIC – Digital image correlation
FEM – Finite element methods
FGM – Functionally graded materials
FML – Fibre metal laminates
Glare – Glass reinforced aluminium
LEFM – Linear elastic fracture mechanics
MBL – Modified boundary layer
MSED – Minimum strain energy density
MSERR – Maximum strain energy release rate
MTS – Maximum tangential stress theory
PZ – Plastic zone
SEN – Single-edge notched
SENB – Single-edge notched bend
SIF – Stress intensity factor
SSY – Small scale yielding

List of Symbols:

a – half-crack length (mm)
a_s – Initial saw-cut length (mm)
A – Crack surface area (mm^2)
B – Biaxial parameter
C – Stiffness matrix
C_b – Correction factor
E_{al} – Young's modulus of aluminium (GPa)
E_{11} – Young's modulus in longitudinal direction (GPa)
E_{12} – Young's modulus in transverse direction (GPa)
G – Strain energy release rate (J/m^2)
G_{12} – Shear Modulus (GPa)
K_{Ic} – Critical stress intensity factor
K - Stress intensity factor (MPa(sqrt(mm^2))
K_I - Stress intensity factor in opening mode (MPa(sqrt(mm^2))
K_{II} - Stress intensity factor in shear mode (MPa(sqrt(mm^2))
K_{br_I} – Stress intensity factor due to bridging in the longitudinal direction
K_{br_II} – Stress intensity factor due to bridging in the shear direction
K_{eff_I} – Effective Stress intensity factor in the longitudinal direction
K_{eff_II} – Effective Stress intensity factor in the transverse direction
K_{m_I} – Stress intensity factor in the metal layers under longitudinal direction (MPa(sqrt(mm^2))
K_{m_II} – Stress intensity factor in the metal layers under shear mode (MPa(sqrt(mm^2))
a/W – Crack length to specimen width ratio
M^e – Mixed-mode ratio
r – Distance from the crack tip (mm)
S – Compliance matrix
t – thickness (mm)
t_{al} – thickness of aluminium layer (mm)
t_f – thickness of fibre layers in the prepreg (mm)
T_D – Distortional energy density
T_v – Dilational energy density
U – Strain energy (J)
γ - Off-axis angle (degrees)
δ_f – Fibre elongation in the longitudinal direction (mm)
δ_{pp} – Prepreg shear deformation (mm)
ε_1 - Longitudinal strain
ε_{11} - Longitudinal strain
ε_{12} - Shear strain
ε_2 - Transverse strain
ε_{22} - Transverse strain
ε_{break} - Elongation at break
θ - Crack angle (degrees)

κ - Shear strain to longitudinal strain ratio

τ_{orth} - Equivalent stress load (MPa)

$\tau_{r\phi}$ - Stress in the shear direction (MPa)

τ_{xy} - Stress in the shear direction (MPa)

υ - Poisson ratio

ρ - Density (g/cm^3)

$\sigma_I - \sigma_{II}$ – Difference in principal stresses of the specimen

σ_r – Stress in the radial direction (MPa)

σ_{ult} – Ultimate strength (MPa)

σ_x – Stress in the radial direction (MPa)

σ_y – Stress in the tangential direction (MPa)

σ_{ys} – Yield strength (GPa)

σ_ϕ – Stress in the tangential direction (MPa)

σ_∞ – Far-field stress (MPa)

σ_{∞_I} – Real longitudinal stress (MPa)

σ_{∞_II} – Real shear stress (MPa)

ϑ_{xy}**(x)** – Crack opening due to fibre bridging in the longitudinal direction (mm)

υ_{xy}**(xy)** – effective crack opening (mm)

$\vartheta_{xy_{br}}$ **(xy)** – effective crack opening due to the bridging load (mm)

υ_{xy_∞}**(xy)** – effective crack opening due to the far-field applied load (mm)

υ_∞**(x)** – effective crack opening in the longitudinal direction (mm)

ς - Transverse strain to longitudinal strain ratio

ϕ -Fracture angle (degrees)

1 Chapter 1: Introduction to damage directionality in Fibre Metal Laminate and hybrid structures

1.1 Introduction

Advances in material research have led to the development of new materials for aerospace structural applications. The success of these applications depends on whether material properties meet the requirements for these applications. In particular, aircraft structures require damage tolerant materials, i.e. low sensitivity to in-service damage, to ensure and maintain safety during the operational life. In the past decades, Fibre Metal Laminates (FMLs) - a class of hybrid materials - have demonstrated to possess the required high damage tolerance.

FMLs are laminated materials comprising alternating layers of metals and fibre reinforced polymers. The fibre composite layers provide additional strength to the isotropic metal layers in their longitudinal directions, while the metals' ductility increases the damage tolerance of the near brittle fibre composites. Thus, FMLs provide the opportunity to utilize the advantages of both constituents to minimize the disadvantages, making them suitable for application as damage tolerant materials in aircraft structures.

A prerequisite to the application of FMLs in aircraft structures is the full understanding of all mechanisms that provide this damage tolerant behaviour. For this reason, both experimental and numerical studies [1-5] have been conducted in the past to understand the slow and approximately constant crack growth behaviour of FMLs. This knowledge has been implemented in analytical models to predict the crack propagation in FMLs, but only when loaded in their principal material orientations. Other studies have illustrated with experiments that the magnitude of crack growth may change significantly, when axial loading is applied under angles with respect to the principal material orientations [6-11].

The first study into the fatigue crack growth mechanisms in FMLs was performed by Marissen [1]. To explain the low crack growth rates of mode I cracks in the aluminium layers of Aramid reinforced aluminium layers (ARALL), an FML based on aramid fibres, Marissen introduced the concept of fibre bridging. Fibre bridging is the mechanism of intact fibres transferring part of the load over the mode I crack in the aluminium effectively reducing the stress intensity at the crack tip. This load transfer imposes shear stresses at the interface between the metal and fibre layers that cause the formation of delaminations in the wake of the crack.

Alderliesten [2] developed a closed form analytical solution to predict crack propagation and delamination growth in the wake of the propagating cracks by reducing the problem to a crack in a single metallic layer and the fibre bridging contribution to that particular layer. Recently, Alderliesten's model has been further developed towards arbitrary FML configurations and different load cases by Wilson [3]. Instead of solving the problem for a single layer, Wilson's model described the growth of all cracks in all metal layers.

All these studies address the magnitude of fatigue crack growth. However, little research has been reported on the directionality of crack growth in FMLs. Only a few studies [6, 7, 10-12] presented experimental results on crack paths under the off-axis loading, but without correct analytical theories explaining the reported crack paths. Zaal's prediction model [9] for

understanding crack paths in Glare3 under off-axis loading does not correlate with the experimental studies [6, 7, 11].

Currently, GLAss REinforced aluminium (Glare) – the FML subject of investigation in the current research – is used in the fuselage structure of the Airbus A380. An aircraft fuselage skin is subject to biaxial loading, i.e. stresses in both hoop and longitudinal direction. This requires Glare grades with fibres oriented both parallel and perpendicular to the aluminium rolling direction. As long as this biaxial loading imposes stresses in the principal material direction of FMLs, the above described models are applicable. However, certain sections of the fuselage also experience shear loading, like for example the aft fuselage, to which the empennage applies also torsion. In these cases, the biaxial stress field may effectively be oriented under an angle with respect to the principal material directions.

In the experiments by Gonesh [6, 7] and Thibault-Liboiron [11], it was observed that there is limited crack deflection in cross-ply Glare grades when loaded under off-axis angles. However, the crack growth rates were observed to increase significantly. In full scale fatigue tests, crack deflection was only observed when cracks approach stiffeners like frames. In those cases crack deflection may terminate the growth in its original direction imposing a flapping mechanism opening the crack, which allows for high residual strengths.

These experimental studies also illustrated that the increase in crack growth rates and the crack deflection may become significant, when unidirectional FMLs are loaded under off-axis angles. This observation is deemed important for the application of FMLs to lower wing structures, where unidirectional FMLs are considered for the high wing bending loads. In this case, the deflection of a crack together with a substantial increase in growth rates, are undesired and require thorough understanding.

The given examples of desired crack deflection in aircraft fuselage structures, and undesired crack deflections in aircraft wing structures raise questions regarding the underlying governing mechanisms. Hence, to extend FML application to more structures in aircraft the following question must be addressed:

What mechanisms affect the crack paths in FMLs under off-axis loading?

1.2 Scientific and engineering objective

To take maximum benefit in both fuselage and wing structures from the advantages of FMLs – lighter than metal, more ductile than fibre composites, orthotropic compared to isotropic metal - , it becomes imperative to understand the phenomenon of damage directionality in FMLs. Hence, a research project was undertaken to develop a better scientific understanding of the mechanisms governing the crack path deflection in FMLs.

The objective of the research presented in this doctoral dissertation is to develop an analytical theory that describes the directionality of damage in FML structures and materials. This theory must be based on the characteristics and interacting mechanisms of the constituent materials of the FML and the loading applied to the FML.

The secondary objective is to develop a model implementing this theory, which allows aircraft manufacturers to assess the direction of crack propagation in FMLs under external loading.

1.3 Research methodology

A combined theoretical and experimental study was performed to achieve the abovementioned objectives. Initially, various crack path theories [18-21] proposed in the literature for metals were reviewed for their applicability to FMLs. For this purpose, the experiments reported by Gonesh [6, 7] and Thibault-Liboiron [11] were used to correlate crack orientations predicted with these theories to data.

Among these theories were the *T*-stress theory [20], the Maximum Tangential Stress theory [19], and Minimum Strain Energy Density criterion [21]. The *T*-stress theory was once used by Zaal [8, 9] to predict crack paths in FMLs. The general observation was that these theories could not be applied to FMLs assuming these laminates represent homogeneous materials. This observation, in fact, is similar to the observations reported in earlier studies by Marissen [1], Alderliesten [2] and Wilson [3]. The crack growth rate could not be predicted assuming that the FML was a homogeneous material. The developed theories approached the FML as a structure, describing the effect of fibre composite layers on the aluminium layers.

Hence, the research aimed at extending the existing crack growth prediction theories to include the mechanisms that cause the crack paths to deflect to orientations other than the direction perpendicular to the applied load. The main hypothesis subject of this approach is that the crack path is influenced by a mode-mix at the crack tip in the metal layer. This mode-mix implies presence of a shear component in addition to the stresses in both principal material directions.

To test this hypothesis experiments were performed in which the Digital Image Correlation (DIC) technique was used to capture the strain field in the crack tip vicinity and to reveal the presence of shear deformation.

The existing crack growth prediction models from Alderliesten [2] and Wilson [3] predict crack growth based on a mode I stress intensity factor at the crack tip in the metal layer. A mode-mix implies that in addition to the tensile opening mode I, a shear mode II is present at the crack tip. The hypothesis here is that this shear component is induced by two different mechanisms:

- The orthotropy of the entire FML; application of a uniaxial tensile load under an off-axis angle imposes a shear component to the panel.
- Off-axis fibre bridging; the transverse component of the bridging forces induce a shear component.

To evaluate this hypothesis, an analytical theory was developed based on a concept similar to the theory of Alderliesten [2], where mode-mix is calculated based on both aspects. In addition, additional experiments were performed to verify and validate this hypothesis and model.

1.4 Thesis outline

Chapter 2 gives a brief introduction to FMLs, in particular Glass Reinforced Aluminium (GLARE), and and to fatigue damage mechanisms in FMLs.

Chapter 3 provides an overview of the crack path theories in monolithic metals. This chapter discusses the fundamental crack path theories in metal and compares them with the past research on the damage directionality in FMLs under off-axis loading. The chapter concludes with an explanation for selecting the mixed-mode theory for predicting crack paths in FMLs.

Chapter 4 presents a review on *T*-stress – the first higher order term on the stress field – and discusses its appropriate role in Linear Elastic Fracture Mechanics (LEFM).

Chapter 5 discusses the investigation of crack paths in FMLs under off-axis fatigue loading that was experimentally performed in the course of this research. The principle, test matrices, specimens, measurement techniques and results from these experiments are discussed. This chapter explains the mechanism governing the crack deflection in FMLs empirically, and defines the hypothesis and principles for developing the analytical model.

Chapter 6 discusses the analytical model for the crack paths in FMLs. The fundamentals, limitations and the outline of the model are provided in this chapter. The experimental results produced during the course of this dissertation and in previous research [6, 7] are briefly presented here and compared with the model prediction results.

Chapter 7 presents the results of quasi-static tests on FMLs to verify the differences in the crack paths between fatigue loading and quasi-static failure. The limitations of the developed analytical model for fatigue loading to quasi-static loading are discussed. Additionally, a plausible approach to predict the quasi-static model using a plasticity similitude approach is presented in this chapter.

Chapter 8 presents the conclusions derived from this research work and the possible applications of the model.

2 Chapter 2: Introduction to Fibre metal laminates and their fatigue damage mechanisms

2.1 Introduction

The current chapter initially defines the nomenclature for Glare, followed by the manufacturing process, and material properties for the components of Glare. The latter part of the chapter summarizes the damage mechanisms in Fibre Metal Laminates (FMLs). These mechanisms are a combination of the damage mechanisms of the FML constituents, i.e. metal and fibres. Because fatigue is the most significant damage mechanism in aircraft structures - major application of FMLs -, a detailed discussion is presented on fatigue in FMLs. Additionally, an overview is provided on the fibre-bridging mechanism – a unique characteristic of fatigue in FMLs – that enhances the fatigue properties of FMLs in comparison to monolithic metals.

To understand crack paths in FMLs under off-axis loading, it was assumed that the crack paths are significantly influenced by the crack growth in metals. Hence, this chapter focusses more on fatigue crack growth in metals compared to delamination of fibres from the metal in FMLs.

2.2 Nomenclature of FMLs

FMLs are made of metals and fibres embedded in resin matrix, therefore, they benefit from the characteristics of both these constituent phases. A typical FML is shown in Figure 2-1. The current research investigated the damage directionality primarily in GLAss REinforced Aluminium (Glare). Although they can be broadly classified as composites, their nomenclature is not similar to composites. Hence, the different nomenclature for FMLs is explained below.

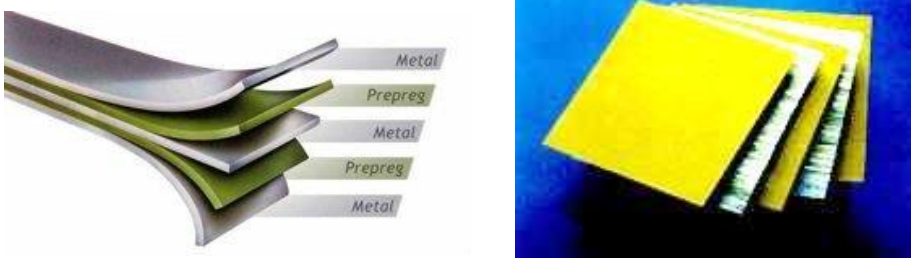

(a) (b)

Figure 2-1. Schematics of the lay-up of a Fibre Metal Laminate (a) and its constituents before bonding (b)

The constituents of FMLs can be configured in various ways to maximize the laminates performance for a given application (e.g. fatigue, strength, impact, shear). This results in many lay-ups leading to several grades of Glare. Hence, a different coding system is used to identify the Glare grade and lay-up correctly. For example, the cross-ply laminate Glare3-3/2-0.3 refers to respectively Glare grade, the lay-up (number of metal and fibre layers) and the aluminium layer thickness. Hence, Glare3-3/2-0.3 is defined as [2, 23]

[2024-T3/0° glass/90° glass/2024-T3/90° glass/0° glass/2024-T3]

The orientation of the fibres in the nomenclature defines their angle with respect to the rolling direction of aluminium. 0° implies that the fibers are oriented along the rolling direction of aluminium i.e. L-direction, and 90° signifies that they are perpendicular to the aluminium rolling direction, i.e. LT direction. Table 2-1 shows some standard Glare grades that have been tested in the course of this research work.

Table 2-1 Nomenclature for tested Glare grades [23]

Glare grade	Glare Type	Fibre prepreg orientation (°)
Glare 2	2A	0/0
Glare3	3	0/90
Glare 4	4B	90/0/90

2.3 Manufacturing and properties of FMLs

An autoclave is used for manufacturing FMLs [23]. For Glare – the FML investigated during this research – the typical metal sheet (aluminium 2024-T3) ranges from 0.3 – 0.5 mm thickness, while the nominal thickness of the S2-glass/FM94-epoxy prepreg is 0.133 mm (single layer). The surface of aluminium sheets are pre-treated – de-greasing and chromic acid anodizing – followed by priming with BR-127 corrosion inhibiting bond primer to ensure proper bonding with the fibre prepregs [2].

Aluminium sheets and the pre-impregnated fibre layers are arranged in the desired lay-up, and then bonded together in an autoclave. The bonding between the layers is achieved at high temperature – 120° C – and a maximum pressure of 6 bar. After the bonding at 120° C the laminate is cooled down to room temperature. The different thermal expansion coefficients of the aluminium and fibre layers results in tensile residual stresses in the aluminium layers and compressive residual stresses in the fibre layers.

2.3.a Post-curing effects

The tensile residual stresses are responsible for the shorter fatigue initiation life in Glare laminates compared to monolithic aluminium [24], because the tensile residual stress in the aluminium layers superimpose to the applied far-field stress. Consequently, metal layers bear higher actual stress than the applied stress. Residual stresses also affect the delamination process because it affects the amount of load transferred through the metal/fibre interface [2, 25]. To mitigate the effects of this unfavourable residual stress system, the method of post-stretching the Glare laminate can be employed [2, 23] in a single direction. During a post-stretching process, the metal layers are strained into the plastic region of the stress-strain curve, while the fibres remain elastic. After unloading, the effects of the unfavourable residual stress system are mitigated or even reversed depending on the amount of the stretching [2]. The properties of Glare's constituents are listed in Table 2-2.

Table 2-2 Material properties [2]

Properties	Unit	Symbol	UD S2 Glass FM94	Aluminium 2024-T3
Young's modulus	[GPa]	E_{11}	48.9	72.4
		E_{22}	5.5	72.4
Shear modulus	[GPa]	G_{12}	5.55	27.6
Yield strength	[GPa]	σ_{ys}	-	345
Ultimate strength	[MPa]	σ_{ult}	2640	470
Poisson's ratio	[-]	ν	0.33	0.33
Elongation at break	[%]	ε_{break}	4.5	5/6
Coefficient of Thermal expansion	[-]	α	6.1e-6	22e-6
Density	[g/cm^3]	ρ	1.98	2.78

2.4 Fatigue mechanism: metals and composites

Aircraft fuselages are cyclically loaded by pressurization cycles each flight, while the wing structures are loaded in wing bending by lift and gust loads. These loads are lower than the nominal maximum stress that the material can sustain. The repeated loading nucleate fatigue cracks at a microscopically small scale, followed by crack growth to a macroscopic length before material failure [26]. Because fatigue failure remains a primary source of damage in aircraft, it is essential to consider the various aspects that could affect the fatigue mechanism in a structure.

The fatigue mechanism in FMLs is defined by both fatigue in metals, and fatigue in composites. However, it was observed in experiments [2, 6, 7, 11, 17] that the delamination growth in FMLs is significantly affected by the crack growth in the metal layers. Therefore, the chapter discusses metallic crack growth in more detail compared to the fatigue mechanism in composite before discussing their combined effect on the fatigue life of FMLs.

2.4.a Fatigue mechanism in metals:

In metals, the fatigue life can be divided into the following phases:

- Crack initiation phase where the nucleated microcracks are slow and erratic in growth and mostly governed by surface conditions.
- Crack propagation phase where the crack growth is regular and governed by the material bulk properties.

Crack initiation phase in metals:

Cyclic slip in the slip bands of a material at stresses lower than ultimate strength leads to the formation of micro-cracks. This is possible due to micro-plasticity that occurs more easily at the material surface because the surface is only constrained by material on one side. The reduced constraint on the plastic deformation at the surface grains permits the deformation to occur at lower stress levels. The inhomogeneity arises from different factors: grain size, grain shape, crystallographic orientation of the grains, and the elastic anisotropy of the material. Fatigue is primarily a surface phenomenon in the crack initiation phase [26].

2.4.b Crack growth phase in metals:

The presence of even a single micro-crack in the material results in stress concentration in the material – most likely at its tip – and an inhomogeneous stress distribution at the microstress level. The presence of adjacent grains increases the constraint on slip displacements [26]. To overcome this constraint, the slip system extends by deviating into a different crystallographic plane, which is generally in the direction perpendicular to shear loading. The constraint can be implicitly interpreted as threshold for the crack growth which depends on cyclic micro-plasticity amongst different slip systems. After the surface grain boundary has been penetrated, the crack growth is relatively high because there is no growth constraint inside the grain, and is again reduced when the next surface grain boundary is reached [26]. The fatigue crack initiation phase in metals is significantly larger than the crack propagation phase.

The crack front must propagate uniformly across all penetrated grains to grow coherently. Besides, for the crack to grow continuously, the whole crack front must propagate at a rate independent of the crack growth rate in the individual grains. This becomes possible after the crack has penetrated a large number of grains, and the crack front is approximated as continuous curve. Its growth rate is determined by the crack growth resistance of the material. Crack growth phase begins after the crack grows independently of the material's surface conditions [26].

2.5 Fatigue in composites:

Fibre reinforced laminated composites exhibit various competing damage modes. These are matrix cracking, delamination, and fibre failure. These damage modes are briefly described below.

2.5.a Matrix cracking

Various fibre layers in the composite are bonded together using a resin matrix. Matrix material generally has low load bearing capacity, and hence, form the location for initial damages in the laminates. As the load reaches the ultimate strength of the matrix, micro-cracks emerge in the matrix that coalesce together to form a crack. Matrix cracks are particularly insidious since an immediate consequence is a loss of load carrying ability in a direction normal to the cracks. This manifests as a reduced stiffness in that direction. Matrix cracks by their very nature, introduce multiple stress concentrations, namely, the crack tips. These crack tips exist at the interface between plies of a laminated composite, and therefore act as potential sites of delamination, thus resulting in damage to the structure on a larger scale.

2.5.b Delamination

Separation of two adjacent plies in a laminate is called delamination. Delamination occurs when local inter-laminar stresses exceed the strength of thin matrix layer between plies. The excess stresses causes the matrix cracking, which leads to delamination. The low cyclic loads applied under fatigue loading are higher than the matrix strength, and hence, they cause matrix cracking which leads to delamination.

In FMLs, delamination occurs between the metal and fibre layers due to shear load caused at the interface between the metal and fibre layers due to bridging stress. The magnitude of the shear loading between the two plies that leads to delamination is affected by parameters such as its thickness, stiffness, delamination resistance of the interface, orientation of the interface and lay-up [2].

2.5.c Fibre failure

The brittle fibres used in composites have lower strain to failure compared to metals. The strain distribution in the fibres comprising the composites is not uniform. Hence, each fibre can break independently of each other at the application of load. Such breakage leads to re-distribution of load amongst the remaining fibres and a possibility of breaking more individual fibres. The broken fibre presents the sites of damage initiation for further damage development. The fibre strength poses resistance to the damage propagation but after the damage overcomes this resistance, damage continues to grow.

2.6 Fatigue mechanisms in FMLs

The fatigue mechanisms in the two constituent phases of FMLs – metal and fibres – was briefly described. Although fatigue life in FMLs can be categorized into similar phases – crack initiation and crack growth – the criterion for distinguishing these phases is different. In metals the crack initiation phase comprised the crack nucleation and micro-crack growth. In composites fatigue is accompanied with transverse matrix cracking, delamination and the failure of the individual fibres.

2.6.a Fatigue crack initiation in FMLs

Using Classical Laminate Theory (CLT) Homan [24] empirically showed that the crack initiation behaviour in FML is described by the actual nominal stress cycle and the peak stress cycle at the notch root. He further showed that the nominal stress cycle and an appropriate stress concentration factor at the notch root enables the application of a fatigue life curve until failure for the monolithic metal to the metal layer in the FML. Spronk and Sen [30] developed this model and further addressed the directionality of crack initiation in FMLs using Lekhnitskii's formulations [31]. Therefore, the directionality of crack initiation in FMLs is not the subject of this thesis. Similar to metals, the crack initiation phase is followed by the crack growth phase. The directionality of crack growth in FMLs is the main subject of this research work.

2.6.b Fatigue crack propagation

The fatigue crack growth phase is governed by crack propagation in the metal layers, similar to monolithic metals. The thinness of the metal layers (0.3–0.5mm) permits the assumption of through thickness cracking in the single metal sheets. Therefore, Linear Elastic Fracture Mechanics (LEFM) can be applied in a one-dimensional manner rather than the crack propagating through the thickness which is normally adopted for monolithic metals. Consequently, the crack growth resistance in FMLs can be dictated by the constituent metal sheet (plane stress), and the local crack tip crack driving force. The studies [1, 2, 5, 17, 24, 27] have shown that delamination and fibre bridging affect the crack tip driving force in FMLs.

These mechanisms further differentiate the fatigue behaviour of FMLs from monolithic metals, and are discussed below.

Delamination

The fibres in the FMLs are affected by the cyclic loading due to the load transfer between the metal and fibre layers. The shear stress between the metal and fibre layers causes delamination to occur at this interface. The delamination growth rate depends on the delamination resistance of the prepreg and the load transfer between the metal and fibre layers in a FML.

Fibre bridging

The fibre bridging mechanism is a distinct characteristic of FMLs compared to fatigue crack growth in monolithic metals. It improves the fatigue characteristics of FMLs because of the load transfer between the metal and fibre layers. It is illustrated in Figure 2-2. Fibre bridging allows the glass fibres to transfer a significant part of the load over the crack and restrain the crack opening. Consequently, the crack opening in Glare is smaller as compared to monolithic aluminium. This leads to a reduced Stress Intensity Factor (K) at the crack tip in aluminium in Glare compared to monolithic aluminium for the same applied stress, which is the main reason for the longer crack growth phase in FMLs compared to monolithic metals. The load transferred over the crack through the fibres is called the bridging load. For fibre bridging it is necessary that the fibres do not break, which would happen if they bear load more than their ultimate strength. However, in fatigue loading the low loads ensure the presence of intact fibres that effectively bridge the crack.

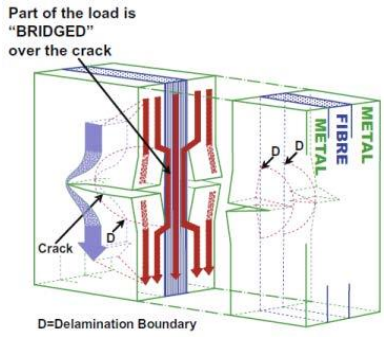

Figure 2-2 Fibre bridging mechanism [5]

Delamination and fibre bridging – a combined study

Marissen [1] identified that the magnitude of the bridging stress is related to the crack opening displacement and the length over which the fibres are elongated. Increase in crack opening increases the fibre strain which leads to higher fibre bridging stress for a given delamination length. However, increasing the delamination length over which the fibres are elongated lowers the strain, which leads to reduced bridging stresses. Therefore, it was initially assumed that the fibre bridging stresses remain constant along the crack length. However, Alderliesten

[2] and Guo and Wu [32] showed that fibre-bridging stresses do not remain constant along the entire crack length.

Besides the cyclic stresses, the delamination growth rate also depends on the delamination resistance of the prepreg. Bridging stresses are affected by delamination and vice-versa [1]. The opening of the crack flanks in aluminium layer during loading leads to elongation of intact fibres over the delaminated zone. It implies that the strains in the fibre layer, and thus, the stresses are determined by the delamination length for a given crack opening. Larger delamination lengths result in small bridging stresses and small cyclic shear stresses at the interface delamination growth rates. In other words, the delamination growth rate and the bridging stresses are in balance, continuously influencing each other [5].

This chapter described the FML nomenclature, its manufacturing process and the fatigue fracture mechanism in FMLs, which is a primary source of damage in aircraft structures. Furthermore, fatigue mechanism in monolithic metals was discussed because the crack growth mainly exists in the metal layers. In FMLs, it was mentioned that the delamination growth follows the crack growth in metal layers.

3 Chapter 3: Literature review of damage directionality in FMLs

3.1 Introduction

Swift [33, 34] performed experiments on shell structures with longitudinal cracks loaded under internal pressure. He observed the cracks flapping above a certain length, i.e. cracks did not propagate in a longitudinal direction above a certain length. Flapping has since then been recognized as a damage tolerance mechanism and a safety mechanism for an aircraft fuselage [15]. To rely on flapping mechanism for safety of an aircraft with Fibre Metal Laminates (FMLs), it is necessary to understand the mechanisms affecting damage directionality in FMLs.

Marissen, Alderliesten and Wilson [1-3] developed methodologies to describe the fatigue damage growth characteristics of FMLs for in-axis loading. These methodologies do not consider the directionality of damage growth, and thus-remain limited to in-axis loading. But significant deviation of crack path under off-axis loading particularly for unidirectional grades of Glare was reported in studies [6, 7, 11]. Up until recently, this deviation is not well understood. In FMLs, damage directionality is mainly determined by the crack paths which remain in the metal layers only. Delamination between the metal and fibre layers occurs after the crack exists. It extends approximately perpendicular to the crack propagation direction. Therefore, the current research problem addresses the damage directionality in FMLs by predicting the crack paths in the metal layers. Hence, crack path theories for metals alone are reviewed in this chapter.

The chapter is divided into three sections. The first section discusses crack propagation using Linear Elastic Fracture Mechanics (LEFM) principles. The second section discusses crack path theories used in LEFM. The final section discusses various studies performed on FMLs under off-axis loading in comparison with the existing crack path theories. This section presents the shortcomings of the existing theories in predicting crack paths in FMLs under off-axis loading. The chapter concludes with the justifications for the approach undertaken in this research to understand the damage directionality in FMLs under off-axis loading.

3.2 Crack propagation in metals: linear elastic fracture mechanics (LEFM) approach

Strain energy concepts for crack growth assume that crack extensions occur when the energy available overcomes the resistance of the material [37, 38]. Griffith [39] demonstrated that a developing crack in a tensile stress field would release strain energy proportional to the fracture surface area that was newly created during its growth. The strain energy released is then equal to the work done in creating the fracture surface area and proportional to the crack length increase. Under increasing stress, the material continues to release the energy by letting the crack grow to a certain length, called the critical length. Beyond this critical length, crack growth is instable.

Irwin [37, 38] extended the theory proposed by Griffith [39] to a mathematical form as:

$$\boldsymbol{G = -\frac{dU}{dA} \geq R} \qquad \textbf{3-1}$$

where, G is the strain energy release rate, U is the strain energy, A is the crack surface area and R is the energy required to create a new surface area in the material. This strain energy balance criterion indicates whether a crack will grow. The strain energy stored in the material is affected by the amount of work performed by the external forces. In loading a panel two cases can be identified: fixed grip and constant load.

The load-displacement graph for the fixed-grip condition is shown in Figure 3-1. During loading upto point A the strain energy stored in the body is represented by triangle OAC. Unloading a specimen results in release of the stored energy. If the specimen is unloaded under fixed-grip by increasing the crack length from a_1 to 'a_1+da', then the straight line OB represents the load-displacement response of the body with a longer crack length a_2 accompanied by a decrease in load from A to B. The increase in crack length results in reduced stiffness of the body, and therefore, point B is below point A. The new elastic energy stored in the body is represented by the triangle OBC. Subsequent removal of load will follow line OB.

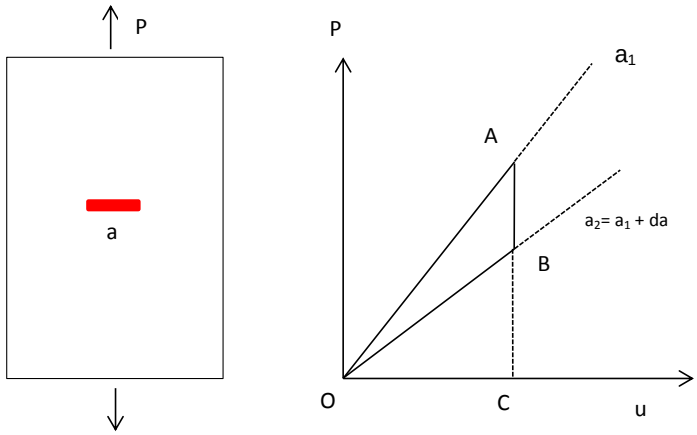

Figure 3-1. Load-displacement response of a cracked plate under fixed grip loading

Although no external work is supplied to the specimen because the specimen remains fixed, the strain energy in the specimen reduced from OAC to OBC during the crack growth process. The amount of strain energy reduced – *excess energy* -, is represented by the triangle OAB. When this available *excess energy* exceeds the energy required to create fracture surface, then instable fracture occurs as:

$$\frac{dU}{da} = -\frac{dOAB}{da}$$

Under constant load, triangle OAC in Figure 3-2 is the amount of elastic strain energy in the component for a crack with size 'a'. The increase in crack size from 'a' to 'a_1 + da' reduces the stiffness of the component. The increased crack size increases the initial amount of stored elastic strain energy OAC to a higher amount of stored elastic strain energy ODE in the load

controlled condition. The excess energy to the system is provided due to the movement of load 'P' from 'Δ' to 'Δ + d Δ'. The strain energy depicted by the area in triangle ABD is provided to the crack growth and rectangle ACED is the work created by the crack extension. In other words the excess energy leads to the crack extension which is equivalent to the created work as:

$$\frac{dU}{da} = \frac{dACED}{da} - \frac{dOAC}{da}$$

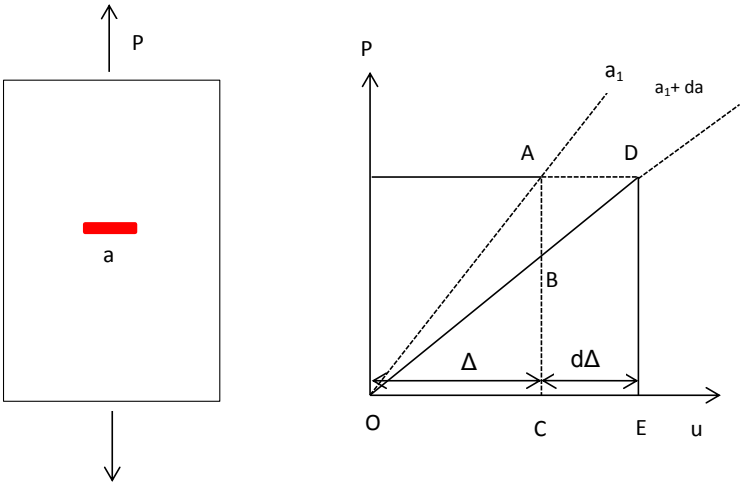

Figure 3-2. Energy based approach to fracture mechanics

For the implementation of LEFM in this research, it is assumed that the material is isotropic and linear elastic. Based on this assumption, the stress field near the crack tip is calculated using the theory of elasticity. The relationship between stress and strain becomes non-linear after the applied stress exceeds the yield strength of the material. The stage of quasi-static fracture is accompanied by large amounts of plastic deformation [40]. LEFM is valid only when the plastic deformation is small compared to the size of the crack, denoted as Small-Scale Yielding (SSY). If large zones of plastic deformation develop before the crack grows, Elastic Plastic Fracture Mechanics (EPFM) must be used. However, fatigue crack growth usually occurs with SSY where these effects are negligible. Therefore, LEFM can be used to describe fatigue phenomena appropriately.

In LEFM, most formulas are derived for either plane stresses or plane strains, associated with the three basic modes of fracture of a cracked body: opening, sliding, and tearing. In the opening mode the load applied is often tensile in nature and applied perpendicular to the plane of the crack. The crack faces open in the direction of loading. In the sliding mode the shear load is applied parallel to the crack faces and the crack faces slide over each other. The crack faces slide in-plane of the material thickness. This plane is marked as OABC in Figure 3-3. In the tearing mode, the crack faces slide over each other but are displaced out of plane of the

material thickness. A combination of any two modes of the crack opening is called mixed-mode. The three modes are illustrated in Figure 3-3 .

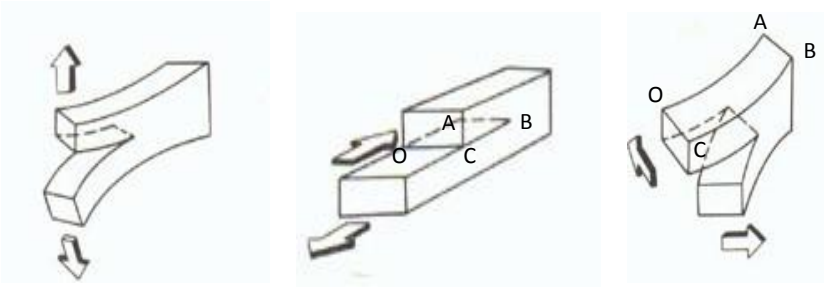

Figure 3-3. Image (a) opening mode (Mode I), (b) sliding mode (Mode II), and (c) shows tearing mode (Mode III) [41]

Elasticity based failure models for cracked specimens start from the description of Westergaard stress functions [42]. The geometrically linear Westergaard functions are used in LEFM to develop solutions for the linear stress field at the crack tip. Westergaard-type solutions predict a standard stress distribution of stresses around any crack tip in an isotropic material, independent of the crack and specimen geometry which describe the stresses that become indefinite in an ideally elastic solid. The stress field at the crack tip, r = 0, obtained using Westergaard functions [41] is:

$$\sigma_r = \frac{1}{(2r)^{0.5}} \cos\frac{\varphi}{2}\left[K_I\left(1+\left(\sin\frac{\varphi}{2}\right)^2\right)+\frac{3}{2}K_{II}\sin\varphi-2K_{II}\tan\frac{\varphi}{2}\right] \quad \textbf{3-2}$$

$$\sigma_\varphi = \frac{1}{(2r)^{0.5}} \cos\frac{\varphi}{2}\left[K_I\left(\cos\frac{\varphi}{2}\right)^2-\frac{3}{2}K_{II}\sin\varphi\right] \quad \textbf{3-3}$$

$$\tau_{r\varphi} = \frac{1}{2(2r)^{0.5}} \cos\frac{\varphi}{2}\left[K_I\sin\varphi+K_{II}(3\cos\varphi-1)\right] \quad \textbf{3-4}$$

Where σ_r is the stress field in the radial direction, σ_φ is the stress in the tangential direction, $\tau_{r\varphi}$ is the stress in the shear direction. This section presented a summary of LEFM principles that are relevant to the current research. The following section reviews the crack path theories used in LEFM.

3.3 Crack path theories in metals

Experiments have often shown that cracks will propagate in a direction perpendicular to the tensile load. Intuitively, researchers concluded that crack paths are determined by the direction of the largest driving force. Irrespective of this intuition, a criterion should exist to predict crack growth direction under various loading configurations. Such a criterion must address two fundamental aspects:

- It should state in which direction the crack will grow.

- It should also predict when will the above path become unstable, i.e. deviate from a crack path locally at the crack tip.

The second must be addressed because it determines the effect of any external disturbances on a propagating crack. Many studies [19, 43, 44] have been performed in the past to address the above two about crack paths and their stability using LEFM principles. Mostly, these theories ignore plasticity effects. In general, these theories use a mixed-mode ratio at the crack tip obtained from Erdogan and Sih's first investigation on crack paths under transverse and shear loading [19]. Using a mixed-mode ratio, the direction for the crack growth can be determined as the direction:

- in which the hoop stress at the original crack tip has a maximum. This is commonly known as the Maximum Tangential Stress (MTS) theory [19, 43, 45-47].
- in which *T*-stress is positive [20].
- in which the energy release rate is maximum. This is known as the Maximum Strain Energy Release Rate (MSERR) [48-50].
- in which the Strain Energy Density is minimum (MSED) [51].
- in which Sih's energy density factor is stationary [21, 51, 52].
- in which mode II stress intensity factor (K_{II}) is reducing and approaching zero [20, 45, 53-57].
- in which the dilatational part of the strain energy density has its maximum. This is known as the *T*-criterion [58-60]. Note that *T*-criterion is based on strain energy, and is not the same as *T*-stress criterion.

Although these theories use different parameters, fundamentally all theories can be related to Griffith's [39] proposed energy release criterion for crack propagation. Exceptions to the above are *T*-stress theory which correlates crack paths to the sign of the first higher order term of William's stress field at the crack tip. An overview of the above listed crack path theories is presented next.

3.3.a Maximum Tangential Stress and Maximum Strain Energy Release Rate

Application of the maximum tangential stress theory (MTS) is straightforward for isotropic materials under uniaxial loading. The direction of the maximum tangential stress or hoop stress from Equation 3-5 can be obtained by calculating the second differential of the σ_{φ} with respect to φ – the fracture angle. The second differential provides Erdogan and Sih's equation [19] for crack path directions:

$$\cos\frac{\varphi}{2}[K_I \sin\varphi + K_{II}(3\cos\varphi - 1)] = 0 \qquad \textbf{3-5}$$

However, when the applied load is at an angle to a crack, then the application of the above theories becomes complicated. The increase in crack angle corresponds to an increase in the mixed-mode ratio, $M^e = \frac{K_{II}}{K_I}$. In brittle materials that fail without developing significant plasticity and in materials with limited ductility, the stress intensity factors describe the stresses around the crack tip. In these brittle materials, Irwin and Kies [40] showed that the

strain energy release rate (G) can be equated to K with the following mathematical relations between G_i and K_i,

$$G_I = K_I^2\left(\frac{1}{E}\right) \quad \textbf{3-6}$$

$$G_{II} = K_{II}^2\left(\frac{1}{E}\right) \; or \; G_I = K_{II}^2\left(\frac{1-\vartheta^2}{E}\right) \quad \textbf{3-7}$$

$$G_{III} = K_{III}^2\left(\frac{1}{2\mu}\right) \quad \textbf{3-8}$$

where *i* represents the mode of crack opening for plane-stress, ϑ is the Poisson's ratio, and μ is the shear modulus. The K based criterion has the added advantage of depending on parameters – crack length, load applied - that can be conveniently measured in experiments. Substituting K_I and K_{II} in Equation 3-5 with G_I and G_{II} using Equations 3-6 – 3-8, the crack path equation for the MSERR becomes:

$$\cos\frac{\varphi}{2}[G_I \sin\varphi + G_{II}(3\cos\varphi - 1)] = 0 \quad \textbf{3-9}$$

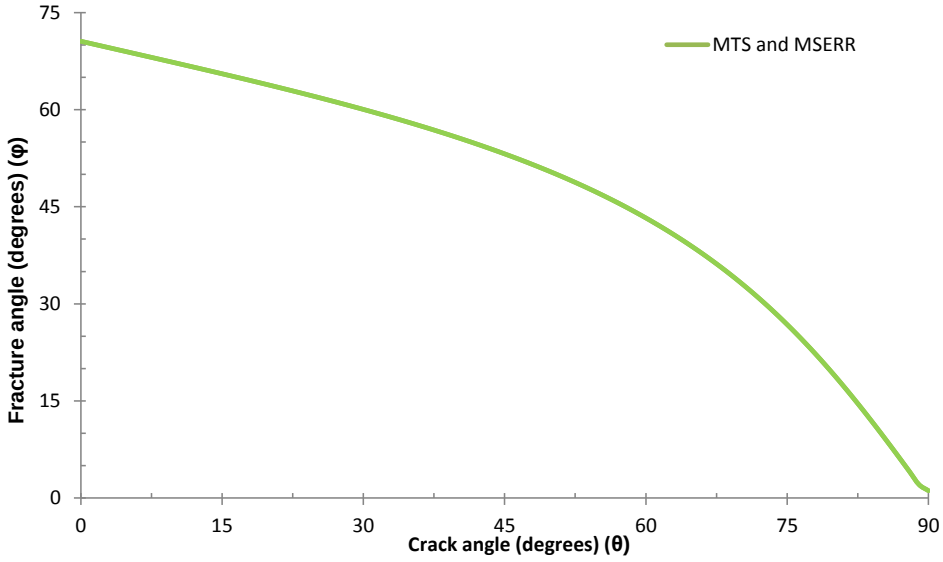

Figure 3-4. Fracture angles with respect to the crack angles for the MTS and MSERR theories

Hayashi and Nemat-Nasser [61] developed expressions using the dislocation theory to verify Irwin's formula for energy release at the crack kinks. Compiling the results of analytical models for crack branching in Hussain *et al*, [49, 62, 63], Nemat-Nasser [64] showed that the fracture angles obtained using the MSERR are the same as MTS. These results are presented in Figure 3-4 and the definitions of the angles is presented in Figure 3-5.

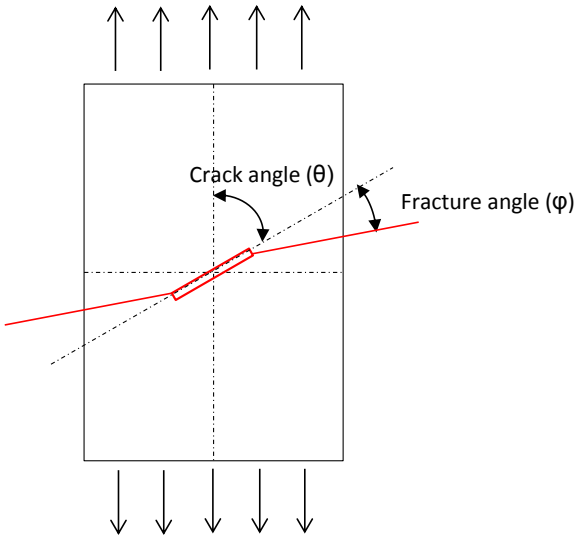

Figure 3-5. Definitions of various angles in specimens under angular loading for a monolithic metal

Therefore, it can be concluded that the crack paths predicted by the MSERR and MTS theory are the same.

3.3.b Minimum Strain Energy Density and the *T*-criterion

A material deforms under the influence of applied loading. The work done by the applied loading is stored as the strain energy in the material as discussed in section 3.2. Strain energy can be separated into distortion energy (T_D) and dilatation energy (T_v). A material yields when there is excessive distortion while excessive dilation leads to fracture. Sih [51] split the stored elastic energy into T_D and T_V to develop the Minimum Strain Energy Density (MSED) criterion for predicting the crack paths.

At the microstructure scale, anisotropy and inhomogeneity affect the distortion and dilation of a material. The stationary value of the 'strain energy density function' (***SED***) is applied [68] to determine the effects of T_D and T_V. This sheds light on the degree of yielding in connection with fracture. If T_D is dominant in total strain energy stored then the crack traverses without deflection, and if T_V is dominant then the crack paths deflect. ***SED*** depends on SIFs following:

$$\boldsymbol{SED = \frac{1}{r}\left(a_{11}K_I^2 + 2a_{12}K_IK_{II} + K_{II}^2\right)} \qquad \textbf{3-10}$$

Where,

$$a_{11} = \frac{1}{16\mu}[(1+\cos\varphi)(\kappa-\cos\varphi)]$$

$$a_{12} = \frac{1}{16\mu}\sin\varphi\,[2\cos\varphi - (\kappa-1)]$$

$$a_{22} = \frac{1}{16\mu}[(\kappa+1)(1-\cos\varphi) + (1+\cos\varphi)(3\cos\varphi-1)]$$

κ – (3-4)/ϑ, where ϑ is Poisson's ratio.
μ – Shear modulus (N/mm^2)

Mathematically, it is important to use a positive definite quantity for assessing the resistance of a material to fracture in order to assess the minimum of ***SED*** which is the fundamental of the MSED theory. Sih [21] postulated that –

- Crack extension will occur at the crack tip in a radial direction along which the strain energy density is minimum, i.e. $\frac{\partial SED}{\partial \varphi} = 0$
- The crack begins to propagate when the strain energy density reaches a critical value, $\boldsymbol{SED} = \boldsymbol{SED_{cr}}$

However, Theocaris and Andrianaopoulos [71] reasoned that MSED continuously sums up T_D and T_V but ignores the fundamentally different natures of the these two quantities. This summation can only distinctly say something about the failure mechanism if either the T_D or T_V are negligible. Additionally, they showed that MSED cannot be used without using the higher order terms of the linear stress field. The usage of the higher order terms would lead to violation of the LEFM principles because of the non-linearity associated with these fields. Hence, MSED cannot be used in conjunction with LEFM theories. To overcome these limitations of the MSED, they developed the *T*-criterion. Theocaris *et al.* [58] developed *T*-criterion based on the dilatational energy density (T_v) and distortional energy density (T_D). Various energy densities can be calculated as :

$$\mathbf{T} = \frac{1}{4G}\frac{1}{1+\vartheta}\left(\boldsymbol{\sigma_r^2} + \boldsymbol{\sigma_\varphi^2} - \mathbf{2}\boldsymbol{\vartheta\sigma_r\sigma_\varphi} + \mathbf{2}(\mathbf{1}+\boldsymbol{\vartheta})\boldsymbol{\sigma_{r\varphi}}\right) \quad \textbf{3-11}$$

$$\boldsymbol{T_V} = \frac{\mathbf{1}}{\mathbf{6}\boldsymbol{G}}\frac{\mathbf{1}-\mathbf{2}\boldsymbol{\vartheta}}{\mathbf{2}(\mathbf{1}+\boldsymbol{\vartheta})}\left(\boldsymbol{\sigma_r} + \boldsymbol{\sigma_\varphi}\right)^{\mathbf{2}} \quad \textbf{3-12}$$

$$\boldsymbol{T_D} = \frac{\mathbf{1}}{\mathbf{6}\boldsymbol{G}}\left(\boldsymbol{\sigma_r^2} + \boldsymbol{\sigma_\varphi^2} - \boldsymbol{\sigma_r\sigma_\varphi} + \mathbf{3}\boldsymbol{\sigma_{r\varphi}}\right) \quad \textbf{3-13}$$

where G is the shear modulus.

The *T*-criterion is evaluated on the boundary of the plastic zone as calculated with Mises yield criterion as illustrated in Figure 3-6. σ_r and σ_φ can be calculated using the stress field calculated by equations 3-2 – 3-4. Hence, K_I and K_{II} are retained in T, T_V and T_D.

Theocaris *et al.* [58, 60, 72] stated that the crack propagated in the direction where the dilatational part of the strain energy density has its maximum along the plastic zone boundary. They reasoned that at this point, the void growth during stable tearing would be maximal since the void growth is controlled by the dilatational part of the energy density. At the plastic zone boundary the deformational energy density – energy used for deforming the material - is constant. However, the *T*-criterion can only be applied to isotropic materials which follow Von Mises yield conditions.

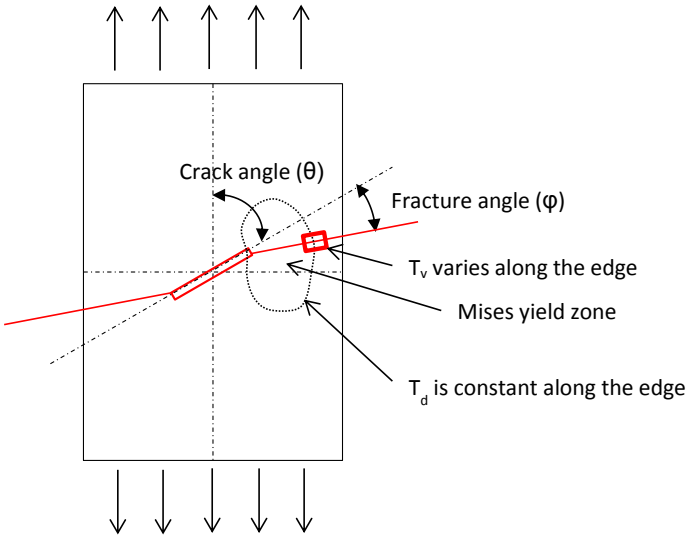

Figure 3-6. *T*-criterion illustration

Although the above mentioned crack path theories use different parameters to determine the crack paths, they all predict the same fracture angle with respect to the change in crack angle [71]. This is primarily because the fundamental for failure in materials is governed by Griffith's theory. The strain energy release rate can be conveniently transformed into K using equation 3-6 – 3-8. Theocaris *et al.* [71] also showed that the fracture angle predicted from all these theories is same as shown in Figure 3-4. Considering the above finding of Theocaris *et al.* [57], the author has decided to compare the FML results with a single theory in Section 3.4 which is the MTS theory.

The common principle of the above theories lies in the fact that cracks will propagate in a direction where K_{II} is vanishing. To improve the results from MTS for materials that have plastic deformations at the crack tip, *T*-stress was incorrectly used in the past to study the size of the crack. An overview of *T*-stress criterion for crack paths prediction is presented in Section 3.3c, and a detailed critical review is presented in Chapter 4.

3.3.c ***T*-stress criterion**

Crack path deviations have also been observed under purely uniaxial loading. To address this observation, a *T*-stress crack path prediction theory was postulated by Cotterell [20]. It's role in predicting crack paths stability is briefly summarized below, and a detailed discussion is provided in Chapter 4.

Sometimes crack paths become unstable – deviate from the straight paths - under applied uniaxial loading. To understand the crack path instability observed in the experiments of Roesler and Benbow [73, 75], Cotterell [20] proposed the use of a higher order term in William's stress field expansion - *T*-stress - for metals under pure Mode I loading. Subsequently, other studies showed the influence of *T*-stress [20] on the crack path. In their study on angled cracks, Williams and Ewing [43] analysed stresses at a distance from the

crack tip (r_c) [45] to calculate the crack paths depending on the sign of *T*-stress. This observation of crack paths with respect to *T*-stress sign is known as the *T*-stress theory for predicting crack path stability. The sign of *T*-stress defines the stability; positive *T*-stress implies that the crack paths are unstable (crack paths deflect) and vice-versa.

Li *et al.* [76] studied crack propagation of a closed crack in compression and used both K_{II} and *T*-stress components - T_x and T_y - with a modified MTS criterion to predict the fracture angle. They concluded that compressive T_y increases the fracture angle by reinforcing K_{II} into the failure mode [77]. But, Leguillon and Murer [78] observed no crack kinking or branching in Double Cantilever Beam (DCB) and Compact Tension (CT) in their finite element method (FEM) study even for positive *T*-stress. Additionally, Williams and Ewing [43] observed in their experiments that the crack path was initially stable for positive *T*-stress before it deviated at an angle. Furthermore, *T*-stress theory's inability to provide correct results for crack paths in dynamic fracture [79-81] raises further concerns with respect to the theory, namely - the inconsistency of the *T*-stress theory in predicting crack paths accurately.

The current section mentioned the widely used crack path theories. It was further stated that *T*-stress is incorrect for predicting crack paths in FMLs. More importantly, it is also shown that the mixed-mode theory is derived from the fundamentals of the MTS. It is, therefore, assumed that a modified form of the mixed-mode theory using SIFs provides a better understanding of damage directionality in FMLs under off-axis loading. A mixed-mode theory using SIFs is assumed to be the best approach because the previous work in fatigue in FMLs was developed using SIFs

3.4 Past studies on off-axis fatigue loading of FMLs

Despite the advances in studying damage mechanisms in FMLs, little knowledge is available on the behaviour of FMLs under off-axis loading [6, 7, 9]. Kawai *et al.* [10, 14, 82] studied the behaviour of Glare2 and Glare3 under off-axis loading for both static and fatigue life tests. They reported the fatigue strength to reduce significantly with the increase in off-axis angle.

Kawai *et al.* [10, 14, 82] observed in Glare3 the fatigue crack growth rates to increase with the off-axis angle up to 45° where the laminate stiffness is minimal. Thibault-Liboiron *et al.* [11] presented the fracture angle results of fatigue test for edge notched specimens, and Gonesh [6, 7] performed fatigue crack growth tests on FMLs under off-axis loading in central notched specimens. Zaal [15] presented a model to predict crack paths in FMLs based on the anisotropic *T*-stress criterion discussed in the next chapter. His model considered the laminate entirely as one homogeneous material, and used different values for the critical distance ahead of the crack tip [5] to predict the fracture angle. However, the experiments by Gonesh [10] and Thibault-Liboiron *et al.* [19] for centrally notched cracks and edge-cracked specimens respectively indicate different angles than what Zaal's theory predicts. The experimental results of Gonesh are tabulated in Table 3-1. In the following section these results are discussed and compared with the mixed-mode theory and Zaal's anisotropic *T*-stress criterion [9].

Table 3-1. Experimental results from Gonesh [6, 7]

Material	Fibre layup with respect to longitudinal axis	Off-axis angle (degrees)	Fracture angle (degrees)
Glare2A-4/3-0.4	0/0	0	0
	0/0	45	31
Glare3-4/3-0.4	0/90	0	0
	0/90	22.5	6
	0/90	45	0
Glare4B-4/3-0.4	90/0/90	22.5	12
	90/0/90	45	5
	90/0/90	67.5	-2

3.5 Discussion on the application of the mixed-mode theory and *T*-stress

The crack path theories previously discussed were specifically developed for metals. Theocaris *et al.* [71] also showed that the fracture angle predicted from all these theories is the same. Hence, the experimental results [6, 7] are only compared with the predicted fracture angles from MTS theory in Figure 3-7.

The MTS theory postulates that the crack path traverses in a direction perpendicular to the maximum tangential stress [19]. Under uniaxial loading in isotropic material this direction of MTS corresponds to the direction of the principal stress direction which is the same direction as the applied loading direction. Anisotropy makes the principal stress in FMLs under off-axis angles different from the loading direction. Therefore, crack paths do not traverse perpendicular to the loading direction in FMLs under off-axis loading as illustrated in Figure 3-7.

Zaal's curve in Figure 3-7 has been reproduced from his thesis [9]. Comparing Zaal's prediction model and the MTS theory with Gonesh's experimental results [6, 7], it is evident that both prediction models predict the fracture angle in Glare incorrectly. Additionally, Zaal approached the problem assuming that the laminate was under purely tensile load. Lastly, Zaal considered the FML as one single homogenous material. These two incorrect assumptions by Zaal resulted in incorrect estimation of the fracture angle. The correct crack angle definition for predicting fracture angle in anisotropic materials was defined by Broberg [22]. Hence, the two assumption used by Zaal yield incorrect results which is explained further.

Firstly, the anisotropy in FMLs make their principal axis different from the loading angle, thereby making the crack angle in FMLs different from the crack angles in metals [22]. Additionally, the effect of unbalanced laminate orthotropy induces shear load into the specimen. The introduction of shear due to laminate orthotropy and fibre-bridging necessitates to use mixed-mode versions of the crack path theories mentioned above.

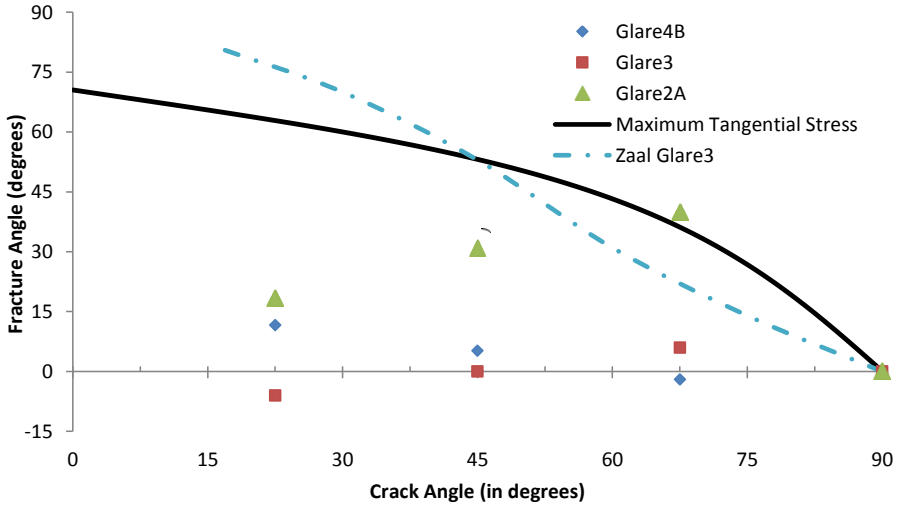

Figure 3-7. FML fracture angles under off-axis loading compared with MTS predicted fracture angle [19]

Erdogan and Sih's [19] postulation that crack path traverses perpendicular to the plane of maximum stress suggests that in Glare3 at 45° off-axis angle the laminate is under pure tensile loading. It is assumed that this is due to the fact that the laminate has balanced orthotropy with respect to the off-axis loading. In Glare3 at 22.5° and 67.5° off-axis angle, the signs of the fracture angle are opposite but same in magnitude. This observation can be understood by assuming that at 22.5° and 67.5° off-axis loading Glare3 has the same magnitude of unbalanced laminate orthotropy with respect to the loading direction, but with opposite signs.

In addition to the laminate orthotropy, the off-axis fibres introduce load in the transverse direction at the crack tip. This causes mixed-mode stress field at the crack tip. However, in comparison to the monolithic metals, the mixed-mode caused is also affected by the off-axis angles and the laminate orthotropy. It is explained as follows.

In monolithic metals the crack angle is changed by changing the crack orientation with respect to the loading axis. Therefore, the principal axis and loading direction continue to be parallel and in the same direction. However, in FMLs under off-axis loading, the initial crack orientation and the loading angle remain same, but the principal axis changes – see Figure 3-8. The change in principal axis affects both the crack angle and the stress induced in the specimen. The amount of shear introduced additionally depends on the fibre-bridging introduced by the transverse component of the off-axis fibres. This causes a different mixed-mode in FMLs under off-axis loading compared to monolithic metals for the same crack angle. Hence, the crack grows with a mixed-mode fracture.

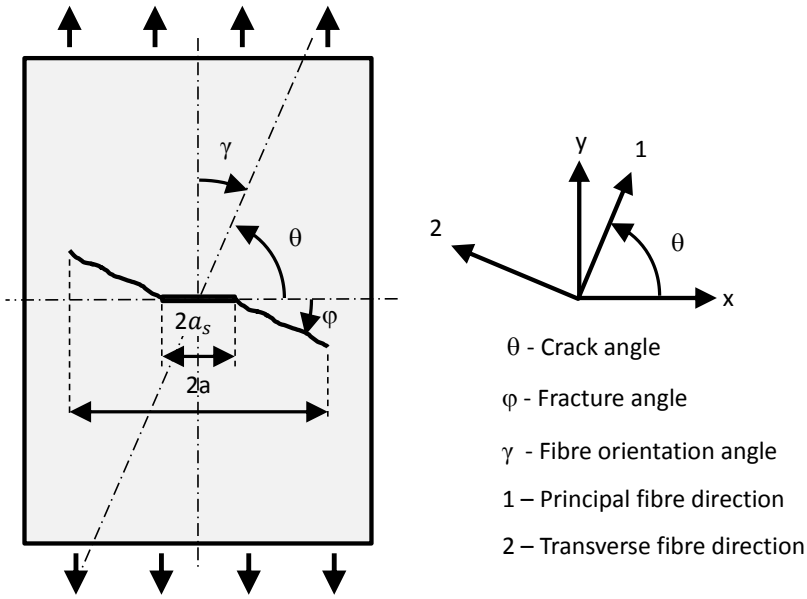

Figure 3-8. Definition of the various angles

The effect of these mechanisms on the crack paths is further explained in Chapter 5. The effect is mathematically included in the prediction model in Chapter 6. The model uses MTS' mixed-mode theory with SIFs that are correctly modified to include the effect of off-axis angles on damage directionality in FMLs[2].

3.6 Conclusions

This chapter discussed only the crack path theories for metals because the damage directionality in FMLs is governed by the crack paths in the metal layers. Comparison of the past studies on damage directionality in FMLs with the SIF based theories existing in their current form highlighted the lack of correlation with the theories. The lack of correlation was attributed to the combined effect of unbalanced laminate orthotropy with respect to loading and off-axis fibre-bridging in FMLs, which are not present in monolithic metals. The *T*-stress role in predicting crack paths in metals in LEFM is discussed in further detail in Chapter 4.

The past work in FMLs fatigue has been developed with an SIF approach, hence, it was concluded that the MTS theory for monolithic materials should be used to incorporate the mixed-mode effects induced in FMLs under off-axis loading. It is assumed that the MTS theory can be appropriately modified to the correct form of mixed-mode for FMLs under off-axis loading by including the following two effects:

(i) mechanism of off-axis fibre bridging - a characteristic of FMLs under off-axis loading and (ii) unbalanced laminate orthotropy with respect to the applied loading direction.

The mechanisms to be included are discussed in details in Chapter 5 and their inclusion in the prediction model is explained in Chapter 6.

4 Chapter 4. A review of T-stress and its effects in Linear Elastic Fracture Mechanics

This chapter is an abridged version of the published article by the author of this thesis. The complete article discusses the role of *T*-stress in Linear Elastic Fracture Mechanics in detail. However, to maintain brevity, only excerpts relevant to this thesis have been presented in this chapter.

4.1 Introduction

A structure's residual strength under fatigue loading can be increased by crack deflection. Some researchers [19, 51, 53] have previously studied the mechanisms and parameters governing cracks paths leading to various crack path theories, such as Maximum Tangential Stress (MTS), Strain Energy Density (SED), and Strain Energy Release Rate (SERR). Cotterell [20] proposed the use of a higher-order term – *T*-stress - to predict crack paths in metals under pure Mode I loading. This became known as the *T*-stress theory for predicting crack path stability, and it used the sign of *T*-stress to predict the stability. Some researchers [85, 86] associated the *T*-stress sign with the crack path stability predictions overlooking its mathematical origin for the far-field boundary correction to the stress field in the transverse direction. Other researchers have used *T*-stress to explain results for other phenomena [43, 45, 87, 88] in fracture mechanics. Hence, it leads to various understandings and interpretations of *T*-stress.

Sherry [89] reviewed the analytical methods used for evaluating *T*-stress, while Chen [90] reviewed the integral equation method for multiple cracks with *T*-stress. This chapter discusses the *T*-stress role in Linear Elastic Fracture Mechanics (LEFM). It discusses various studies comprising the origin of *T*-stress, phenomena associated with *T*-stress, experimental results, methods of evaluating *T*-stress, and its application in various fields. The chapter provides a critical review for the crack path stability predictions with *T*-stress sign considering its origin.

The chapter begins with an introduction to the origin of *T*-stress followed by various experimental studies to understand *T*-stress in fracture mechanics. Finite Element Methods (FEM) that have been developed to increase the accuracy of the calculated *T*-stress values are discussed subsequently. Finally, the results are critically discussed and the conclusion is presented for *T*-stress associated phenomena in LEFM.

4.2 The origin of *T*-stress

The use of the Westergaard equations to understand the stress field in a cracked specimen is one of the oldest and most popular methods. The Westergaard equations have played an important role in the development of LEFM to analyze the stress field in a cracked specimen. In 1939, Westergaard [42] developed a description of the biaxial stress field for internal cracks in pressurized cylinders. He demonstrated that ''in a restricted but important group of cases the normal stresses and the shearing stress in the *x* and *y* - *directions* at the crack tip can be stated in the form'' [41]

$$\begin{Bmatrix}\sigma_x\\ \sigma_y\\ \tau_{xy}\end{Bmatrix} = \frac{K_I}{\sqrt{2\pi r}}\cos\frac{\theta}{2}\begin{Bmatrix}1-\sin\frac{\theta}{2}\sin\frac{3\theta}{2}\\ 1+\sin\frac{\theta}{2}\sin\frac{3\theta}{2}\\ \sin\frac{\theta}{2}\cos\frac{3\theta}{2}\end{Bmatrix} \qquad 4-1$$

The terms in equation 4-1 are illustrated in Figure 4-1. For Mode I cracks, the boundary condition $\tau_{xy} = 0$ along the entire *x*-axis is automatically satisfied with the above equation. Westergaard equations that were originally developed for a biaxial stress field were subsequently applied for uniaxial loading. However, they produce a σ_x component at the boundary edges along the crack axis for a purely uniaxial load. This is expected because Westergaard's solution was developed for a biaxial loading. To eliminate this transverse component, Irwin [37] suggested the use of a transverse component of stress and called it *T*-stress.

$$\sigma_x = \frac{K_I}{\sqrt{2\pi r}}\cos\frac{\theta}{2}\left\{1-\sin\frac{\theta}{2}\sin\frac{3\theta}{2}\right\} - \sigma_{0x} \qquad \textbf{4-2}$$

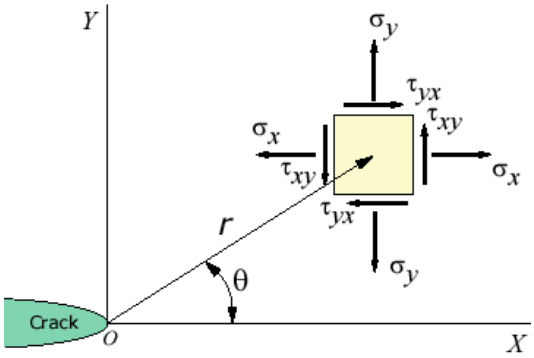

Figure 4-1. Crack tip parameters

Including this non-singular stress, σ_{0x} (*T*-stress), explained the observed tilt of the isochromatic fringe loops away from the normal in the work of Wells and Post [91]. Later, Williams [92] showed the presence of *T*-stress at the edge of a wedged crack through the eigen series expansion of the stress field. Thereafter, *T*-stress became widely regarded as the stress acting parallel to the crack tip in the x-direction.

Cotterell and Rice [53] developed analytical solutions for the stress intensity factors (SIFs) at the tip of a slightly curved crack or kinked two-dimensional cracks. Using the hypothesis 'crack paths propagate in a direction of $K_{II} = 0$' they demonstrated crack path stability to be predicted by the sign of *T*-stress, i.e. crack paths are stable for T<0 and vice-versa. Pham *et al.* [93] showed that this criterion for crack path prediction was universal with respect to all loading and geometrical situations for small crack growth. Recently, there have been many other studies in the past 50 years on *T*-stress through experimental, analytical and FEM which relate *T*-stress with other phenomena. These studies are discussed in this chapter. The

following section discusses the various experimental studies on *T*-stress and its associated mechanisms.

4.3 Experimental studies on *T*-stress

4.3.a Photoelastic tests on *T*-stress

Principle of the photoelastic tests

The isochromatic fringes observed in the photoelastic tests relate to the geometric locus of material points that present the same principal stress differences. The stress-optic law relates the principal stress differences ($\sigma_I - \sigma_{II}$) with the measured isochromatic fringe order *N*, according to equation 4-3:

$$\boldsymbol{\sigma_I - \sigma_{II} = \sqrt{\left(\left(\sigma_x - \sigma_y\right)^2 + 4\tau_{xy}{}^2\right)} = \frac{N}{t} f_\sigma} \qquad 4-3$$

where 't' is the thickness of the specimen at the point under analysis and f_σ is the stress fringe value that depends on the photoelastic material and the wavelength of the light used in the observation. Since $\sigma_I - \sigma_{II}$, is continuous, *N* varies in a continuous manner. The locus of points at which *N* = 0 forms a light band and the locus of points at which *N* = 1/2 forms an adjacent dark band. Another light band is formed by rays traversing the photoelastic material at points where *N* = 1. Successive dark and light bands are formed for increasing values of *N*. These bands are called fringes. The change from dark fringe to an adjacent light fringe represents an increase or decrease of 1/2 in the value of *N*; to assign any other magnitude would violate the principle of continuity. The number of these fringes increases in proportion to the external forces. Thus, the isochromatic pattern can be used to obtain the magnitude of $\sigma_I - \sigma_{II}$ throughout the specimen.

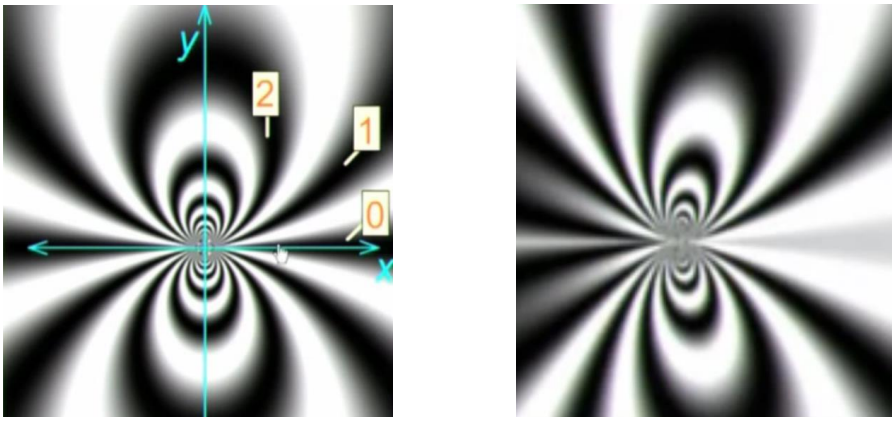

(a) **(b)**

Figure 4-2. Photoelastic fringes without *T*-stress (a) and the forward tilted photoelastic fringes with the *T*-stress (b). 0, 1 and 2 in (a) indicate the photoelastic fringe order. [94]

Using photoelastic tests, Ramesh *et al.* [95] studied the equivalence of the multi-parameter equations proposed by Westergaard [42], Sanford [96], and Atluri and Kobayashi [97] to

calculate the crack-tip stress state. They proposed an over-deterministic least squares technique to evaluate the mixed-mode stress field parameters by photoelasticity. While Christopher *et al.* [98] performed a quantitative evaluation of fatigue crack shielding forces using photoeleasticity and evaluated the interfacial shear stress intensity and retardation intensity at the crack tip, both of which possibly cause the shielding effects. This was similar to the results obtained by Jian-Jun and Yi-Heng [99] in their study of the *T*-stress effect for the interaction problem of an interface macrocrack with a near-tip microvoid in the process zone of the main crack tip with the 'pseudo traction edge dislocation' method. Colombo *et al*. [100] showed that the positive *T*-stress has an amplification effect and the negative *T*-stress has a shielding effect on the crack. FEM results of Spaniel *et al.* [101] who also showed that the Paris relation is not applicable for cases with different *T*-stress. They also showed that under small scale yielding (SSY), the crack direction prediction based on both original MTS and with *T*-stress is sufficiently accurate.

Cotterell [20] studied an isochromatic pattern in a compact tension (CT) specimen similar to the one obtained by Guernsey and Gilman [102] in a cleavage specimen. Cotterell [15] showed the influence of higher order terms on the stress field ahead of the crack tip. The crack deviated away from the expected straight path under assumed purely Mode I opening. Cotterell [20] found a correlation between the crack path's direction and the sign of the first non-singular term, *T*-stress, (referred to as a_2 by Cotterell in [20]), and between the isochromatic fringes and the sign of *T*-stress. When *T*-stress was positive, he observed that the crack deviated and then the isochromatic fringe pattern tilted backward. This effect of the *T*-stress on the rotation of the isochromatic fringes was also shown by Ayatollahi and Safari [103, 104].

Zakeri *et al.* [105, 106] found that the K_{II} and *T*-stress calculated from the photoelastic methods correlated well with the numerical values obtained through FEM. Zanganeh *et al.* [107] used thermoelastic stress analysis and FEM to determine *T*-stress and mixed-mode SIFs using pure mode I, mixed-mode I and II, and interacting cracks as case studies. They obtained a more accurate solution of *T*-stress using three terms of William's stress field formulation compared to using only the first two terms of the expansion. Their studies highlight the correction in the stress field that is obtained by using *T*-stress which is expected because the higher order terms increase the accuracy of a stress field.

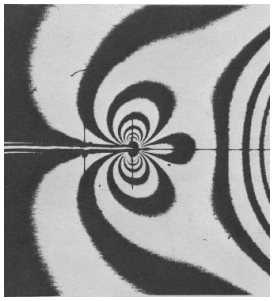

Figure 4-3. Sanford's [96] experimental results

In contradiction to Cotterell's [20] theory for the crack path stability with the *T*-stress sign, Sanford [96] observed the crack path to be stable in the vicinity of the specimen edge in CT specimen even though *T*-stress was positive. Sanford used the Modified Boundary Layer (MBL) to explain the photoelastic effect but the observed crack path was in disagreement with the *T*-stress theory. MBL uses the *T*-stress to calculate the stress field at the crack tip. Besides, Sanford [96] observed photoelastic results in which the fringes tilted forward with positive *T*-stress, as shown in Figure 4-3 which was similar to Ramesh *et al.* [95]. Sanford [96] observed the photoelastic pattern closer to the specimen edges thus highlighting the role of *T*-stress at the boundary edges similar to the FEM results of Shahani and Tabatabaei [77]. This is further discussed in section 4.5.

4.3.b Crack paths with *T*-stress

Several studies [43, 45, 86, 108-115] have evaluated crack paths in materials using the *T*-stress theory. Llopart *et al*. [112] studied crack turning behaviour using the *T*-stress theory in integral structures. Their results showed higher potential for crack turning in a region far away from the stringers where the parameters K_I and *T*-stress are less sensitive to the stringer design. Matvienko [113] predicted fracture angles using *T*-stress, and observed consistency between predictions and the experimental data for mixed-mode I/II crack growth behaviour of Guiting limestone.

Ki [114] studied various criteria for kinking outwards of interface cracks between dissimilar materials with experiments. He concluded that the slightly modified MTS to accommodate the *T*-stress effect could be used for the kink initiation point under assumption of tough interface, but that it cannot be used to determine whether-or-not to kink.

Williams and Ewing [43] observed that the crack in an angled crack problem extended initially in a stable crack path with positive *T*-stress which is in contradiction with what is expected from the *T*-stress crack path theory. This was also observed by Finnie and Saith [55] in their photoelastic tests. They suggested the application of the *T*-stress at a critical distance ahead of the crack tip which was mathematically justified by Finnie and Saith [45] to be a function of the fracture toughness of a material. Williams and Ewing [43] used the α, (α = 2c/a, where 'c' is an empirically determined distance ahead of the crack tip, and a is the crack length) in their angled crack problem to predict crack paths. They included the *T*-stress in MTS and SED theories for predicting crack paths, and obtained improved correlation between the experimental results and prediction values.

Leevers *et al.* [109-111] studied the effect of *T*-stress on fatigue cracks of various specimen geometries implicitly by defining a biaxial parameter B. They reported an increasing curvature of crack paths with increasing biaxiality, defined with B is

$$\boldsymbol{B = \frac{T\sqrt{\pi a}}{K_I}} \qquad \textbf{4-4}$$

where $T = p_x - p_y, p_x = \text{load in x} - \text{direction}, \quad p_y = \text{load in y} - \text{direction}$. However, Leevers *et al.* [109-111] observed that *T*-stress predicted the crack path for pure Mode I opening differently in Double Cantilever Beam (DCB) and Compact Tension (CT) specimens

compared to the other specimens. They found more negative B values (negative *T*-stress) in longer cracks. For shorter cracks (crack length to width ratio (a/w) <0.4), B values were significantly different in the externally notched specimens such as Single Edge Notched (SEN), single edge notched bend (SENB), CT, double cantilever beam (DCB), and tapered double cantilever beam (TDCB) compared to larger cracks (0.4<a/w<0.7). They concluded that the longer cracks had more negative *T*-stress values because no constraint on bending was allowed.

In their CT specimens, they noticed negligible change in K_I for different loading with respect to specimen width (0.4<a/w<0.7), although the B values were significantly different for shorter cracks to with respect to specimen width (a/w<0.4). Leevers *et al.* [109-111] reasoned that *T*-stress and B were affected by the bending stresses in the specimens. In another experimental study on the fracture toughness of a material with *T*-stress, Joyce [116] found that *T*-stress had no effect on K_{Ic} for CT and three point bend specimens for the a/w range 0.45 – 0.7. After comparing the *T*-stress results from the specimens' tests, he recommended them to be tested at a/w=0.7 because at this value, *T*-stress was equal for the two geometries.

Hallback and Nilsson [115] investigated mixed-mode fracture in aluminium 7075-T6 with experimental and numerical studies. Experiments performed exhibited only small differences in the mode mixity values for which a shift in the initial crack growth appearance occurred. Thus, they concluded *T*-stress only had a minor influence on the crack transition angle.

The role of *T*-stress in dynamic fracture resistance has been studied are reported in [79, 117-124]. These studies on dynamic fracture observed that the *T*-stress theory for predicting crack paths in dynamic fracture inapplicable. A summary of these experimental studies highlights the different observations by different researchers for the crack path stability prediction with the *T*-stress. These results raise concerns for the inconsistent predictions with this crack path theory. The authors address the cause for this inconsistency of *T*-stress crack path stability theory in section 4.5.

4.3.c Fracture toughness with *T*-stress: constraint parameter

The plastic strains in the vicinity of the crack-tip are restrained which results in a triaxial stress state at the crack tip. This effect is called crack tip constraint and it affects the fracture toughness of a material. This subsection discusses studies that investigated the role of *T*-stress at crack tips with regards to its influence on the crack tip constraint parameter.

The papers [105, 106, 113, 125-157] present other work of Ayatollahi *et al.* who have extensively explored the role of *T*-stress in LEFM through combined experimental, numerical and analytical work. Their modification of the MTS criterion by the inclusion of *T*-stress and in some cases other higher order terms improved the correlation with the experimental results in comparison to conventional MTS in a variety of problems ranging from graphite rocks and soda lime glass to double cleavage drilled specimens (DCDC). Smith *et al.* [86] showed substantial influence of *T*-stress for mode II tests using a shear specimen under tension and compression to obtain positive and negative *T*-stress values respectively. They showed an inverse relationship between *T*-stress and fracture toughness implying that negative *T*-stress increases mode II fracture toughness.

The following studies [120, 158-165] undertook experiments to study the influence of *T*-stress on fracture toughness of various materials. These studies demonstrated that the apparent fracture toughness of the material varied with specimen geometry or the constraint level, and highlighted that the non-singular *T*-stress term must be accounted for to accurately measure the fracture resistance in functionally graded materials (FGM). Sumpter and Hancock [166] observed a significant J_c increase in crack tip opening displacement (CTOD) bend specimens when a/W is reduced below 0.3. The increase in toughness was attributed to loss of constraint due to break back of the plastic zone (PZ) at shallow crack depths.

Some other studies [167-172] investigated the crack tip constraint with different parameters - *T*-stress, Q-parameter, and the multiaxiality quotient, q. The J-T (*J*-integral with *T*-stress) analysis results based on an MBL solution showed that as the applied load increased, the solutions departed from the MBL solutions. These studies demonstrated that loss of constraint due to increasing plastic deformations is not captured well by the elastic *T*-stress.

The relation between *T*-stress, constraint and transition temperature were investigated in [170, 173, 174]. Wallin [174] developed and verified the relation between *T*-stress and the master curve transition temperature. His two-parameter (K-*T*-stress) model predicted constraint loss similar to more detailed models based on Weibull analysis.

In [115, 175] Hallback *et al.* performed experiments on mixed-mode loading configurations. With the inclusion of *T*-stress, their prediction were in good agreement with experiments. However, in [115], they did an evaluation without *T*-stress and their results in [115] showed a shift between mode I and mode II type crack growth initiation that was fairly well predicted without the *T*-stress. They concluded that the inclusion of *T*-stress does not improve the understanding of the observed geometry and size dependence on fracture toughness. Wang and Xu [176] concluded that high SIFs of incident cracks easily induce interfacial debonding initiation, and changing the *T*-stress sign is an effective way to control interfacial debonding initiation (negative *T*-stress suppresses interfacial debonding initiation).

In general, the studies concluded that *T*-stress captured loss of constraint well at low loads, but at higher loads or deep cracks the correlation was not sufficient. The mismatch at the higher loads or deeper cracks can be attributed to the plastic flow under large scale yielding (LSY) that relieves the stresses at the crack tip and reduces them below the MBL solution.

4.4 Finite Element Studies in *T*-stress

Larsson and Carlsson [87] computed *T*-stress as the average difference between the σ_x for a specimen and the corresponding value obtained from the Boundary Layer (BL) approach – no inclusion of *T*-stress in the Westergaaard equations - where σ_x was obtained from the elastic-plastic finite element method. In the elastic-plastic solution, they observed the plastic region to grow linearly with K_I^2 and the elastic region to grow linearly with K_I. They showed different plastic strains at the crack tip for different specimen geometries by the MBL method. For CN and Double edge-cracked (DEC) configurations, MBL computed more plastic strain elements compared to the BL method. Conversely, for CT and bending specimens the number of plastic strain elements compared was lower, compared to the value of the first plastically-

yielding element. Furthermore, MBL calculated larger PZ sizes at the crack tip compared to BL. Larsson and Carlsson [87] also showed an increasing PZ in the internally notched specimen with the MBL approach and a reduced PZ in externally notched specimens (Bend specimen and CT) similar to Leevers *et al.* [109-111]. These results provide evidence for an effect of *T*-stress on the PZ size but do not provide the mechanism of this effect.

Rice [177] explained Larsson and Carlsson's [87] results of limited range of validity by SSY, whereby small crack tip PZ are correlated in terms of the SIFs. He explained their results by considering *T*-stress in a plane strain yielding model. Rice claimed *T*-stress has less effect on crack tip parameters such as crack opening displacement (COD) and *J*-integral compared to the yield zone size. Inclusion of *T*-stress as a second crack tip parameter characterizes the small plane strain yield zone more adequately.

Ayatollahi *et al*. [178] explored the direct use of FEM for calculating *T*-stress. *T*-stress was determined for a test configuration designed to investigate brittle and ductile fracture in mixed mode loading. *T*-stress was calculated in mode I by direct use of displacement along the crack flanks. Their results for the mixed-mode specimen under real loading conditions showed the biaxiality ratio in mode II is much higher than in mode I conditions.

4.4.a FEM for *T*-stress for specimen geometries

The following studies [179-182] employed FEM to investigated the role of *T*-stress in various cases – Single edge cracked plate (SECP), double edges cracked plate (DECP) and centrally cracked plate (CCP) specimens [179], SIFs and *T*-stress for edge cracks aligned along the gradient in finite size elastically graded plates [181]. Other studies pertaining to the crack paths stability with *T*-stress are discussed below.

Chen *et al.* [183] and Petit *et al* [182], showed the necessity and influence of *T*-stress in predicting crack paths correctly for aircraft fuselages. Similarly, Becker Jr *et al.* [184] incorporated *T*-stress to predict crack paths correctly when the SERR criterion failed to accurately predict the kink direction.

Al-Ani and Hancock [185] studied short cracks in tension and bending. Edge-cracked bars with an a/W ratio less than 0.3 in bending and 0.5 in tension lose J-dominance. This loss was attributed to compressive *T*-stress. Geometries which exhibited tensile *T*-stress retained *J*-dominance in agreement with MBL formulations. This was similar to the experimental results reported in [166] and re-establishes the influence of *T*-stress on crack tip constraint.

Leguillon and Murer [78] observed no crack kinking or branching in DCB and CT configurations even for positive *T*-stress until a threshold was reached. They used both the energetic and the stress fracture criterion [186] to define a positive *T*-stress threshold below which no branching can occur in a biaxial stress field. They concluded that no kinking can occur below the aforementioned critical/threshold *T*-stress value provided the size of the inhomogeneities is much smaller than the characteristic length. Later, Selvarathinam and Goree [186] explained that if a crack slightly kinks due to micro-inhomogeneities with *T*-stress below threshold *T*-stress, it will instantaneously realign itself along with the primary crack.

Zafosnik *et al.* [187, 188] investigated a gear tooth root. Formulation of modified SED and MTS criteria was based on the asymptotic stress field that comprises the stress intensity factors K_I, K_{II}, the *T*-stress, tractions on crack surfaces caused by pressure trapped inside the crack and the critical distance r_c. The results for the influence of stress distribution around the crack tip showed that *T*-stress can be neglected for crack propagation in the tooth's root. The crack propagation path could be modelled accurately when only stresses described with SIFs were considered.

Jayadevan *et al*. [79, 81] studied *T*-stress evolution in dynamically loaded fracture specimens by performing two-dimensional plane strain, elastodynamic finite element analyses of SEN specimens. Their results demonstrated that dynamically loaded specimens are subjected to larger negative *T*-stresses in the early stages of loading as compared to static loading, and that the crack opening profile and opening stress at a finite distance from the tip are strongly affected by the magnitude and sign of the *T*-stress at any given crack speed.

This subsection again highlights the contradiction and unreliability in predicting crack path stability with *T*-stress. However, the results mentioned in this subsection verify the influence of *T*-stress on the constraint parameter.

4.4.b FEM for *T*-stress in anisotropic, functionally graded and adhesive materials

The following studies [189-193] investigated *T*-stress role in anisotropic materials, Functionally graded materials (FGMs) and adhesive materials. Zhang [194] calculated the effect of *T*-stress for the spot welds to improve his earlier results in [195]. The obtained SIFs closely matched with the results from [196].

Lugo and Daniewicz [197] showed that the crack closure transient behaviour is different for positive and negative *T*-stress. While positive *T*-stresses show a typically monotonic plane stress behaviour, negative *T*-stress display an initial increase till a peak and decreases subsequently. Lee and Kim [198] showed the plastic mismatch as well as compressive *T*-stress in bi-materials to affect the interfacial crack-tip constraint substantially through FEA similar to the findings in the analytical studies of [199] where elastic mismatch was found to influence the *T*-stress in anisotropic materials.

Through FEA and numerical analysis, Chen and Dillard [200-203] analysed the crack paths in adhesively bonded joints. They found that *T*-stress significantly influenced the crack paths in such joints, and similar to homogeneous materials, crack paths were unstable for positive *T*-stress and stable for negative *T*-stress. This was consistent with the predictions made by Fleck, Hutchison and Suo in [204] and with the *T*-stress crack path stability theory. Chen *et al.* [203] also, reported that *T*-stress is closely related to adhesive layer thickness.

4.4.c FEM studies for *J*-integral and *T*-stress

Several researchers [205-210] studied the *T*-stress relationship with *J*-integral with FEM. Meliani *et al.* [209, 210] assessed the gouge defect in a pipe subjected to internal pressure based on the mesofracture Modified Notch Failure Assessment Diagram approach. They used MBL to study the fracture resistance, and found that the notch fracture toughness is a linearly decreasing function of the critical effective *T*-stress ($T_{eff,c}$-stress).

Burstow and Howard [211] showed the existence of high constraint at the crack tip for ductile crack growth due to dominance of *J*-integral over *T*-stress, but the constraint reduced significantly once the crack grew as the *J*-integral influence reduced. In [212-214] Burstow *et al.* showed homogeneous *T*-stress cannot reproduce the complex stress fields due to material mismatching in welded joints, but that the *T*-stress has a similar effect on the geometrical constraint in overmatched materials as in homogeneous materials. However, in an under matched specimen, *T*-stress has little to no effect on the crack tip stress field. Karstensen [215] showed J-T characterization of crack tip stress fields failed at high levels of deformation. Hence, *T*-stress fails to capture deformations correctly under LSY conditions.

Roy and Narasimhan [216] found that in mixed mode cases, positive *T*-stress retards the plastic flow localization in the ligament, and that zero and negative *T*-stress results in rapid accumulation of plastic strain in the ligament. Roy and Narasimhan [217] found that positive or zero *T*-stress favoured *J*-dominance for the full range of near-tip mode mixity, while negative *T*-stress causes loss of *J*-dominance within a narrow range of near-tip mixity close to mode I loading. Kim and Kang [218] in their elastic-plastic FEM studies on mode-mixity showed that the shear stress remains unaffected by *T*-stress with increasing mode-mixity, but that normal stresses are significantly affected in a manner similar to that seen in [219, 220].

4.4.d Other studies on T-stress

Castro *et al.* [221] and Sousa *et al.* [222] compared the PZ at the crack tip. They estimated the PZ using various methods such as Equivalent Inglis plate, William's series only, William's series, *T*-stress, SIF + *T*-stress etc. They showed that neither SIF nor SIF+*T*-stress can predict the PZ correctly at the crack tip correctly. It may be influenced by the nominal stress far away from the crack tip. Sousa *et al.* [222] concluded that *T*-stress improvements to the PZ are limited only to the medium nominal stress to yield strength ratio.

Yeh *et al.* [223] studied the influence of *T*-stress on the PZ size of a precracked isotropic composite plate using various failure criteria under tensile loading conditions. Their investigation indicated that the stress field with *T*-stress always yields a larger PZ.

Hello *et al.* [224] developed the higher order stress field coefficients at the crack tip under mixed mode conditions. They transformed Westergaard's exact complex solutions into polar power and Laurent series defined in closed form and derived exact analytical values of SIFs and *T*-stress from the power series definitions. Li and Xu [225] studied the change of *T*-stress before and after crack kinking in two-dimensional elastic solids using the asymptotic analysis and the Westergaard function method to estimate *T*-stress and SIFs of an infinitesimal kink. The contribution of the *T*-stress before crack kinking was shown in both the *T*-stress and SIFs of the kinked crack. Besides this, they concluded that the sign of the kinked open crack *T*-stress might be different from that of a main crack. Hence, simply using the sign of the *T*-stress before crack kinking is insufficient to determine the crack growth stability. Li *et al.* [226] came to a similar conclusion.

4.5 The role of T-stress in Linear Elastic Fracture Mechanics: a discussion

The previous review presented the various applications of *T*-stress in LEFM. Its origin lies in the correction of the Westergaard biaxial stress field when applied to uniaxial loading. Amongst the aforementioned studies, *T*-stress has consistently been used for PZ correction, and as a constraint parameter. However, the results obtained from *T*-stress have lacked consistency in predicting crack path stability.

T-stress corrects the stress field ahead of the crack tip and thus it enables us with more accurate estimation of fatigue life as evidenced in [227]. Besides, the studies [228-233] have also mentioned that using further higher order terms improves the stress field estimation. This is in compliance with the mathematical origin and function of the higher order terms. However, the use of these higher order terms cannot create a new physical mechanism at the crack tip and thereby cannot create an influence on the crack propagation but only improve their numerical evaluation.

Li *et al.* [76] studied the crack extension results from a closed crack in compression. They used K_{II}, T_x and T_y with a modified MTS criterion to predict the crack kink angle. They concluded compressive T_y increases the kinking angle, and reinforced apparent mode-II fracture toughness and vice-versa. The results in [77] reported similar observation for *T*-stress values. Leguillon and Murer [78] observed no crack kinking or branching in DCB and CT even for positive *T*-stress in their FEM study, whereas, Williams and Ewing [43] observed in experiments that the crack path was initially stable for positive *T*-stress before it deviated at an angle. The *T*-stress theory's inability to provide correct results for crack paths in dynamic fracture as discussed in section 4.3.c raises further concerns on the physics of the theory.

These results highlight the inconsistency of the *T*-stress theory in predicting crack paths accurately. In the following subsections, the authors critically discuss the *T*-stress crack path stability theory and other mechanisms associated with *T*-stress in LEFM considering the origin of *T*-stress

4.5.a T-stress: a correction to the Westergaard's biaxial stress field

T-stress was introduced to the Westergaard's solution in order to eliminate the effect of the transverse stress which arises in uniaxial loading. Westergaard took advantage of symmetry in problems to bring the two complex stress functions into one single Westergaard function. Therefore, it implicitly states that the fracture mechanics problems under consideration or analysis with the Westergaard functions must be symmetrical, similar to a biaxially loaded specimen.

Eftis [234] showed that symmetry is a correct condition for the application of the *T*-stress (the constant term in [234]) to satisfy the boundary value problem. The *T*-stress when correctly applied in coherence with its origin would reduce the CN specimen problem to the symmetrical problem. Considering the arguments by Eftis [234], the correct application of *T*-stress should reduce the problem to a biaxially symmetric stress field problem. The CN specimen is one particular geometry which satisfies this boundary condition. However, *T*-stress has repeatedly failed to predict the crack paths correctly in such specimens -

experiments [43], dynamic fracture [79, 117-123], and analytical model for biaxial stress field [76, 78]. Crack paths in CT specimens are predicted correctly using the *T*-stress crack path stability theory even though the CT specimens do not satisfy the boundary conditions necessary to use the theory.

4.5.b The origin of T-stress crack path prediction – a retake

Cotterell [20] established the *T*-stress theory for crack path prediction in CT specimens where he correlated the sign of *T*-stress term in his paper to the direction of the isochromatic fringes which was similar to the fringes obtained by Guernsey and Gilman [102]. There have also been cases [96] where the theory failed. However, Cotterell [20] overlooked the appropriate symmetry condition that *T*-stress should produce in the specimen in order to produce the biaxial stress field of Westergaard [42]. It is necessary to simulate the correct symmetry condition in order to maintain the relevance of *T*-stress origin with its mathematics.

Cotterell [20] studied the isochromatic pattern of Guerney and Gilman [102] who used Berry's [235] specimen as reference for their study. In their specimen the maximum tensile stress does not lie in a plane perpendicular to the crack but in a plane whose normal is at an angle of roughly 80° to the direction of crack propagation. Hence, crack paths in cleavage specimen have the tendency to deflect away from the expected straight path [102]. Therefore, to control crack paths in cleavage specimen, Berry [235] used a groove, and Benbow and Roesler [73] used compressive stress to keep the crack path stable. Guernsey and Gilman [102] initially used compressive transverse stresses similar to Benbow and Roesler [73]. The compressive forces were used to eliminate any tensile forces parallel to the crack surfaces and keep the crack paths stable. Guernsey and Gilman [102] obtained their fringe pattern after removing both the compressive stresses and the wedge. Their crack paths were stable, and the isochromatic pattern observed by them [102] was leaning backward implying that the *T*-stress was positive. Furthermore, their [102] cleavage specimen was constraint against in-plane bending specimen while Cotterell's [20] study of the similar isochromatic fringes with CT specimen has no such constraint. Cotterell's [20] correlation of positive *T*-stress with unstable crack paths, and backward tilting fringes seems incorrect because Guerney and Gilman [102] reported their crack paths to be stable with the backward tilting isochromatic fringes.

The specimen studied in Cotterell [20] is more similar to Benbow and Roesler [73] who applied the wedge through a pair of clamps fastened to the specimen edge. These clamps provide compressive forces through a sliding motion and Benbow and Roesler [73] attributed this external compressive forces to produce the stable path. They mentioned the possibility of obtaining straight crack paths in certain materials without the use of compressive forces and also showed evidence that applied lengthwise compression could produce stabilization of crack paths. They reasoned that the bending nature of the CT specimen make the crack paths deviate from their stable paths. Leevers *et al*. [109-111] investigated this with the biaxiality parameter that affected the crack paths stability.

One could argue that *T*-stress could represent the applied transverse stresses to the specimen and their sign represents tensile (positive) and compressive (negative) nature. However, the application of external transverse stresses modifies the problem to a biaxial loading problem

whereas, the original suggestion by Irwin [37] to use *T*-stress was to correct the unaccounted stress that results ahead of the crack tip in the *x*-direction under uniaxial loading. Therefore, using *T*-stress to represent the applied transverse stresses violates the mathematics of the origin of *T*-stress.

Therefore, the *T*-stress theory for predicting crack paths which originated from Cotterell's [20] observation must be modified considering other parameters such as the *T*-stress at a critical distance ahead of the crack tip as suggested in [45, 231] or possibly discarded. Pook [236] suggested an alternative to *T*-stress for predicting crack path stability. He considered this because *T*-stress fails to predict crack paths under certain conditions – cracks were stable for positive *T*-stress. He suggested using the *T*-stress ratio as $T_R = 0.01T/K_I$, where T_R is the ratio of *T*-stress (*T*) with respect to Stress intensity factor in opening mode (K_I). Besides, the origin of *T*-stress implies that the its application should make the problem symmetrically biaxial like CN specimen and it cannot be applied to CT specimens. The failure to predict crack paths correctly in CN specimens, where the fundamentals of its origin are adhered to, raises concerns over the application of the theory. It is successful in CT specimens where it does not adhere to the fundamentals of the origin.

4.5.c Plastic zone and T-stress

One may argue that the *T*-stress effects on PZ is analogous to the fringes lobes. However, one must remember that K_I also relates to PZ. *T*-stress correction to PZ is the consequence of the crack-tip constraint mechanism, and not because of the crack path theory. Besides, close examination of the study [108, 115, 131] also shows that the increase and decrease of *T*-stress is associated with K_I decrease or increase respectively. Llopart [112] showed the influence of *T*-stress on K_I, i.e. increasing *T*-stress reduces K_I. The work done by an applied load in the material can be used by the material for elastic deformation, plastic deformation or to extend the crack growth. Under SSY, defining elastic energy strain release rate as G, is mathematically stated as:

$$\boldsymbol{G = \frac{1-\vartheta^2}{E} K^2} \qquad \textit{(plane strain)} \qquad \textbf{4-5}$$

Where $\boldsymbol{\vartheta}$ is the Poisson's ratio, *E* is the young's modulus and K is the stress intensity factor. Steady-state crack growth requires that the energy imparted to the material by the applied load be equal to the sum of (a) the energy released at the crack tip, (b) plastic work in the active PZ, and (c) the residual strain energy deposited in the wake in a unit of crack advance (see Figure 4-4). The energy stored at the crack tip is the incremental strain energy that is used to extend the crack length at the crack tip by breaking the surface bonds. Materials develop a PZ at the crack tip over a certain load, and as the applied load increases, the PZ increases in size until the crack grows and the material behind the crack tip unloads, forming a wake where the residual strain energy is stored.

Elastic strain energy is trapped within the plastic wake during steady crack growth, and it has no effect on the crack front inelastic deformation. Larger plastic wakes also remove energy that would otherwise be available for the crack front loading. Any increase in the plastic work

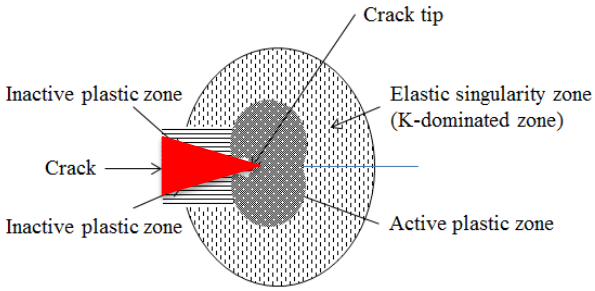

Figure 4-4. Various zones at the crack tip

or residual strain energy deposited in the wake must reduce the energy released at the crack tip, because the total sum of the energy in the material remains constant under constant amplitude loading. Accordingly, the strain energy released at the crack tip for crack growth is reduced and becomes negligible compared to the plastic work and the elastic strain energy in the PZ. The lower energy at the crack-tip reduces the plastic deformation ahead of the crack front which results in a decrease in the near field quantities – displacements, strains and stresses – which reduces K.

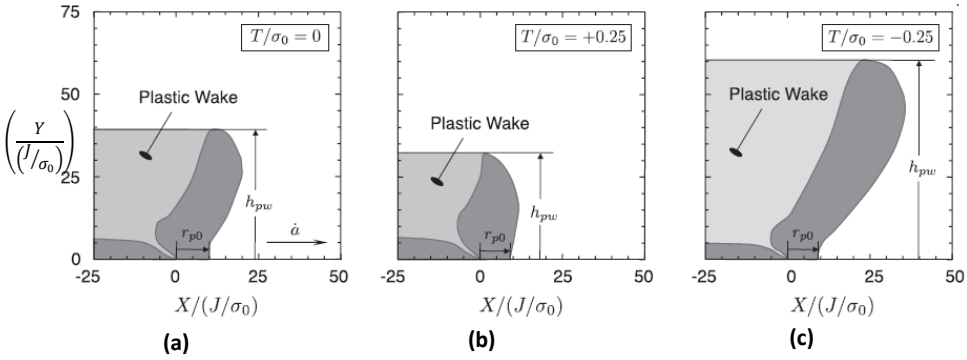

Figure 4-5. Active yielding regions for a steadily advancing crack under plane-strain above the crack plane – h_{pw} – and ahead of the advancing crack front on the crack plane, r_{p0} conditions for imposed zero (a), positive (b) and negative T-stress (c) [237]

Sobotka *et al.* [237] showed that the variation in the plastic wakes with various *T*-stress levels, plastic work and elastic strain energy are associated with the plastic wake height, h_{pw} (see Figure 4-5). The *T*-stress effect limits the amount of plastic deformation ahead of the advancing crack front (r_{po} in Figure 4-5). The large plastic wakes accompanied with negative *T*-stress store more elastic strain energy, reducing the energy at the crack tip that extends the crack growth. This results in reduced near-field quantities under negative *T*-stress. One may expect, based on the energy balance argument and the fact that the overall PZ size is smaller for $T=0$ compared to $T<0$**,** that near-tip strain levels will decrease for any loading with

negative *T*-stress (i.e. larger PZ), which in turn reduces K. The reduction of K values with negative *T*-stress has been reported in [108, 115, 131].

4.5.d Mechanism of crack tip constraint with T-stress

T-stress plays a role in improving the PZ size at the crack tip in SSY in accordance with its mathematical origin, i.e. to compensate the σ_{0x} that arises due to Westergaard's function in uniaxial loading. It can be understood as a parameter affecting the stiffness of the material under uniaxial loading, thus influencing the crack tip opening displacement and the crack tip constraint. This in turn affects the PZ size, thereby correcting the PZ estimation when used with K to determine its size. *T*-stress changes the value of K as expected from global conditions in LEFM by implicitly including the 'constraint effect'.

The following studies [238-247] have shown *T*-stress to affect the constraint parameter. The constraint effect of *T*-stress influences the size and shape of the PZ near the crack tip which results in a progressive loss of crack tip constraint as *T*-stress became negative. The negative *T*-stress retards the mechanisms of ductile fracture. Application of negative *T*-stress suppresses the multiple void growth mechanism, thereby increasing the crack growth resistance

The discussion in this section highlights the limitations of the original crack path theory stability associated with *T*-stress, and why it should not be used for predicting the crack paths. It also discusses the role of *T*-stress in LEFM with consideration of the energy balance to understand its influence on the PZ and crack tip constraint.

4.6 Conclusion

The chapter presented the origin of *T*-stress, various experimental results for *T*-stress on crack path stabilities, analytical techniques and FEM techniques for evaluating *T*-stress, and *T*-stress effects on the plastic zone and constraint parameter. The author emphasize the following about *T*-stress:

- *T*-stress is a boundary effect as evidenced by the following studies [77, 96, 248].
- *T*-stress affects the plastic zone size [80, 87, 249].
- *T*-stress affects the crack tip constraint [237, 250, 251].
- Although there are studies linking the *T*-stress with the crack path stability, several studies exist - experimental [96, 109-111, 175, 252], analytical [85, 253] that contradict this theory. Therefore, it is imprudent to pursue this theory without caution and it must be reassessed with relevance to its mathematical origin.
- The *T*-stress sign and magnitude are affected by the material non-homogeneity [199, 254]. T-stress in anisotropic materials is affected by the anisotropy and mismatched elasticity [199]**.**
- In *T*-stress studies on piezoelectric and pressure-sensitive materials, [255-260], it was shown to be affected by the elastic and electric constants (positive charge increased the *T*-stress), affect the crack kinking behaviour, and the PZ shapes.
- *T*-stress is unable to predict crack paths in dynamic crack growth [79, 117-123].
- The sign of *T*-stress determines the shielding or anti-shielding behaviour of the plastic zone shape and size at the crack tip [88, 99, 261, 262]**.**

5 Chapter 5. Investigation of the crack paths in Fibre Metal Laminates under off-axis loading

5.1 Introduction

The previous chapters reviewed crack path theories [9, 19-21, 64, 263] and past experimental results [6, 7, 11] on damage directionality in Fibre Metal Laminates (FMLs) under off-axis loading. In chapter 3 it was concluded that the most suitable theory to predict crack paths in FMLs under off-axis loading is the mixed-mode theory using SIFs. Mixed-mode theory implies the presence of both tensile and shear loading at the crack tip. The objective of this chapter is to investigate the presence of shear at the crack tip. To this aim, some fatigue tests were performed using Digital Image Correlation (DIC) to investigate the strain field at the crack tip. DIC was previously used by Rodi *et al*. [10] to study the strain field in FMLs. Additional to Goensh' tests [6, 7] that were repeated in this research, fatigue tests were performed to understand the general relationship between laminate orthotropy – unbalanced and balanced with respect to the applied loading – and the crack path behaviour.

This chapter first explains the objectives of the experiments. Thereafter, the experiments are discussed and results are presented. After discussion of these results the chapter ends with concluding remarks.

5.2 Research objectives

The primary objective of the experiments was to investigate shear loading at the crack tip. This is necessary to verify whether crack paths in FMLs indeed deflect under off-axis loading as result of mixed-mode loading. Therefore, a first series of three configurations were tested:

- Glare2A under in-axis loading
- Glare2A under 45° off-axis loading
- Glare3 under 45° off-axis loading

Cracks have been observed to propagate straight under in-axis loading in Glare2A, and to deflect under 45° off-axis loading [265], so comparison between the first two cases should reveal absence of shear in the in-axis loading condition and presence of shear in the off-axis loading condition. Similarly, correlation of strain fields for both off-axis loading – i.e. under 45° off-axis angle - conditions in Glare2A and Glare3, should reveal the contribution of balanced and unbalanced laminate orthotropy in combination with off-axis fibre bridging.

In addition to these three configurations, a second series of fatigue tests was performed. In this series, a number of fatigue tests previously reported by Gonesh [7,8], were repeated to investigate the reproducibility of reported fracture angles. Additionally, a number of tests were performed at off-axis angles not previously tested to extend the total range of off-axis angles.

5.3 Materials and specimen

FMLs can be classified into two categories – unidirectional and cross-ply FMLs. Unidirectional FMLs such as Glare2A and Glare2B have the fibre layers aligned in a single direction, while cross-ply grades such as Glare3 and Glare4B have fibre layers in two perpendicular directions. Due to the different number and orientations of the fibre layers, the

effect of fibre bridging and laminate orthotropy will be different in the unidirectional and cross-ply grades.

Glare2A has the fibre layers along the rolling direction of aluminium, while Glare2B has the fibre layers along the transverse direction. Considering the negligible effect of monolithic aluminium on the overall laminate orthotropy, Glare2A under 22.5° off-axis angle is considered equivalent to Glare2B under 67.5° off-axis angle. Therefore, investigating Glare2A also provides information for Glare2B. In cross-ply FML grades the fibre layers are oriented in two directions. Their influence on the laminate orthotropy is different in magnitude compared to the unidirectional FML grade. The amount of fibre layers in the two directions can be equal like in Glare3 or unequal as in Glare4B which influences the laminate orthotropy differently in different cross-ply Glare grades. For example, in Glare3 the crack traverses without deflection under 45° off-axis loading, while in Glare4B the crack path deflects. To demonstrate the contribution of the different amount of cross-ply fibre layers, both Glare3 and Glare4B were tested.

For this investigation a similar centre crack tension specimen geometry has been selected as adopted by Gonesh [7,8]. In this case the specimens were 540 mm in length and 140 mm in width, as illustrated in Figure 5-1. The total initial starter notch length was $2a_s$ = 5 mm, created by drilling a 3 mm diameter hole in the specimen centre with two saw-cuts of each 1 mm at both sides transverse to the direction of loading.

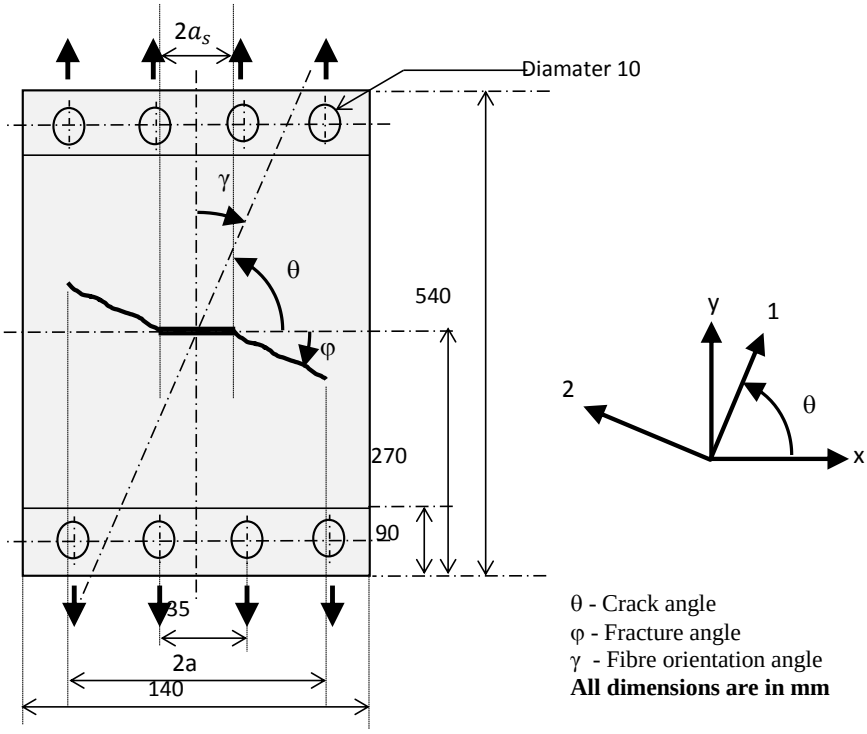

Figure 5-1. Specimen configuration for crack growth under off-axis loading tests specified in Table 1

Specimens were tested until a crack length ($a-a_s$) of 42.5mm was reached, which is more than half the length between the starter notch and the specimen edge. As the primary objective of the experiments was to observe crack deflection in the propagating crack, tests were terminated after this length was achieved. This was done because cracks were observed to continue in their deflected direction without further deflection.

5.4 Fatigue test procedure

After the specimens were machined to the dimensions illustrated in Figure 5-1, they were bolted to clamping plates, which were then mounted to the fatigue machine using a pin joint. The specimens were tested in the 60kN fatigue machine at Delft Aerospace Structures and Materials Laboratory (DASML) at a frequency of 10Hz. The tests were performed under force controlled constant amplitude loading conditions at a maximum stress of S_{max} = 100 MPa and a stress ratio of R = 0.05. The test matrix is presented in Table 5-1.

Table 5-1. Fatigue test matrix

Specimen	Off-axis angle (α – (°))	S_{max} (MPa)	DIC measurement
Glare2A-4/3-0.4	0	100	Yes
	22.5	100	No
	25	100	No
	45	100	Yes
	50	100	No
	67.5	100	No
Glare3-4/3-0.4	0	100	No
	22.5	100	No
	35	100	No
	45	100	Yes
	55	100	No
	67.5	100	No
Glare4B-4/3-0.4	22.5	100	No
	25	100	No
	35	100	No
	45	100	No
	67.5	100	No

The forces corresponding to the minimum and maximum stress were calculated using the measured thicknesses of the various laminates. Thereafter, the required machine inputs – force amplitude and mean – were calculated and used as inputs to control the machine.

First, the machine was run for a minimum number of 10k cycles. In absence of visible cracks the machine was subsequently run in batches of 5k cycles. After the initial crack and the

deflection was recorded, the number of fatigue cycles was increased until the cracks reached a length ($a-a_s$) of 42.5mm, after which the specimens were unclamped from the machine. Depending on the specimen tested and its off-axis angle, the number of cycles required to reach the half ($a-a_s$) of 42.5mm would vary between 80 to 120 kcycles.

Table 5-1 indicates that three tests were conducted using DIC to measure the strain field at the crack tip. Because the DIC measurements on the first three specimens demonstrated the presence of shear at the crack tip and thereby confirmed the hypothesis of mixed mode loading conditions, it was deemed unnecessary to perform DIC measurements in the other tests. The tests were performed at stress ratio of 0.05.

5.5 Digital Image Correlation (DIC)

5.5.a Reason for selecting some specimens for DIC

In Chapter 3 it was postulated that crack paths in FMLs deflect as result of mixed-mode loading at the crack tip induced by the off-axis fibres. The experimental results in [7-9] recorded the crack growth and the fracture angle under off-axis loading. Amongst these results, Glare3 under 45° off-axis loading poses an interesting case, because the crack does not deflect. It was postulated that this occurs due to the laminate being balanced in the off-axis direction, (i.e. the shear produced by the 45° fibre layers, is nullified by the shear produced by the -45° fibre layers).

This concept of cancellation of shear at the crack tip can be verified by observing the presence or absence of a shear strain field at the crack tip using DIC. To reference the observed strain field in Glare3 under 45° off-axis loading, it was compared with two other specimens: Glare2A under in-axis loading, and Glare2A under 45° off-axis loading. In the first case, the crack path was observed to traverse without deflection, while in the second case it deflected to a certain angle.

The presented hypothesis implies that absence of crack path deflection under in-axis fatigue loading in Glare is accompanied with absence of shear at the crack tip. This implies that the deformation observed with DIC should be similar in various Glare grades under in-axis loading to that of Glare3 at 45° off-axis loading. On the contrary, crack path deflection in Glare under off-axis loading should be accompanied with a shear deformation. The DIC measurements were undertaken to study the difference in the deformation field at the crack tip between these two categories – crack paths without deflection and crack paths with deflection.

The primary reason for selecting Glare2A was the larger crack deflection compared to Glare4B under 45° off-axis loading. It was assumed that the larger crack deflection under off-axis loading will be accompanied with significant shear which could be observed more easily using the DIC technique. Therefore, Glare3 at 45° off-axis loading, Glare2A under in-axis loading, and Glare2A under 45° off-axis loading were selected for the DIC strain field observation.

5.5.b DIC principle

DIC is a measurement technique that provides information on the deformation field of an object. It is a fully non-contact and non-destructive image evaluation technique used to track the surface displacements of deforming materials [11, 12]. DIC is based on the analysis of displacements between two images – source image (Figure 5-2a) and deformed image (Figure 5-2b). This is done by tracking the deformation on the material's surface using one particle (or pixel or speckle) between these images. The source image is taken initially before any load is applied to the specimen, i.e. the image of the unloaded specimen with the initial saw-cut. Thereafter, new images are collected after a predetermined number of fatigue cycles. These images are called the deformed images which are compared with the source image (the unloaded pristine crack image). In post-processing, a speckle (one of the black speckled dots) is selected in a region near the crack tip. The procedure is illustrated in Figure 5-2. In DIC, the area of interest – area near the crack tip for the current test – is selected in the images and marked by a rectangle.

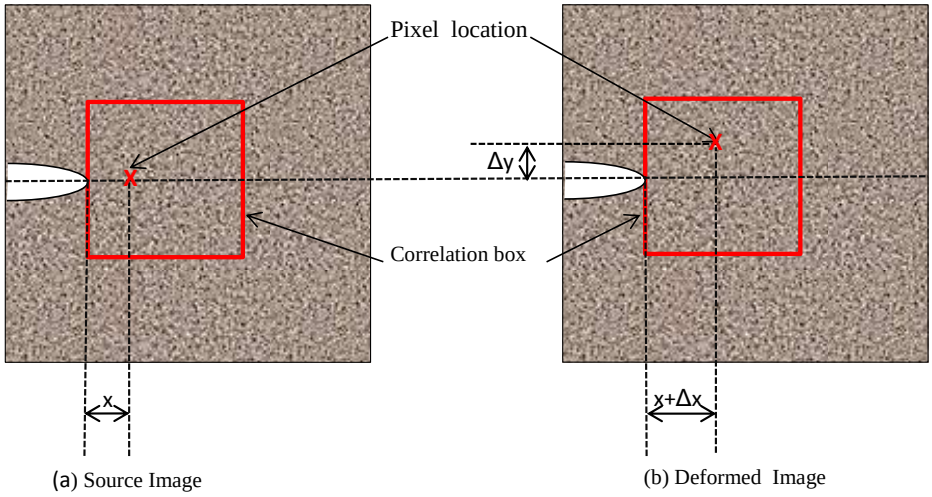

Figure 5-2. Post-processing stages in the DIC calculation. Image (a) shows the selection of the black dot, and image (b) shows the new position of the selected dot with reference to the crack tip process

The marked rectangle in Figure 5-2 is further illustrated in more details (in terms of pixels) in Figure 5-3. The area is divided according to the pixels – represented by the empty squares in Figure 5-3 by the VIC-3D software [13], while the filled squares represent the originally selected pixel. The distance travelled by the selected speckle within this region - from the position marked x in Figure 5-2a to the position marked x in Figure 5-2b – is calculated in terms of the pixels. This data is further calculated as relative strain by the software. The Δx and Δy in Figure 5-3 is the displacement of the selected speckle in the x and y-directions respectively in terms of the pixels. The change in the selected speckles with respect to its original position, which is also calculated in terms of pixels, calculates the strain in the

marked square with respect to the selected speckle. The post-processing analysis in the current research was done using a commercial software called VIC-3D [13].

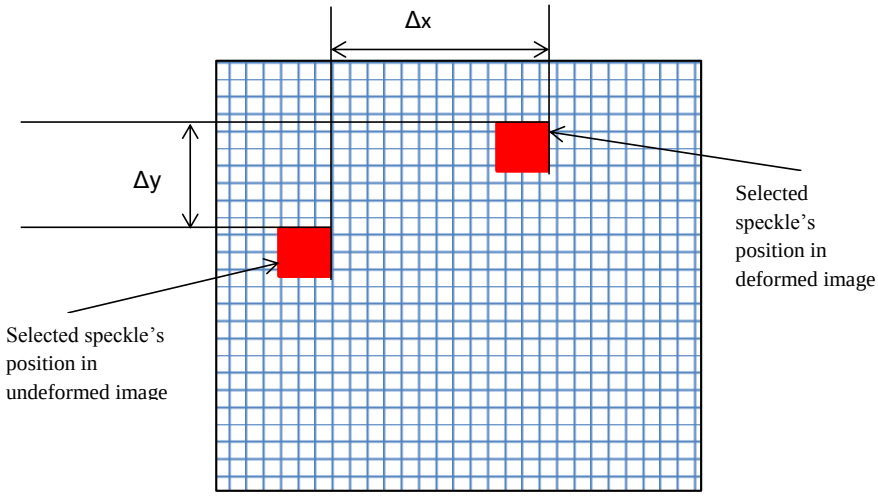

Figure 5-3. The movement of the selected speckle pattern between the undeformed image and the deformed image

To prepare the specimens for DIC, a speckle pattern was applied on the selected specimens' surface – white background with black speckled dots. The specimen is thereafter, loaded in the fatigue machine, and the source image is captured. The source image is the unloaded specimen with the initial saw-cut.

Thereafter, the load is applied and the test conducted for a pre-determined number of fatigue cycles. After the pre-determined number of cycles is achieved, the maximum load is applied on the specimen, and a new image is captured. This image is the deformed image. Then the test is conducted further to the pre-determined number of cycles and the deformed image thereafter, captured at the maximum applied load. This is repeated until the crack length (a-a_s) of 42.5mm is achieved. The collected set of deformed images is then correlated with the source images to calculate the relative strain according to the abovementioned principle.

5.5.c Shear Strain results

The DIC strain fields at the tip of the saw-cut for Glare2A at 0° off-axis, Glare3 under 45° off-axis and Glare2A under 45° off-axis loading, are presented in Figure 5-4. The plastic zone, indicated by the white areas in the three images was determined with $\varepsilon_{yy} > \varepsilon_{yield}$, where ε_{yield} was taken as the strain determined with the intersect between the stress-strain curve and the 0.2% offset of the linear part of the curve. Although this assumption incorrectly estimates the plastic zone, correlation between the three images was deemed sufficient to draw conclusions on the mode mix at the crack tip.

In Glare2A under in-axis loading, and Glare3 under 45° off-axis loading, the 'wing-angle' ($2\theta_w$) defined in Figure 5-5 [11], and the extension of the plastic zone at the crack tip (r_p) are similar. Rodi [10] showed that orthotropic fibre bridging influences the deformation field at the crack tip vicinity in FMLs. The 'butterfly wing-angle' obtained in Glare2A under in-axis loading and Glare3 under 45° off-axis loading are similar to Rodi's experimental result for Glare3 under in-axis loading [14]. These 'butterfly wing-angles' were accompanied with a crack observed to traverse straight without deflection. In Glare2A under 45° off-axis angle the 'butterfly wing-angle' is smaller, and it is accompanied with a deflected crack path.

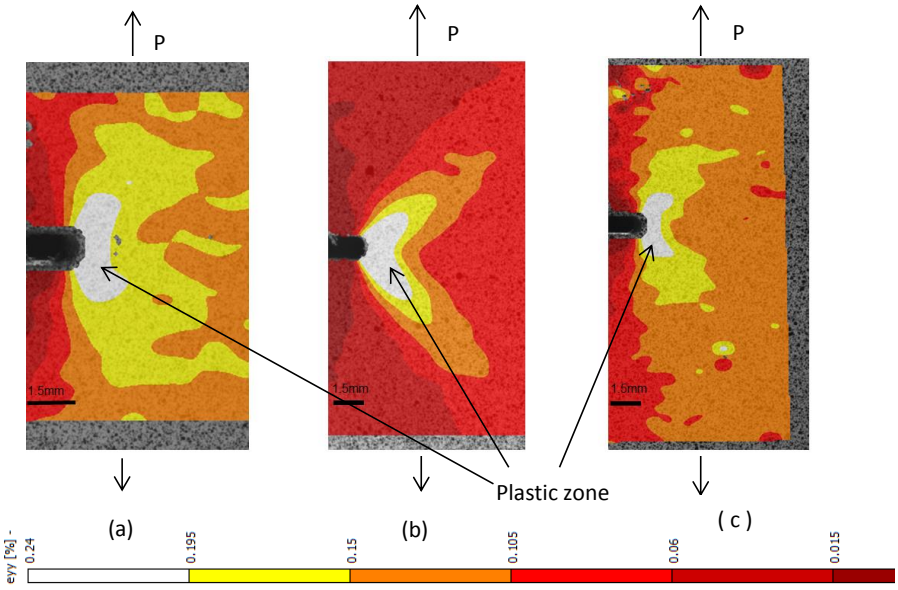

Figure 5-4. Strain fields at crack tip obtained by DIC technique in a) Glare2A-4/3-0.4 at 0° in-axis loading, b) Glare2A-4/3-0.4 at 45° off-axis loading and c) Glare3-4/3-0.4 at 45° off-axis loading.

Figure 5-5 shows a qualitative illustration for the strain field at the crack tip obtained from DIC. When the 'butterfly wing-angle' is narrower and the angles θ_I and θ_{II} are not equal the crack deflects from its straight path. Additionally, in Glare2A under 45° off-axis loading, it was observed that OA is not equal to OB. The complete strain field for both sides of the crack tip in Glare2A under 45° off-axis loading is shown in Figure 5-6. These observations in Figure 5-4 and Figure 5-6 are further discussed in the following sub-section.

5.5.d Discussion

The difference between Glare without crack path deflection, and Glare with deflected crack is related to the amount of fibre bridging and laminate orthotropy. For the specimens without crack path deflection, the strain fields extend in the longitudinal direction with an extremely wide 'butterfly wing-angle' such as different Glare grades under in-axis loading [11].

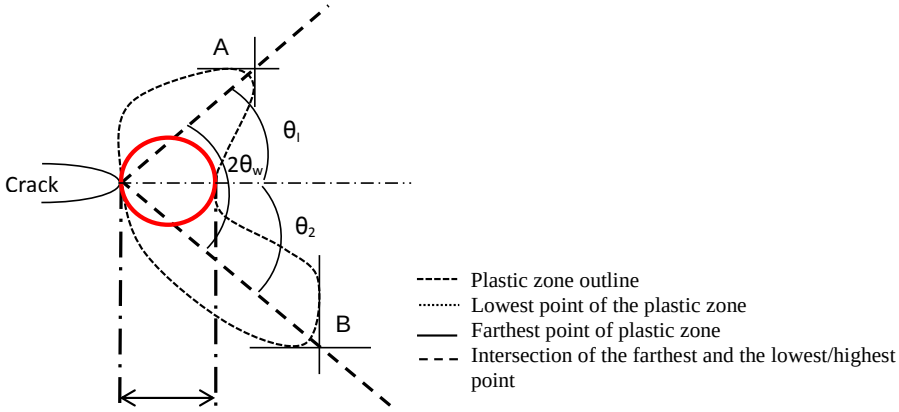

Figure 5-5. 'Butterfly wing-angle' and plastic-zone in the DIC image [4]

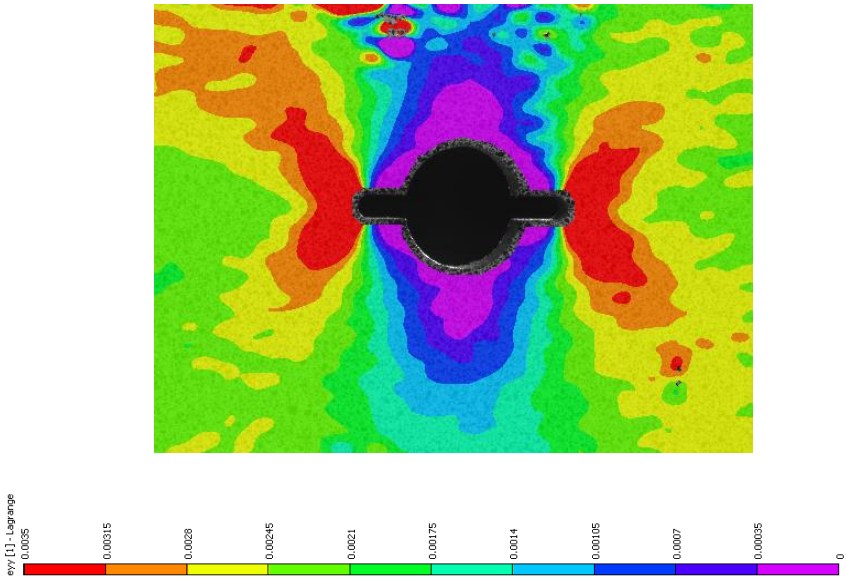

Figure 5-6. Strain field of Glare2A at 45° off-axis loading obtained from DIC

However, in Glare2A under 45° off-axis loading the deformation is affected by the orthotropic fibre bridging, and therefore, the 'wing-angle' is narrower. The difference is that in Glare2A under 45° off-axis fibres, there are 2 fibre layers at 45° with respect to the applied loading direction. This angular orientation of the fibre leads to transverse deformation in the specimen. Consequently, the 'butterfly wing-angle' is narrower. This is mainly due to the

following two mechanisms – clamping effect due to laminate orthotropy, and fibre-bridging component in shear.

The effect of laminate orthotropy and shear strain on the crack path can be explained from the following figures that show the variation of two quantities $\varsigma = \frac{\varepsilon_2}{\varepsilon_1}$ and $\kappa = \frac{\tau_{12}}{\varepsilon_1}$, – where ε_2 is transverse strain, ε_1 is longitudinal strain, and τ_{12} is shear strain – with respect to the off-axis angle as shown in Figure 5-7. The quantity ς shows the effect of laminate orthoropy on the transverse strain, and κ depicts the effect of laminate orthotropy on the shear strain.

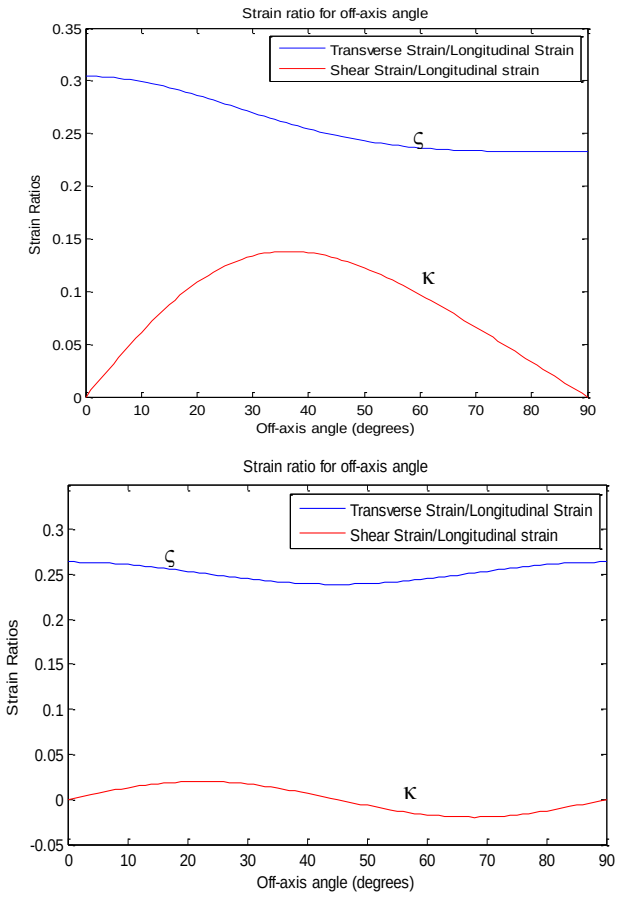

Figure 5-7. Strain ratios with respect to Off-axis angle for Glare 2 (top image) and Glare 3 (bottom image)

ς has a non-zero value for all values of the off-axis angle in both Glare2A and Glare3. A non-zero value for ς suggests the presence of the transverse strain in the laminates which is due to the laminate orthotropy. The non-zero values at Glare2A under in-axis loading where the crack paths do not deflect, and Glare3 at 45° off-axis angle suggests that the laminate orthotropy does not affect the crack path in FMLs alone. They affect the crack path behaviour in combination with a non-zero κ.

κ is non-zero in Glare2A between 0° and 90° of the off-axis angles. Besides the 0° and 90°, for Glare3, κ is zero at 45° off-axis angle also. When κ is zero, it can be noted that the crack traverses without deflection – Glare2A under in-axis loading, and Glare3 at 45° off-axis loading, but when it is non-zero – Glare2A under 45° off-axis loading – crack path traverses at an angle. Additionally, it was observed that in Glare3 under 22.5° off-axis loading, the crack path traverses at an angle when κ is non-zero.

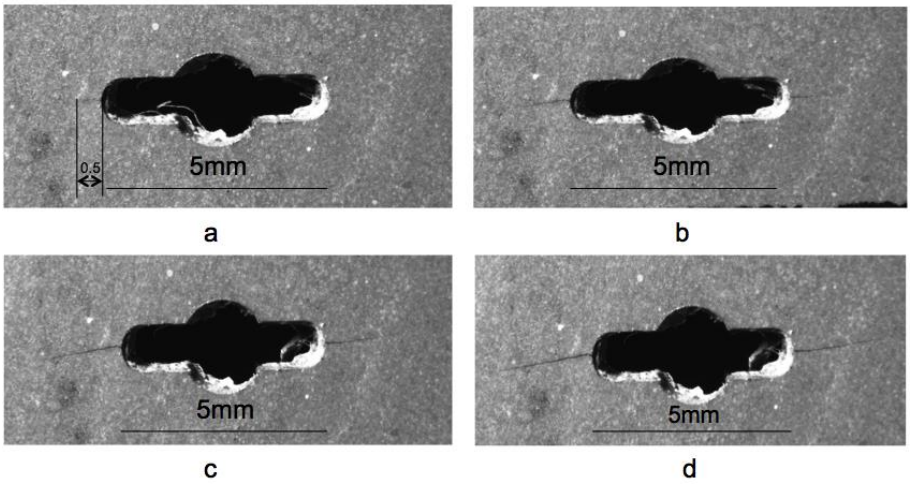

Figure 5-8. Crack propagation in Glare3-4/3-22.5° off-axis loading at various stages of fatigue loading - a) 19000 cycles, b) 20000 cycles, c) 30000 cycles and d) 40000 cycles.

Figure 5-8 shows the crack propagation sequence in Glare3 under 22.5° off-axis loading. It is observed that the crack traverses without deflection for a crack length ($a-a_s$) of 0.5mm before it deflects. This crack path is observed because the crack is initially only affected by the stress concentration factor [24, 30, 269]. The effect of stress concentration on crack paths is discussed in detail in Chapter 6. After the crack has propagated 0.5mm, the off-axis fibres bridge the crack in its wake thereby, affecting the strain field. The affected strain field induces mixed-mode deformation at the crack tip which causes the crack path to deflect.

This section presented the DIC test results and correlated their findings with the effect of ς and κ. It was found that the crack paths deflected when κ was non-zero. Therefore, it was concluded that the crack paths in FMLs under off-axis loading traversed at an angle only when shear stress was introduced in the laminate due to the imbalance in the fibre-bridging and laminate orthotropy. This is explained in detail later in the chapter.

5.6 Fatigue tests

The specimens listed in Table 5-2 were tested until the crack length ($a-a_s$) grew to a length of 42.5mm. The cracks were opened to their maximum fatigue loads, and a black line was marked on the specimen to sketch the extended crack path. The fracture angle was measured with this extended line using a protractor.

For confirmation, the fracture angles were re-measured between the rolling direction of aluminium and the above sketched line on the specimen because the off-axis fibres are at a pre-determined angle with the initial saw-cut. The angle measured with respect to the rolling direction of aluminium (Δ), off-axis angle and the fracture angle should be equal to 90°. However, due to errors these angles do not sum upto 90°.

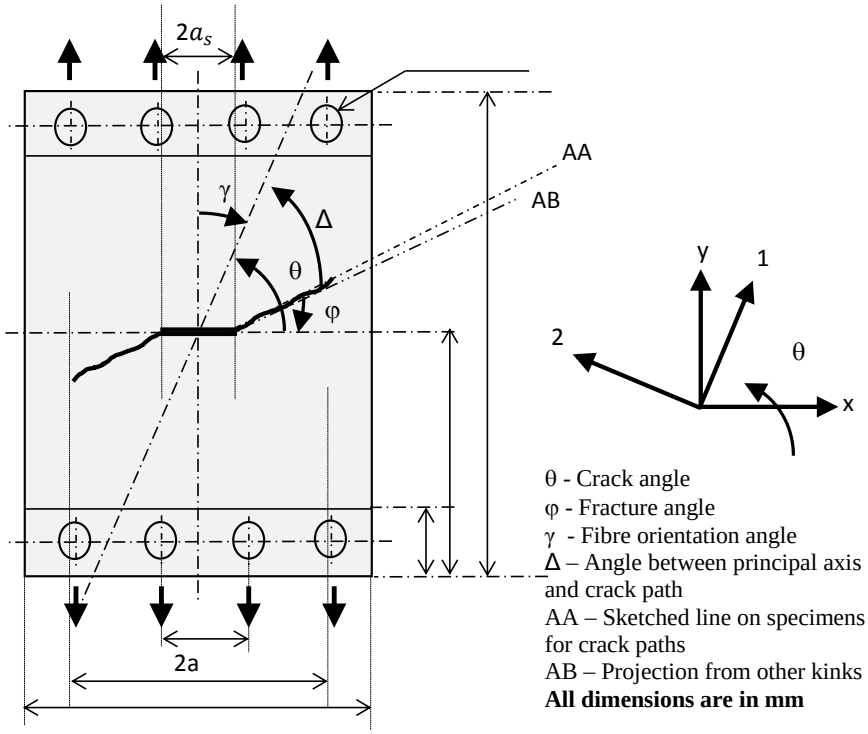

Figure 5-9. Fatigue Test results

The author recognizes two major sources of errors. First error arises due to the possibility that the fibres were not placed at the correct angles during the lay-up process for manufacturing. This is a manufacturing error. The second error arises from ignoring the angular kinks that arise from the waviness of the cracks. Crack waviness leads to a possibility of different projections of the crack path from the initial crack-tip which causes an error in accurate measurement of the fracture angle as shown in Figure 5-9.

These errors are represented by the error bars in the results shown in figures from Figure 5-10 to Figure 5-12. The results obtained from the fatigue tests are presented in Table 5-2. Figure 5-8 show the results for Glare3 , Figure 5-11 shows Glare4B results and Figure 5-12 shows the images for Glare2A results In Glare2A under 50° off-axis loading, the initial curve deflected to an angle of 22° and continues at that path for approximately 25000 cycles. This deflection is significant compared to the biaxial grades of Glare.

Table 5-2. Fatigue test results

Specimen	Crack angle (°) (γ)	S_{max} (MPa)	Stress ratio	No. of cycles (*1000)	Fracture angle (°) (φ)	Crack path with respect to principal axis (°) (Δ)	Fracture angle calculated from principal axis measurement (°) (Δ - θ)
Glare2A-4/3-0.4	0	100	0.05	100	0	90	0
	20	100	0.05	100	13	5	15
	22.5	100	0.05	100	19	4	18.5
	45	100	0.05	100	23	20	25
	60	100	0.05	80	15	43	17
	67.5	100	0.05	100	12	57	10.5
Glare3-4/3-0.4	0	100	0.05	100	0	90	0
	22.5	100	0.05	100	6	27	4.5
	35	100	0.05	100	3	50	5
	45	100	0.05	140	0	45	0
	55	100	0.05	100	-3	51	-4
	67.5	100	0.05	100	-6	60	-7.5
Glare4B-4/3-0.4	0	100	0.5	100	0	0	0
	22.5	100	0.05	120	14	8	14.5
	45	100	0.05	80	6	37	8
	55	100	0.05	80	0	57	2
	65	100	0.05	100	-2	62	3
	67.5	100	0.05	100	-3	65	2.5

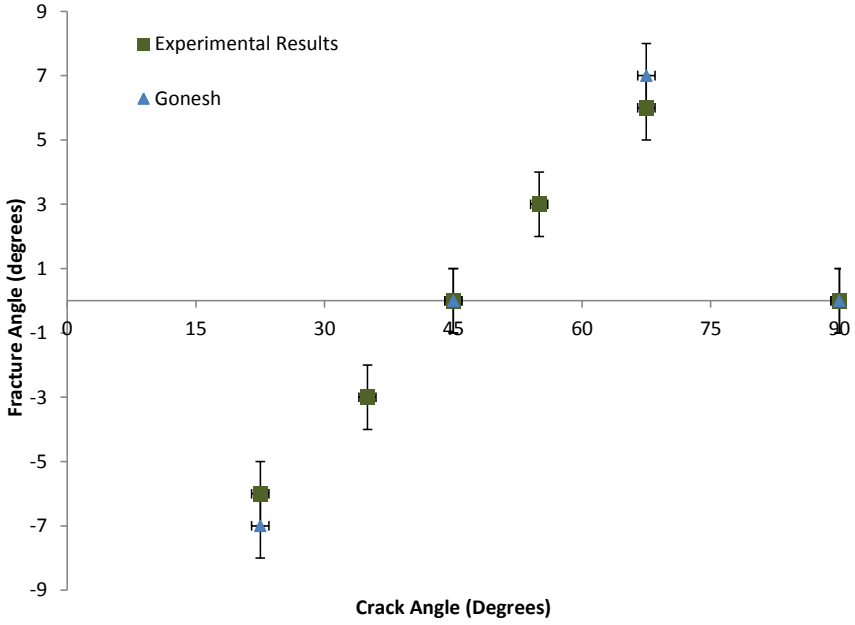

Figure 5-10. Crack propagation and fracture angle as measured with the specimen in the machine for Glare3 and compared with Gonesh [6, 7]

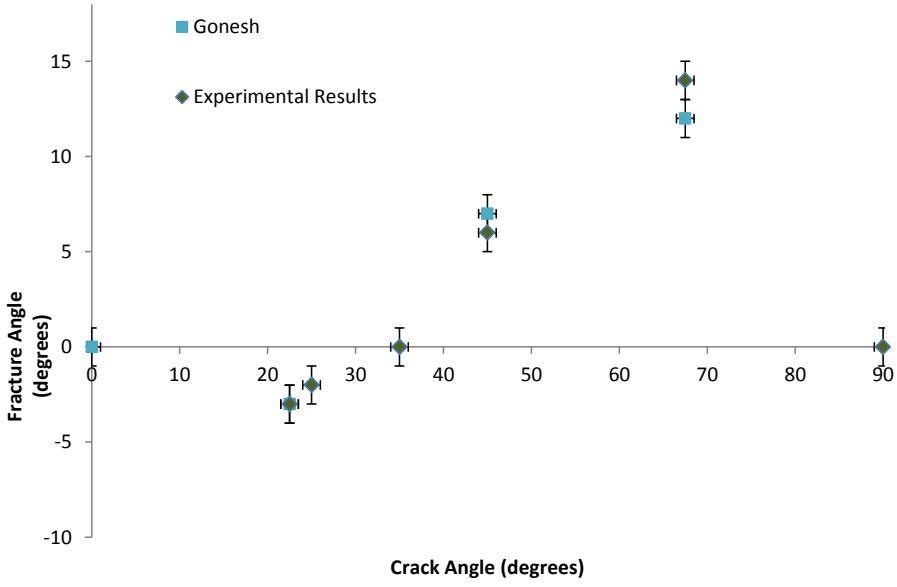

Figure 5-11. Crack propagation and fracture angle as measured with the specimen in the machine for Glare4B and compared with Gonesh [6, 7]

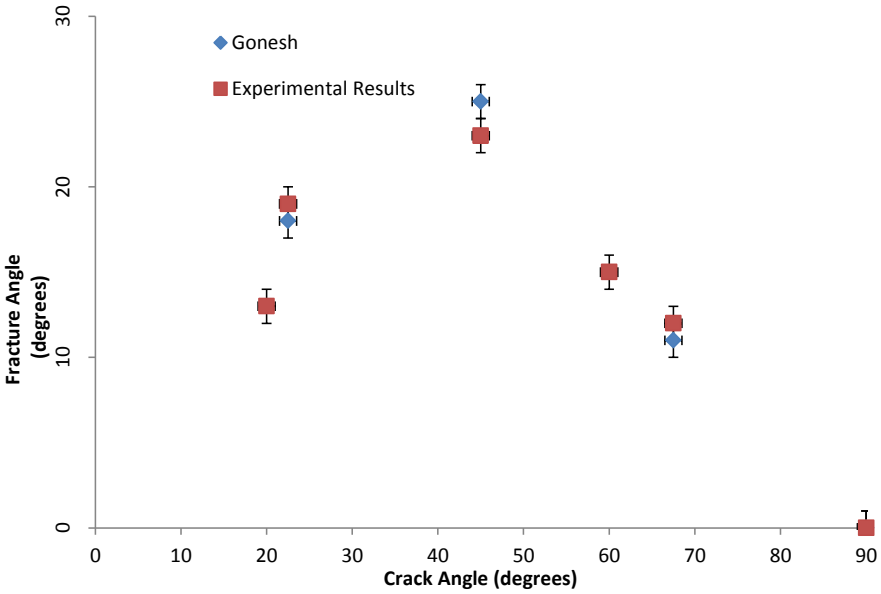

Figure 5-12. Crack propagation and fracture angle as measured with the specimen in the machine for Glare2A and compared with Gonesh [6, 7]

5.7 Discussion

The results from fatigue tests were discussed in more detail in [265]. A concise summary for the results is presented below.

5.7.a Fracture angle in Glare3

Glare3 at an arbitrary off-axis angle (γ) is illustrated in Figure 5-13. Consider Glare3 in Figure 5-13 at 22.5° off-axis angle, i.e. a fibre layer at 22.5° angle with respect to loading, and another layer perpendicular to this. These layers bear a certain portion of the vertical load and bridge the crack in the vertical direction. The deformation of the fibres along the off-axis angle introduces a transverse component of loading at the crack tip in the metals and these transverse components are not balanced at 22.5°. This induces a Mode II component at the crack tip, and thus the crack begins to incline depending on the mixed-mode loading at the crack tip.

In Glare3 at 22.5° and 67.5° as explained by the equation in Figure 5-10, the fracture angles have the same magnitude, but extend in opposite directions with respect to the crack plane. They extend in opposite direction of the crack plane because the fibres are rotated by the same amount about the loading axis. Now, consider Figure 5-13 for 45° off-axis angle in Glare3. The crack propagation angle of 0° implies there is a Mode I component acting on the crack. The off-axis deformation is zero because of the balanced fibres at 45° that results in zero Mode II acting at the crack tip.

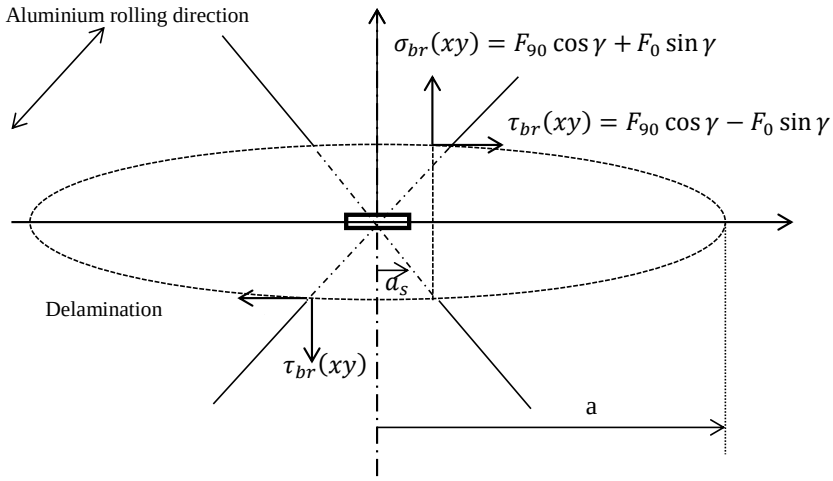

Figure 5-13. Effect of off-axis fibres on crack path in Glare-3

5.7.b Fracture angle in Glare4B

The illustration of Glare4B at an off-axis angle is given in Figure 5-14. Consider Figure 5-14 for 45° off-axis angle in Glare4B. The crack propagates at an angle compared to Glare3 at 45° off-axis angle where the crack propagates without deflection. This occurs due to an unequal number of fibre layers in the two directions, which results in an unbalanced laminate orthotropy. Consequently, a Mode II component at the crack tip in the metal exists resulting in mixed-mode loading at the crack tip. Hence, the crack propagates at a slight angle to the transverse direction compared to Glare3.

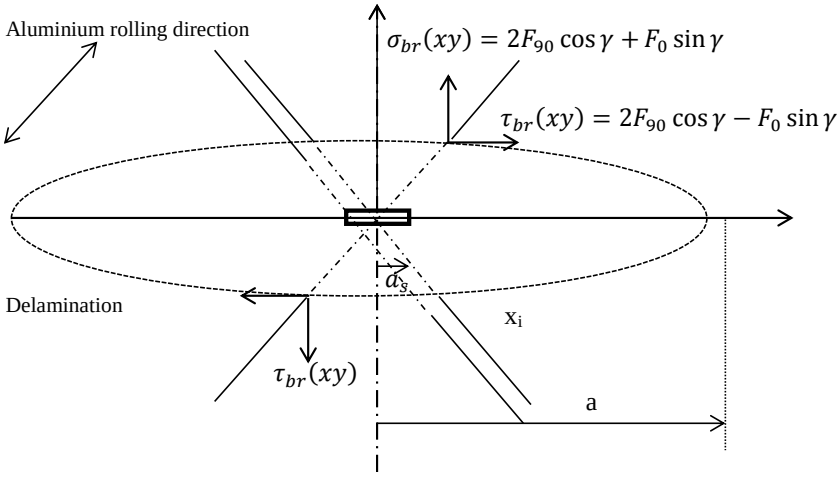

Figure 5-14. Effect of off-axis fibres on crack path in Glare-4B

For Glare4B at 22.5° and 67.5° off-axis angle the fracture angles have opposite signs similar to the results in Glare3. This is due to the symmetry of the unbalanced laminate orthotropy with respect to the transverse axis. However, the magnitudes of the fracture angles are unequal in Glare4B. The magnitudes of the fracture angles are different because the change in unbalanced laminate orthotropy affects the mixed-mode differently. At 22.5° off-axis angle there are two fibre layers closer to the transverse axis which increases the shear stiffness of the laminate. Hence, the shear strain is higher, and consequently, the fracture angle at 22.5° is higher in magnitude compared to the 67.5° off-axis angle which only has one layer closer to the transverse axis.

5.7.c Fracture angle in Glare2A

Glare2A at an general off-axis angle is illustrated in Figure 5-15. Consider Glare2A at 22.5° off-axis angle, there are two layers of fibres at 22.5° angle with respect to loading but no layer is perpendicular to these. These layers bear a certain portion of the longitudinal load and bridge the crack in the longitudinal direction. The deformation of the fibres along the off-axis angle also introduces a transverse component of loading at the crack tip in the metals. This component is not balanced by any perpendicular layers as is the case in bidirectional Glare grades as shown in Figure 5-15. Hence, the component of mode II induced is higher that leads to higher fracture angles in unidirectional Glare grade compared to bidirectional Glare grades.

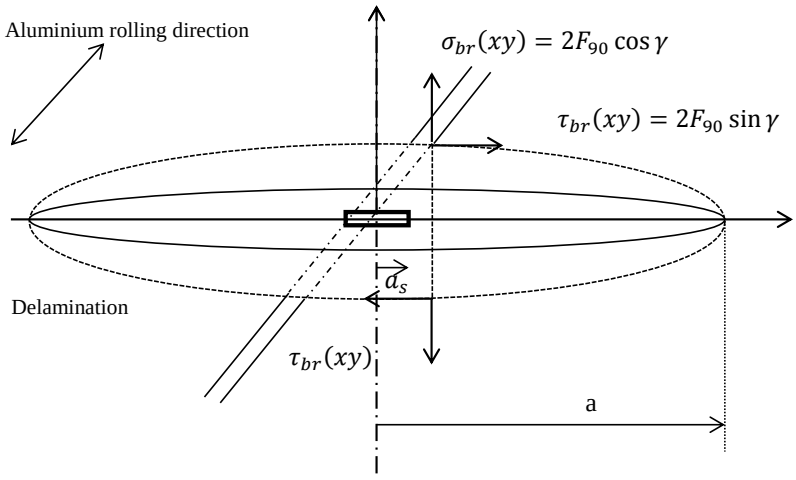

Figure 5-15. Effect of off-axis fibres on crack path in Glare-2A

5.8 Conclusions

In summary, cracks in off-axis loaded FMLs deflect due to mixed-mode effects induced at the crack tip by the fibre bridging mechanism and laminate orthotropy as discussed in Section 5.5.*d*. The laminate is initially under tensile loading and off-axis fibres induce a shear load to provide equilibrium. However, it is observed that the crack deflects only after it has propagated in the transverse direction for a certain length (Figure 5-8). Crack deflection

occurs because of fibre bridging at the crack tip in two directions also. Therefore, it is postulated that the crack path in FMLs can be better understood by applying the mixed-mode approach at the crack tip along with the laminate orthotropy.

6 Chapter 6: Predicting crack path orientations in FMLs under off-axis fatigue loading

6.1 Introduction

In the experiments presented in Chapter 5, shear deformation was observed in the vicinity of the crack tip. This shear deformation was attributed to fibre-bridging in the off-axis direction and to the imbalance in laminate orthotropy with respect to the applied loading direction. The induced shear strain at the crack tip introduces a mixed-mode effect causing the crack path in Fibre Metal Laminates (FMLs) to deflect under off-axis loading.

The objective of this chapter is to present the analytical model for predicting the crack path in FMLs under off-axis fatigue loading. It discusses the developed analytical model, which is an extension of the mixed-mode crack path theory for metals to FMLs, in combination with existing fatigue crack growth models for FMLs [2, 17].

Hence, the chapter begins with a discussion of the existing in-axis fatigue models for FMLs followed by a summary of the assumptions for Linear Elastic Fracture Mechanics (LEFM). Initially, the effect of laminate orthotropy on crack paths is discussed, and thereafter, the chapter discusses the method to calculate the fibre-bridging component in the longitudinal and transverse direction. Subsequently, the fracture angle in terms of the FML's mixed-mode parameter is derived, combining the influence of laminate orthotropy and fibre-bridging on the crack paths. Finally, the crack path orientations predicted with the analytical model for various off-axis angles are presented and compared with experimental results.

6.2 Fatigue models for in-axis loading of FMLs

Intensive research has been undertaken in the previous years to understand the fatigue mechanisms in FMLs. Marissen [1] introduced the concept of fibre bridging to explain the reduced crack growth rates of Mode I cracks propagating in metal layers of ARALL. Alderliesten [2] developed a closed form analytical solution to predict crack propagation and delamination growth in the wake of the propagating cracks. He reduced the damage problem to a crack in the metallic layer with the fibre bridging contribution to that particular layer. Alderliesten's model [2] was further developed towards arbitrary FML configurations and different load cases by Wilson [3, 16]. An overview of these models is provided hereafter.

6.2.a Marissen's model [1]

Marissen [1] assumed that the bridging load is distributed equally along the delamination boundary. He observed that when delaminations were large the crack growth became faster. The faster crack growth occurs because larger delaminations are accompanied with lower bridging stresses, reducing the bridging effect on the crack tip Stress intensity factor (SIF). On the contrary, when the delaminations are small, the bridging stresses are high, which reduces the SIFs at the crack tip retarding crack growth. Marissen [1] called this interaction between the delamination and crack growth the 'self-balancing nature of delamination'.

Marissen [1] assumed an elliptical shape for the delamination shape. An elliptical delamination shape implies that bridging stresses are constant along the crack length. This was later corrected by Guo and Wu [27, 270] and Alderliesten [2] because they found through experiments that the bridging stresses do not remain constant. Their analytical models revealed that the bridging stress distribution peaked near the crack tip. This peak was highly

dependent on the exact delamination shape at that location and this peak affected the SIF significantly.

6.2.b Alderliesten's model [2]

Alderliesten [2] used deformation compatibility between the fibre and metal layers at the delamination edge to develop the equations required for crack opening and bridging load. He developed his analytical model using an iterative framework, because the effective crack opening depends on the bridging stress. He developed an integral to calculate the bridging stress and approximated it using the numerical solution. The obtained *H*-matrix cannot be calculated using a closed-loop equation, hence, he inversed the *H*-matrix. In his iterative method, Alderliesten [2] calculated the crack opening superimposing

- Crack opening due to the stress in metal layers from the far-field load.
- Crack opening due to the bridging stress. Algebraically, this opening effect is subtracted from the overall crack opening, because bridging stress effectively reduces the stress at the crack tip which is equivalent to closing the crack.

Alderliesten [2] calculated the bridging stress at discrete points along the continuous delamination contour. To calculate these points, he discretized the crack length into two-dimensional bar elements. The element's width represented the crack increment in the transverse direction, while their length approximated the delamination length. The width of these bridging elements depend on the initial crack length and the initial number of elements. In the model, the crack length increment was taken equivalent to the width of a single bar element. The bridging stresses are calculated at the mid-point of the bridging elements at their maximum length using the matrices derived from the inverse of the integral.

An initial delamination was assumed to start the iteration. The model thereafter calculates the propagating crack length and the corresponding delamination geometry. The calculated crack length is used to estimate the SIF that arises due to the stress in the metal layers from the far-field load. The fibre bridging stress is used to calculate the SIF due to fibre bridging. These two SIFs are superimposed in a linear manner to calculate the effective SIF for the crack opening which is used to estimate the crack growth in FMLs under in-axis loading.

For Glare, Alderliesten [2] attributed the fibre shear deformation to the entire fibre layer, because the resin rich layer in Glare is thin as compared to ARALL. At zero delamination length, Alderliesten [2] hypothesized that no crack opening due to prepreg shear deformation is possible which adheres to the assumption that the fibres are uniformly distributed over the entire fibre layer. He further demonstrated that after a certain delamination length is reached the magnitude of prepreg shear deformation becomes independent of the delamination length.

6.2.c Method of Guo and Wu [27, 270]

Alderliesten derived his model from Guo and Wu's model [27, 270]. The difference in the two models lies in the principle of calculating the crack opening in the metal. Guo and Wu [27] used Green's functions to calculate the crack opening, while Alderliesten [2] utilized the approximated opening function. Guo and Wu [27, 270] used the entire FML stiffness to

calculate the metal crack opening. This is incorrect because the crack opening is affected only by the metal stiffness.

6.2.d Wilson's model [17]

Wilson [17] extended Alderliesten's crack growth model for application to the individual metal layers in FMLs. He used the intersection of the centre line of the bridging element and the delamination contour as the point for bridging stress similar to Alderliesten. However, Wilson used the second order Chebyshev polynomial in the model to interpolate the bridging stress between two elements. The use of second-order Chebyshev polynomial's allowed Wilson to distribute bridging elements of different widths over the crack length. At the crack tip, there are relatively more and smaller bridging elements compared to the vicinity of the starter notch. Consequently, Wilson's method improved the accuracy of Alderliesten's model compared to the experimental results [16, 17]. He further developed the model to also understand the effect of multiple thicknesses, multiple crack lengths, and multiple alloys within the FML, and the effects of bending.

The current research investigated symmetric lay-ups of Glare specimens and therefore, ignored bending effects. Besides, all tested specimens had equal crack lengths in all metal layers. Therefore, Alderliesten's simpler model was used instead of Wilson's more accurate model [3] to create the crack path prediction model using the mixed-mode theory [19].

6.3 Approach to developing the analytical model

The two major fracture mechanisms in FMLs under fatigue loading are cracks in metal layers and delamination at the interface between metal and fibre layers. To address crack path directionality, it is necessary to understand the following aspects subject to this research.

6.3.a Linear Elastic Fracture Mechanics

LEFM originated from Griffith's experiments [39] and was extended by Irwin [37, 38, 40]. It is a simple, linear theory that deals with crack growth and damage in elastic bodies for which the following conditions are satisfied:

- Structure obeys Hooke's law of deformation
- Global deformation of the material is linear
- Small scale plasticity exists at the crack tip

The theory assumes that the material deforms elastically everywhere except for a very small region at the crack tip where the stresses are really high. These high stresses are likely to introduce a certain amount of inelasticity in this region which remains confined within this region while deformations outside this zone are entirely elastic in nature. Under LEFM it is assumed that these elastic stresses can be used to estimate the inelastic fracture process at the crack tip. To satisfy this assumption, the inelastic zone must be significantly smaller relative to the elastically deformed zone of the body. To achieve this condition of Small Scale Yielding (SSY), the loads applied must be sufficiently low so that the plastically deformed zone is confined to the crack tip vicinity in comparison to the physical dimensions of the specimen. Under fatigue loading in monolithic metals, the low crack growth rate implies that loads applied are low in magnitude. Due to the fibre bridging of the crack in the metal layers,

the crack growth rate in FMLs is even lower than in monolithic metals. Therefore, it is assumed that FMLs satisfy the SSY criterion for LEFM under fatigue loading. Hence, the model in this research was developed using the LEFM approach.

6.3.b Strain energy release rate or Stress intensity factor

Crack deflection usually occurs due to the presence of shear at the crack tip. In FMLs under off-axis loading, the fibres are aligned at an angle with respect to the loading direction. Such angular orientation of fibres introduces shear into the laminate when the specimen is clamped and then loaded. This causes the resultant laminate orthotropy to become unbalanced with respect to the loading axis which introduces shear into the laminate.

The fibre orientation also causes a transverse component of bridging stress into the laminate. This transverse component of bridging stresses also produces shear at the crack tip. The total shear produced due to the laminate orthotropy and the fibre-bridging components in combination with the applied load produces a mixed-mode effect at the crack tip. This mixed-mode effect causes the crack to deflect. Hence, to evaluate the crack path, an appropriate mixed-mode theory must be used.

The selected mixed-mode theory [18, 263] for assessing crack path orientations in FMLs under off-axis loading can be applied with both the Strain Energy Release Rate (G) and the SIF because they provide the same information of the fracture process. They are both equated using equation $G = \frac{K_I^2}{E}$ for plane stress, and $G = \frac{(1-\vartheta^2)K_I^2}{E}$ for plane strain as discussed in Chapter 3.

The SIF describes the stress field singularity at the crack tip to calculate the crack growth. For the cracks in the metal layers of FMLs, it is convenient to use SIF because it allows for linear superposition. Linear superposition implies that the SIF due to far-field and bridging are added algebraically to obtain the effective SIF at the crack tip locally. However, at an interface between dissimilar materials, it is mathematically difficult [1-3] to calculate SIF because of the non-uniform stress field. The non-uniform stress field applies to the delamination between metal and fibre layers in FMLs. Hence, it is more convenient to calculate G between dissimilar materials. Therefore, to calculate the crack growth in metals K is used and G is used to calculate the delamination between the metal and fibre layers.

6.3.c Effect of delamination on the crack orientation

In the experimental results it was observed that the crack path initially traversed perpendicular to the loading direction, and then deflected at an angle. Thereafter, it traversed along the same angle. The accompanying delamination also traversed similarly, i.e. delamination shape and orientation remains constant after the initial deflection of the crack. The constant shape of the delamination with the traversing crack shows that an equilibrium exists between the crack path and the delamination shape after the initial deflection.

Erdogan and Sih's [18, 19] postulated that crack paths traverse perpendicular to the plane of maximum tension. Considering Erdogan and Sih's postulation and the constant delamination shape along the traversing crack, it can be concluded that delamination does not affect the

crack path after the initial deflection. Hence, the developed analytical model assumes delamination effects to be negligible on the crack path after the initial deflection with the exception of stiffened FML panels. The crack paths in stiffened panels is discussed in the following chapter.

Under pure opening mode I (K_{eff_I}), there is only one direction of maximum stress. However, in reality pure mode I loading rarely exists and therefore, it is necessary to first find the plane of maximum stress. Erdogan and Sih [19] developed the mixed-mode theory to find the plane of maximum tension which uses the following relation between the SIF in the opening mode (K_{eff_I}) and SIF in the shear mode (K_{eff_II}) to calculate the fracture angle.

$$\cos\frac{\varphi}{2}\left[K_{eff\_I}\sin\varphi + K_{eff\_II}(3\cos\varphi - 1)\right] = 0 \qquad \textbf{6-1}$$

Where φ is the fracture angle. In the experiments presented in Chapter 5, it was observed that the crack initiates in a transverse direction and then deflects. Initially, the stress concentration dominates the crack propagation followed by the effect of clamping and transverse fibre bridging effect. Stress concentration at the notch tips in FMLs under off-axis loading was determined by Homan [24]. Later Spronk *et al.* [30] used Lekhnitskii's anisotropic formulation [31] to determine the influence of stress concentration on crack initiation direction in FMLs under off-axis loading. They showed that the stress concentration only influences the crack initiation direction upto a certain D/W ratio – where D is the initial notch diameter, and W is the specimen width.

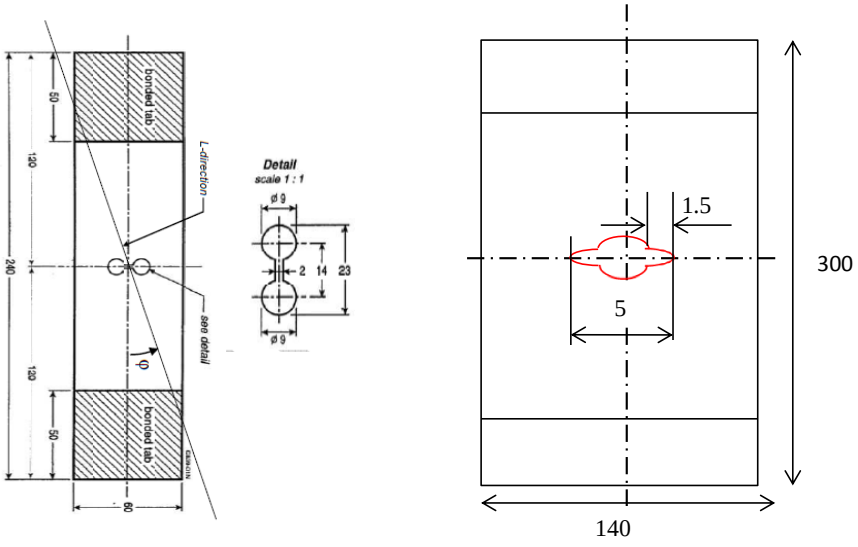

Figure 6-1. Image (a) shows the specifications for the NLR specimen [271]and image (b) shows the specimens tested during this research

In FMLs with low D/W under off-axis loading, the stress concentration does not lie along the transverse axis, and therefore, the crack paths initiate at the deflected angle from the

beginning. However, as the D/W ratio reduces, the influence of the stress concentration reduces on the crack initiation [30]. This is evident from the fact that the crack paths initiate at a deflected angle in NLR specimens (Figure 6-1) which have a high D/W ratio compared to Gonesh's specimens [6, 7] and the specimens tested during this research. Consequently, the mixed-mode changes at the crack tip and the crack path deflects as observed in the experiments and the experimental results presented in Chapter 5.

6.3.d Averaged fibre bridging over the entire laminate

FMLs can have different lay-ups depending on the number of metal and fibre layers, as mentioned in Chapter 2. The developed analytical model used Alderliesten's principle of averaged fibre bridging over the layers. A crack is described in a single layer, and the bridging to the crack is considered as the effective bridging for that particular layer. For the laminate, the bridging contribution is averaged by dividing the total bridging effect of all the fibre layers with the number of metal layers.

6.4 Analytical model for SIFs of FMLs under off-axis loading

The analytical model is developed with the mixed-mode theory to predict the crack path orientation. Initially, the effect of unbalanced orthotropy with respect to the loading direction is discussed followed by the effect of off-axis fibre bridging. The Alderliesten model [2] is applied to calculate the longitudinal component of the off-axis fibre bridging, which is subsequently modified to calculate the transverse fibre-bridging stress in a similar manner. Thereafter, the effective SIFs in the two directions are calculated. Finally, the mixed-mode ratio is calculated and the crack path angles are predicted from these ratios for different Glare grades.

In FMLs under in-axis loading, the effective longitudinal SIF depends on two types of stresses – the far-field applied stress and the bridging stress. Under off-axis loading, there exists transverse applied loading additionally to the longitudinal load due to the clamping effect. The orientation of the fibres further induce two components of bridging – longitudinal and transverse bridging stress. Therefore, under off-axis loading the effective SIFs in the longitudinal and transverse directions depend on the far-field applied stress, the fibre bridging components similar to in-axis loading, and the clamping effect.

Under off-axis loading the laminate orthotropy is unbalanced with respect to the applied uni-axial loading with the exception of Glare3 under 45° off-axis loading and Glare4B at an angle of approximately 35°. The resultant unbalanced orthotropy induces a lateral reaction force in the laminate induced by clamping that produces shear in the specimen. This unbalanced orthotropy of the laminate creates a transverse loading on the laminate in addition to the longitudinal far-field applied loading. The applied loading on the specimen with respect to the off-axis fibres and the methodology to dissect the problem is illustrated in Figure 6-2.

In other words, first the SIFs for the opening and shear mode are calculated for both the problems. Subsequently, the SIF for the opening mode in the two problems are linearly superimposed and similarly the shear mode stress intensity factors are superimposed. The

mixed-mode for the entire problem is calculated from these effective SIFs. Finally, the fracture angle is calculated from this obtained mixed-mode ratio.

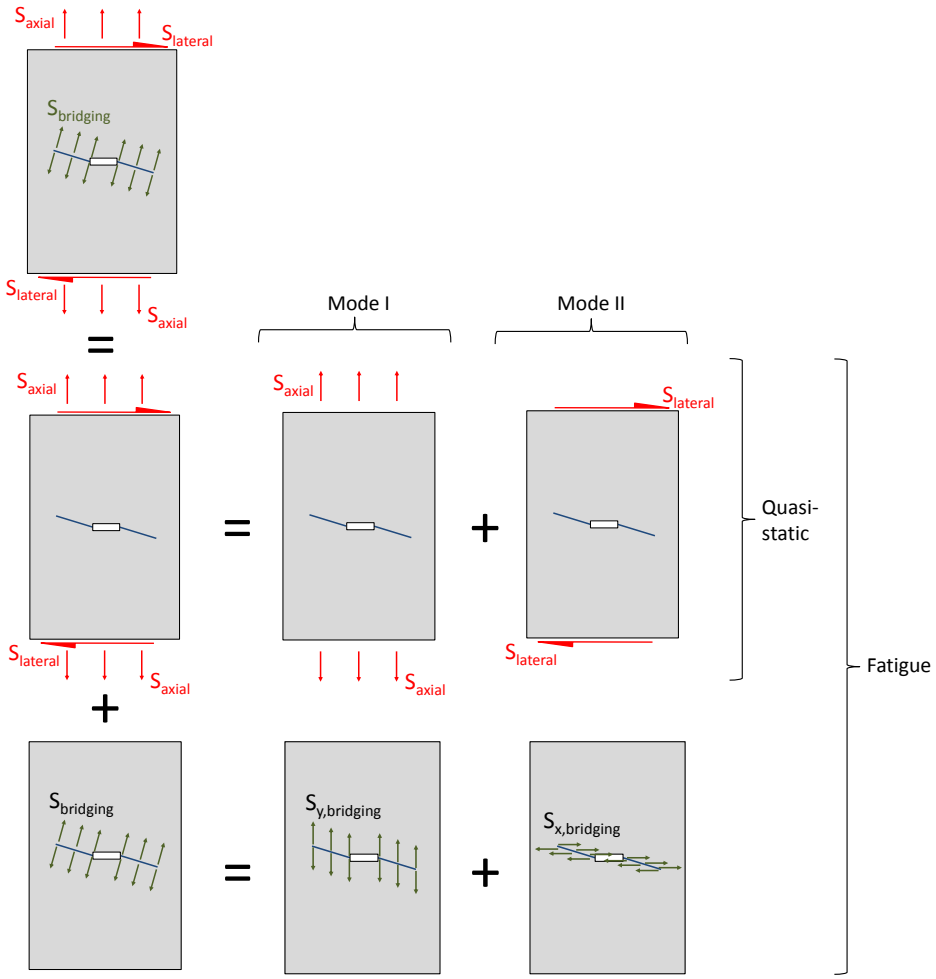

Figure 6-2. Concept illustrating the dissection of individual cases using superposition principles for SIF

6.4.a Shear coupling with laminate orthotropy

When the off-axis fibres are not symmetric with respect to the loading axis, they cause an imbalance in the laminate orthotropy. This causes shear to be introduced into the laminate. This was explained by Herakovich [272] who states that orthotropic materials exhibit normal-shear coupling effects when the material is loaded in directions other than the principal material coordinates. This means that effectively, not only an axial load is applied to the specimen, but that with clamping also a transverse load is applied.

Herakovich further introduced two 'coefficients of mutual influence' to calculate this shear stress using the material properties. The first coefficient is used to calculate the effectively applied normal stress from the applied shear load, and the second coefficient is used to

calculate the shear applied by application of a longitudinal load. Using the Classical Laminate Theory (CLT), he derived the following expression for the coefficient of mutual influence of the second kind (the coefficient relevant to our application):

$$\eta_{xy,x} = \frac{nm\left[m^2\left(2+2\nu_{12}-\frac{E_1}{G_{12}}\right)+n^2\left(-2\frac{E_1}{E_2}-2\nu_{12}+\frac{E_1}{G_{12}}\right)\right]}{\left[m^4+m^2n^2\left(-2\nu_{12}+\frac{E_1}{G_{12}}\right)+n^4\frac{E_1}{E_2}\right]} \quad \textbf{6-2}$$

where n is the cos(α), m is the sin(α) - (α is the fibre orientation angle), nu is the Poisson's ratio, E is the Young's modulus, and G is the shear modulus of the material. The various angles are defined in Figure 6-3.

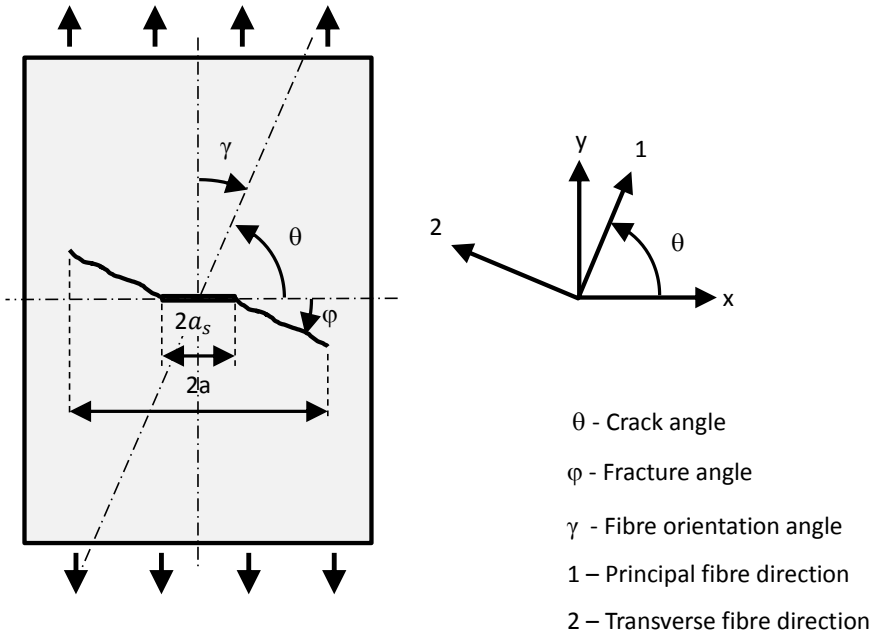

Figure 6-3. Schematics of the various angles used in the analytical model

In the current research, a more elaborate but mathematically simpler approach is used to incorporate this coupling effect. This is illustrated in Figure 6-4 on the following page, where S is the compliance matrix, σ_∞ is the far-field load, C is the stiffness matrix and ε is the strain. Assuming an applied load P, the shear strain in the entire laminate is calculated using the CLT with the following equation:

$$\begin{bmatrix}\varepsilon_{11}\\ \varepsilon_{22}\\ \varepsilon_{12}\end{bmatrix} = S\begin{bmatrix}\sigma_\infty\\ 0\\ 0\end{bmatrix}$$

The obtained shear strain component in the strain vector is caused by the laminate orthotropy. To eliminate the effect of clamping, the equivalent stress (τ_{orth}) that causes the non-longitudinal strain in the strain vector is calculated with:

$$\begin{bmatrix} 0 \\ 0 \\ \tau_{orth} \end{bmatrix} = C \begin{bmatrix} 0 \\ 0 \\ \varepsilon_{12} \end{bmatrix}$$

The correct stress applied to the laminate is the summation of the far-field stress σ_∞ and the equivalent stress that causes the transverse load due to clamping τ_{orth}.

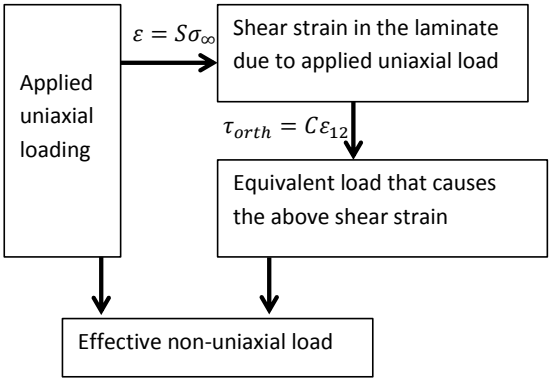

Figure 6-4. Calculating the real load in the laminate

The SIFs in the metal layers in the longitudinal direction (K_{m_I}) and the transverse direction (K_{m_II}) due to the far-field load can be calculated using the following equations:

$$\boldsymbol{K_{m\_I} = \sigma_{\infty\_I}\sqrt{\pi a}} \qquad \textbf{6-3}$$

$$\boldsymbol{K_{m\_II} = \tau_{\infty\_II}\sqrt{\pi a}} \qquad \textbf{6-4}$$

Where σ_{∞_I} and τ_{∞_II} are the longitudinal and shear stress obtained after the real stress has been calculated as shown in Figure 6-4.

6.4.b Off-axis fibre bridging

The effective crack opening in FMLs is the summation of the crack opening due to applied loads and crack opening due to fibre bridging. Under off-axis loading, both crack openings – far-field and fibre bridging – have their longitudinal and transverse components. The effective crack opening in FMLs under off-axis loading is therefore, expressed as shown in equation 6-5 and is illustrated in Figure 6-5,

$$\boldsymbol{\vartheta_{xy}(x) = \vartheta_{xy\_\infty}(x) - \vartheta_{xy_{br}}(x)} \qquad \textbf{6-5}$$

where $\vartheta_{xy}(x)$ is the effective crack opening, $\vartheta_{xy\_\infty}(x)$ is the crack opening due to the far-field applied load, and $\vartheta_{xy_{br}}(x)$ due to the bridging effect from the off-axis fibres.The direction for the crack bridging is different from Alderliesten's model [2], due to the different fibre orientation. To compute the fibre bridging correctly, it is resolved into two components - longitudinal and transverse component. The longitudinal component is calculated using Alderliesten's model [2] which is summarized first.

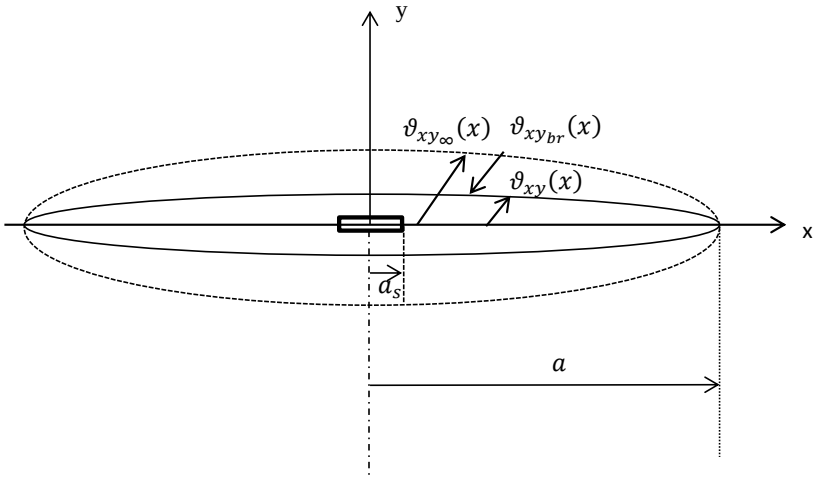

Figure 6-5. Definition of an arbitrary crack under off-axis loading

Longitudinal component of fibre bridging

The current model uses the reduced longitudinal stiffness properties – due to the off-axis directions – to calculate the longitudinal component of fibre bridging. The reduced stiffness was calculated using CLT. Alderliesten [2] applied compatibility of displacements in the metal and fibre layers at the delamination boundary. He assumed that the displacement at the delamination boundary is nearly equivalent to the crack opening. This crack opening is a resultant of the far-field opening and the longitudinal component of fibre-bridging. He developed the following equation to express this compatibility for the in-axis loading.

$$\boldsymbol{\vartheta_{br_\infty}(x) - \vartheta_{br}(x) = \delta_f(x) + \delta_{pp}(x)} \qquad \textbf{6-6}$$

where, $\vartheta_{br_\infty}(x)$is the crack opening at x, $\boldsymbol{\vartheta_{br}(x)}$ is the crack opening due to the fibre bridging in the longitudinal direction, $\boldsymbol{\delta_f(x)}$ is the fibre elongation in the longitudinal direction, and $\boldsymbol{\delta_{pp}}$ is the prepreg shear deformation. The longitudinal crack opening due to the far-field applied stress is calculated with [41],

$$\boldsymbol{\vartheta_\infty(x) = 2\frac{\sigma_\infty}{E_{al}}\sqrt{a^2 - x^2}} \qquad \textbf{6-7}$$

Where σ_∞ is the far-field stress in the aluminium layer in the longitudinal direction calculated using CLT, E_{al} is the Young's modulus of aluminium, a is the half crack length and x is the location in the crack wake in the transverse direction in Figure 6-6.

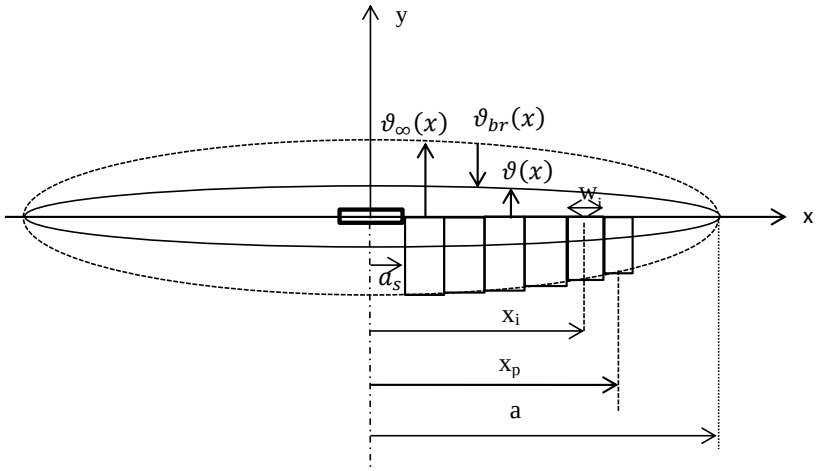

Figure 6-6. Definition of the crack opening of an arbitrary crack under in-axis loading

The numerical solution of equation 6-6 requires the bridging stress to be calculated over the entire delamination profile as point loads. This is achieved by discretizing the crack wake into bar elements along which the bridging stress is acting at the delamination contour. Although, the developed model has been derived from Alderliesten's model [2], Wilson's [3] approach of Chebyshev polynomial was used for the width of the element widths along the crack length. The equation to determine the element width is presented below:

$$w_i = \frac{\pi(a-a_s)}{2N}\cos\left(\frac{\pi}{4}\frac{2*j-1}{N}\right) \qquad \textbf{6-8}$$

After the bar element width is calculated, the integral for the non-uniform bridging stress is approximated as the summation of the bridging stress on these element widths. Alderliesten [2] calculated the crack opening due to point loads integrated over the entire crack profile with the following equation:

$$\vartheta_{br} = \int_{a_s}^{a} \vartheta(x, x_p)\,dx_p \qquad \textbf{6-9}$$

In this equation, a_s is the saw-cut length where no fibre-bridging is present, and $\vartheta(x, x_p)$ is the crack opening displacement at location x due to a point load applied at location x_p - distance from the crack centre as illustrated in Figure 6-6. To calculate the bridging stress over the entire crack opening profile, first the effect of each bridging element must be calculated individually. The cumulative effect from all these bridging elements determines the fibre bridging stress on the cracks.

The crack opening due to a single point load acting on one bridging element can be approximated as described by Tada [41]. For $x < x_p$,

$$\vartheta(x, x_p) = \frac{4P(x_p)}{\pi E}\left(\tanh^{-1}\sqrt{\frac{a^2-b^2}{a^2-x^2+b^2}} + \frac{0.5(1+\nu)b^2}{x_p^2-x^2+b^2}\sqrt{\frac{a^2-b^2}{a^2-x^2+b^2}}\right) \qquad \textbf{6-10}$$

For $x > x_p$,

$$\vartheta(x, x_p) = \frac{4P(x_p)}{\pi E}\left(\tanh^{-1}\sqrt{\frac{a^2-b^2}{a^2-x_p^2+b^2}} + \frac{0.5(1+\nu)b^2}{x^2-x_p^2+b^2}\sqrt{\frac{a^2-b^2}{a^2-x_p^2+b^2}}\right) \quad \text{6-11}$$

In the equations above, E is the young's modulus of the metal in the longitudinal direction, $P(x_p)$ represents the bridging load at distance x_P from the crack centre, ν is the Poisson ratio, and b is the distance from the crack flanks (thus at location of $P(x_p)$). The remaining terms are illustrated in Figure 6-6. The fibre elongation δ_f in the longitudinal direction can be calculated as:

$$\delta_f(x) = \varepsilon_f(x)b(x) = \frac{S_{f,tot}(x)}{E_f}b(x) = \frac{S_f+S_{br}(x)}{E_f}b(x) \quad \text{6-12}$$

Where b(x) is the delamination length at location x. The shear deformation of the fibre layer can be calculated with:

$$\delta_{pp} = \gamma t_f = \tau_f \frac{t_f}{G_f} \quad \text{6-13}$$

Where γ is the shear strain, τ_f is the maximum shear stress at the delamination tip, G_f is the shear modulus of the fibre layer and t_f the fibre layer thickness. Alderliesten [2] further developed these equations into the following equation for uniaxial Glare:

$$\delta_{pp}(x) = C_b S_{al} t_{al}\sqrt{\frac{t_f}{G_f}\left(\frac{1}{F_{al}}+\frac{1}{F_f}\right)} \quad \text{6-14}$$

And for the Glare with cross-ply fibre layers,

$$\delta_{pp}(x) = C_b S_{al} t_{al}\frac{t_{fi}}{G_{fi}}\sqrt{\left(\frac{G_{f1}}{t_{f1}}+\frac{G_{f2}}{t_{f2}}\right)\left(\frac{1}{2F_{al}}+\frac{1}{F_{f1}+F_{f2}}\right)} \quad \text{6-15}$$

where C_b is the correction factor to account for the minimum delamination length that must be obtained before the crack opening is affected by the maximum shear stress. The subscripts 'x1' and 'x2' represent the principal fibre direction and the direction perpendicular to it respectively (see Figure 6-3). The correction factor for uniaxial grade of Glare is:

$$C(b) = 1 - \left(\cosh\sqrt{\propto_{UD}}\, b - \tanh\sqrt{\propto_{UD}}\, b \sinh\sqrt{\propto_{UD}}\, b\right) \quad \text{6-16}$$

For cross-ply grades of Glare α_{UD} is replaced by $2\alpha_{CP}$ under the assumption that they are equal. In the current analytical model the values for α_{UD} and $2\alpha_{CP}$ are calculated using the Young's modulus and shear modulus in the off-axis direction as:

$$\alpha_{UD} = \frac{G_x}{t_x^2} \text{ and } \alpha_{CP} = \frac{\frac{1}{t_{f1}E_{x1}}+\frac{1}{t_{f2}E_{x2}}}{\frac{t_{f1}}{G_{x1}}+\frac{t_{f1}}{G_{x2}}}$$

Where G_x is the shear modulus. E_{x1} is the Young's modulus of the fibre along the principal direction of the laminate, E_{x2} is the Young's modulus of the fibre in the transverse direction of the laminate, and t_{f1} and t_{f2} are the thickness of the fibres. In fibre directions, the stiffnesses can be calculated from the CLT as following:

$$\frac{1}{E_x} = \frac{m^2(m^2 - n^2\vartheta_{12})}{E_1} + \frac{n^2(n^2 - m^2\vartheta_{12})}{E_2} + \frac{m^2n^2}{G_{12}}$$

$$\frac{1}{G_{xy}} = \frac{4m^2n^2(1 + \vartheta_{12})}{E_1} + \frac{4m^2n^2(1 + \vartheta_{21})}{E_2} + \frac{(m^2 - n^2)^2}{G_{12}}$$

Where E_x is the stiffness in the fibre direction, E_1 is the fibre stiffness in the longitudinal direction, E_2 is the fibre stiffness in the transverse direction, and G_{12} is the shear stiffness. The bridging stress is calculated as

$$\boldsymbol{S_{br} = H^{-1}Q} \quad \textbf{6-17}$$

Where,

$$\boldsymbol{H = \sum_{j=1}^{N} \frac{v(x_i,x_j)}{S_{br}(x_j)} - \frac{b(i)}{E_f}\delta(i,j)} \quad \textbf{6-18}$$

$$\boldsymbol{Q = v_{\infty}(i) - \delta_{pp}(i) - \frac{S_f}{E_f}b(i)} \quad \textbf{6-19}$$

The prepreg layer consists of several fibre layers. The cumulative bridging effect of these layers on the individual metal layer is calculated with:

$$\boldsymbol{S_{br,al} = S_{br} \sum_{i=1}^{i=Z} \frac{n_i t_i}{n_{al} t_{al}}} \quad \textbf{6-20}$$

where Z is the sequence number of fibre layers in the prepreg. Where, $S_{br,al}$ is the bridging stress, t_i is the thickness of the fibre prepreg, n_{al} is the number of aluminium layer, and t_{al} is the thickness of a single aluminium layer. To estimate the effect of bridging in the longitudinal direction, K_{br_I}, is calculated as

$$\boldsymbol{K_{br\_I} = 2\sum_{i=1}^{N} \frac{S_{br,al}(x_i)w}{\sqrt{\pi a}} \frac{a}{\sqrt{a^2 - x_i^2 + b_i^2}} \left(1 + 0.5(1 + \nu)\frac{b_i^2}{a^2 - x_i^2 + b_i^2}\right)} \quad \textbf{6-21}$$

Where $S_{br,al}$ is the bridging point stress. The effective SIF is then calculated using the algebraic superposition of the far-field longitudinal SIF (equation 6-3) and bridging SIF in the longitudinal direction (equation 6-21) as:

$$\boldsymbol{K_{eff\_I} = K_{m\_I} + K_{br\_I}} \quad \textbf{6-22}$$

Where, K_{eff_I} is the effective SIF, K_I is the SIF due to the far-field applied load, and K_{br} is the SIF due to bridging. These two constituents are linearly superimposed to calculate K_{eff_I}.

Transverse fibre-bridging

The previous sub-section applied Alderliesten's approach to calculate the longitudinal component of the off-axis fibre bridging stresses. A similar approach is used to calculate the transverse fibre-bridging component. The problem is illustrated in Figure 6-7 and the principle to calculate the fibre-bridging stress is similar. The major differences are mentioned below.

The off-axis fibre orientation induces transverse stresses in the specimen which produces a shear at the crack tip. The shear inducing transverse component is caused due to the reaction

forces at the clamps and the transverse component of fibre bridging at the crack tip. The transverse component of stress at the clamps was discussed at the beginning of this section. The current section discusses the transverse component of the fibre-bridging stress at the crack tip.

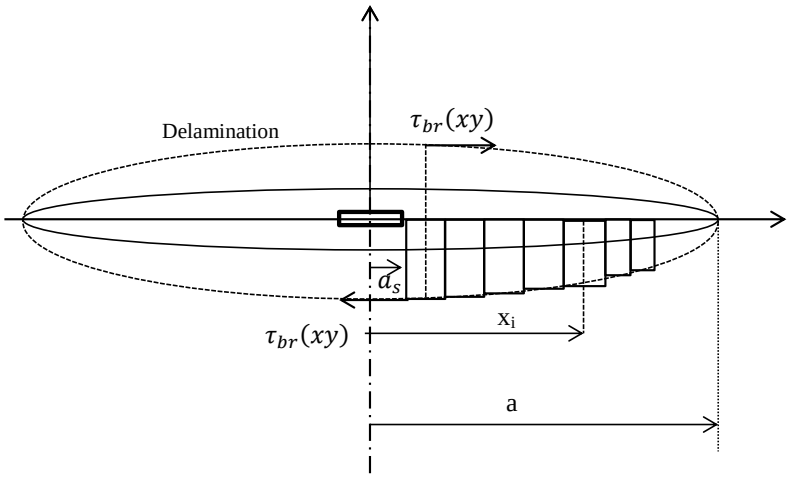

Figure 6-7. Illustration of the transverse component of off-axis fibre bridging under off-axis loading

The transverse component of the fibre-bridging causes the two crack faces to slide over each other as mentioned in Chapter 3. The equation for the crack sliding (ϑ_{II}) due to the fibre bridging in the transverse mode is taken from Tada [41]

$$\vartheta_{II}(x, x_p) = \frac{4P(x_p)}{\pi E}\left(tanh^{-1}\sqrt{\frac{a^2-b^2}{a^2-x^2+b^2}} - \frac{0.5(1+\nu)b^2}{x_p^2-x^2+b^2}\sqrt{\frac{a^2-b^2}{a^2-x^2+b^2}}\right) \quad 6\text{-}23$$

And the SIF in the transverse direction due to fibre bridging is:

$$K_{br\_II} = 2\sum_{i=1}^{N}\frac{S_{br,al}(x_i)w}{\sqrt{\pi a}}\frac{a}{\sqrt{a^2-x_i^2+b_i^2}}\left(1 - 0.5(1+\nu)\frac{b_i^2}{a^2-x_i^2+b_i^2}\right) \quad \textbf{6-24}$$

The effective SIF in the transverse direction can be obtained from the superposition of equation 6-4 and 6-24.

$$K_{eff\_II} = K_{m\_II} + K_{br\_II} \quad \textbf{6-25}$$

Where, K_{eff_II} is the effective SIF in the transverse direction.

In this section, Alderliesten's model was modified to calculate the crack opening, crack sliding, and the fibre bridging components in the two directions – longitudinal and transverse. The equations for the effective SIFs in the two directions – equation 6-22 and equation 6-25 - were presented.

6.5 Fracture angle prediction

The previous section presented the method to determine the Stress Intensity Factors. These parameters are required for predicting the fracture angle in FMLs, especially under mixed-mode conditions as shown by Erdogan and Sih [19]. They showed that the fracture angle for a crack traversing under mixed-mode load can be predicted by the following equation:

$$\cos\frac{\varphi}{2}\left[K_{eff\_I}\sin\varphi + K_{eff\_II}(3\cos\varphi - 1)\right] = 0 \qquad \textbf{6-26}$$

The solution to this equation provides the following two solutions at the two extremes of mixed-mode condition:

- Mode II is zero, i.e. $K_{eff\_II} = 0$, $\varphi = 0, \pi$
- Mode I is zero, i.e. $K_{eff\_I} = 0$, $K_{eff\_I}\sin\varphi \quad + K_{eff\_II}(3\cos\varphi \quad - 1) = 0$

Between these two extremes the latter equation must be solved with the mixed-mode ratio (M^e) which is defined as.

$$M^e = \frac{K_{ef\_II}}{K_{eff\_I}} \qquad \textbf{6-27}$$

After trigonometric analytical manipulation, the fracture angle is calculated from the mixed-mode ratio with:

$$\varphi = 2\frac{180}{\pi}\left(\tan^{-1}\left\{\frac{(-M^e)-\sqrt{M^{e2}+8}}{4}\right\}\right) \qquad \textbf{6-28}$$

The above equation is solved to calculate the fracture angle. The detailed derivation is provided in Appendix A. The computer programme to analyse the results from the analytical model was developed in MATLAB software. After the fracture angles are predicted with the initial loading conditions, the crack continues to grow without deflection. Therefore, the model presented in this work is only limited to predicting the initial fracture angle. The computer program structure is illustrated in Figure 6-8 on the following page.

6.6 Results and discussion

The experimental results from Gonesh [6, 7] provided an insight into the crack paths mechanism in FMLs. The predictions with the analytical model are compared with Gonesh results [6, 7] and with additional experimental results from tests conducted during the course of this doctoral work. The comparison is presented in 6.7. Alderliesten [2] compared the influence of different delamination shapes on the fatigue crack growth rate. This is discussed in section 6.8.b.

6.7 Comparison with experiments

In chapter 5 and in [266] it was hypothesized that the crack paths in FMLs under off-axis loading are caused due to the imbalance in the fibre-bridging in the off-axis directions and the laminate orthotropy. This mechanism is mainly influenced by the load bearing capacity of the prepregs in the transverse direction which depends on the principal axis of the laminate which depends on the crack angle.

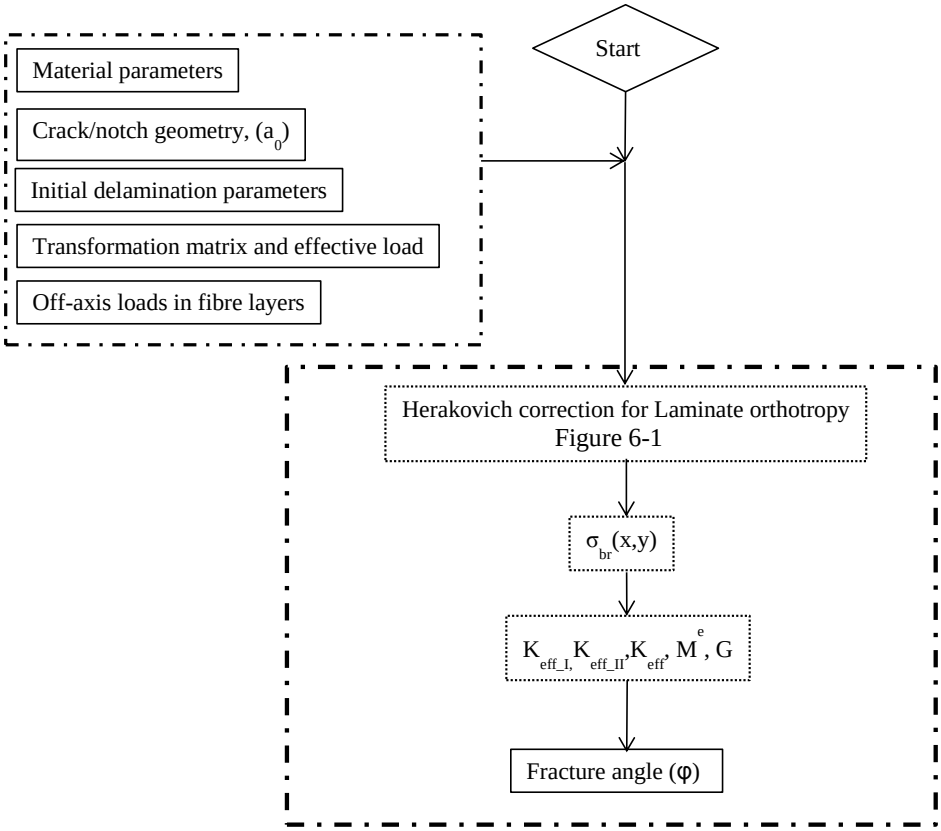

Figure 6-8. Schematic for the numerical program implementation for fracture angle prediction

Figure 6-9 depicts the fracture angle variation with the change in the crack angle for bidirectional Glare3. The 0° fracture angle observed at 45° crack angle is because the mutually perpendicular fibre-layers in the prepreg cancel the fibre-bridging effects in the transverse direction as explained in Chapter 5 and in [266].

Figure 6-10 depicts the fracture angle variation with the change in the crack angle for bidirectional Glare4B. The 0° fracture angle observed at 35° crack angle is because the mutually perpendicular fibre-layers in the prepreg cancel the fibre-bridging effects in the transverse direction as explained in Chapter 5 and in [266] . This angle is different in Glare4B compared to Glare3 because the number of fibres layers in the mutual perpendicular directions is unequal.

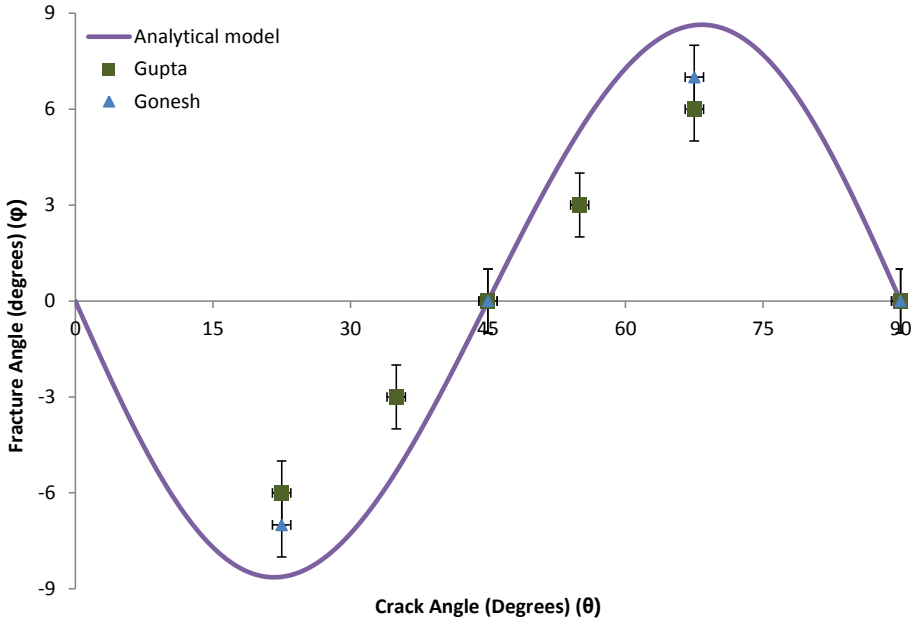

Figure 6-9. Comparison of analytical model results with Gonesh [6, 7] and Gupta for Glare-3 [7]

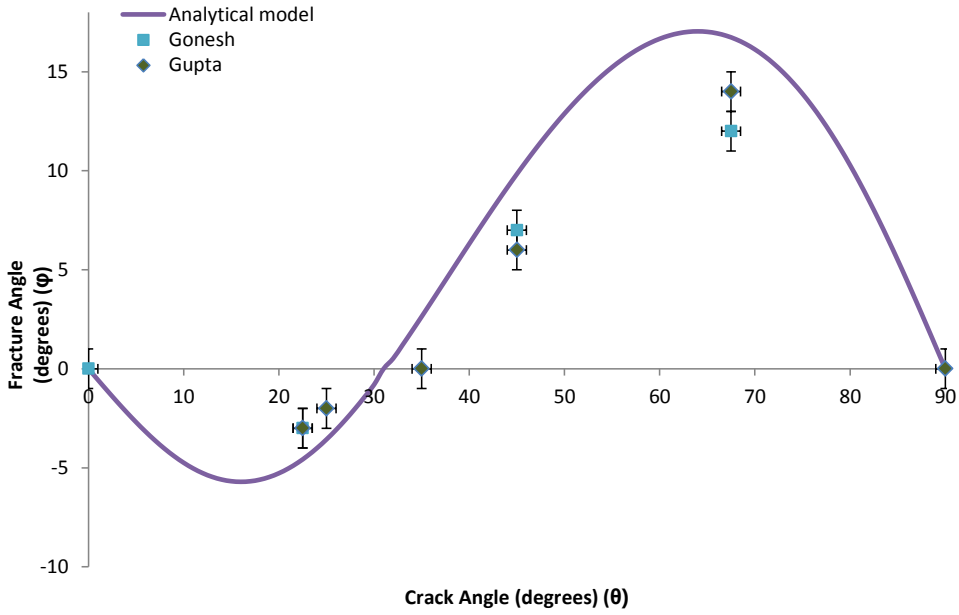

Figure 6-10. Comparison of analytical model results with Gonesh [6, 7] and Gupta for Glare-4B [7]

In unidirecitional Glare2A, the decrease in fracture angle with the increase in crack angle from 30° to 78° in Figure 6-11 with a fracture angle peak value of 22° at the crack angle of

30°. Between the crack angles 78° and 90°, the fracture angle is approximately 0°. In the experiments 0° fracture angle was recorded at a crack angle of 75°. The 0° fracture angle occurs because the off-axis fibres do not bear transverse load that is sufficient enough to influence the transverse component of fibre-bridging.

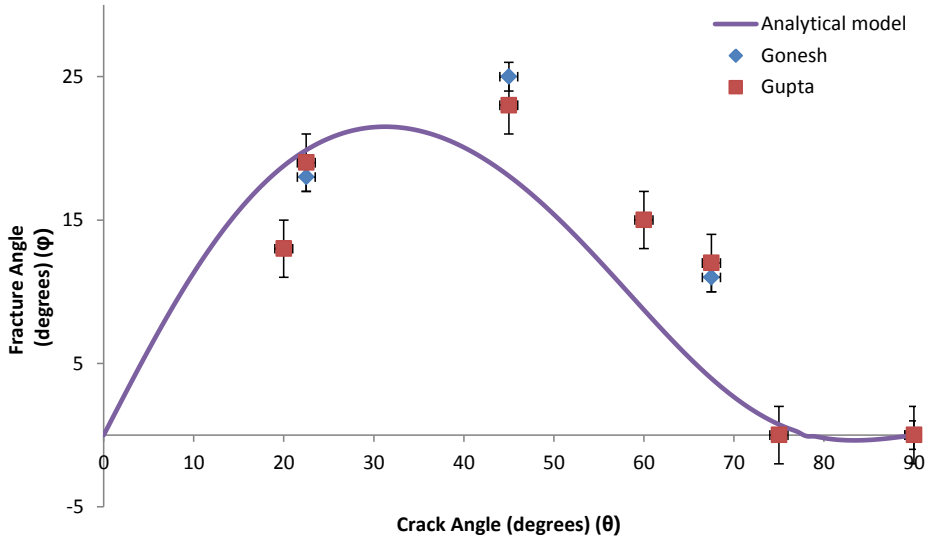

Figure 6-11. Comparison of analytical model predictions with Gonesh [6, 7] and Gupta for Glare2A

It was seen that the trend of fracture angles predicted from the implemented model matches the experimentally observed fracture angle. In terms of the values predicted there is a difference between the model and the experimental results. However, these errors are within 4° of the predicted value except for Glare2A under 67.5° off-axis angle where is differs by 7°. The cause of these errors were discussed in Section 5.6.

The principal stress direction changes with the change in the laminate's Young's modulus. These are influenced by the amount of fibres in the following two directions: along the rolling direction of aluminium and perpendicular to it. A change in the direction of fibres influences the crack angle, and hence, the crack path.

As the crack angle reduces, the fibres induce higher bridging stress in the laminate's transverse direction. This changes the principal direction because a higher component of bridging in the transverse direction affects the stress field in the laminate. Therefore the crack paths changes. The amount of change in principal stress direction depends on the amount of fibres in the mutually perpendicular directions and their bridging effect at the particular crack angle.

The above influence of the fibres in the transverse direction can be easily understood by discussing the particular example of Glare3 where the amount of fibres in the mutual perpendicular directions is same. In Glare3, it is noted that the crack paths initially increase in the positive direction and thereafter decrease to a zero degree fracture angle. Simultaneously, it is observed that the axial stiffness of the laminate decreases with the off-axis angle (Figure 6-3, Figure 6-9 and Figure 6-12), and its gradient continuously changes with respect to the off-axis angle. This is due to two phenomena influencing each other.

1. The change in axial stiffness changes the principal stress direction, and therefore, the crack path deflects.
2. The reduction in the crack angle influences the amount of fibre-bridging in the transverse direction.

As the Laminate's Young's modulus reduces, the material's principal axis changes (it no longer lies along the longitudinal direction) and therefore, the fracture angle increases because crack paths traverse perpendicular to the principal axis [18]. Additionally, as the crack angle reduces the fibre perpendicular to the rolling direction of aluminium induces higher transverse bridging compared to the fibre along the rolling direction. As the crack angle is further reduced to 45°, the net effect of the fibre-bridging in the two directions nullify the effect of fibre-bridging in the two direction as explained in chapter 5 and Gupta *et al*. [266]. Therefore, the fibre-bridging does not influence the crack path and the crack paths traverse without deflection at 45° off-axis angle. On further reduction of the crack angle, the net fibre-bridging is non-zero and the cracks deflect. Beyond the 45° crack angle the laminate is simply symmetric about the transverse axis. The amount of deflection is same but in the opposite direction with respect to the transverse axis of the laminate. Similarly, the fibre-bridging mechanism in the transverse direction influences the fracture angles in the bidirectional Glare4B and unidirectional Glare2A.

Considering the above two mechanisms' influence on the crack path, it is expected that as axial stiffness of the material decreases with respect to the off-axis angle the fracture angle will increase. The change in the laminate's Young's modulus with respect to the off-axis angle for bidirectional Glare grades is illustrated in Figure 6-12, while for the unidirectional Glare2A, it is shown in Figure 6-13. The slopes of the curves approximately provide the fracture angles for the cracks in the Glare specimens under the off-axis angles [273].

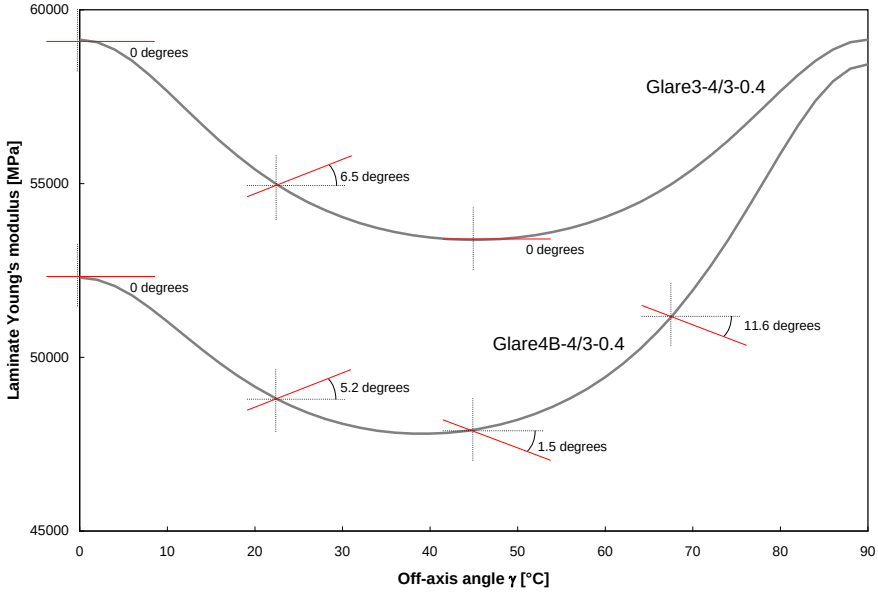

Figure 6-12. Change in Laminate's Young's modulus for bidirectional Glare with respect to off-axis angle [273]

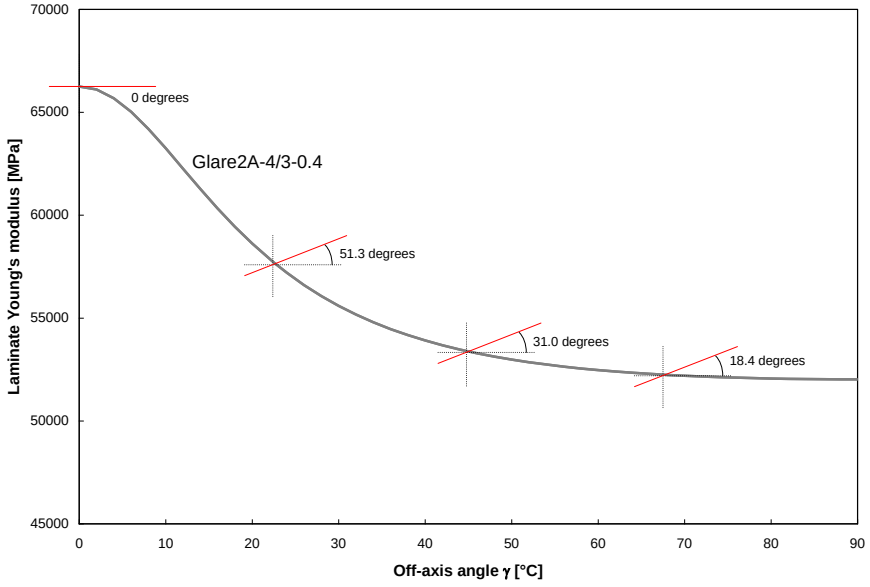

Figure 6-13. Change in Laminate's Young's modulus for unidirectional Glare with respect to off-axis angle [273]

6.8 Model robustness

The following assumptions were made for the analytical model.

- Element widths have an effect on the fracture angle
- Initially assumed delamination shape affects the crack path
- The principle of symmetric laminate can also be applied to other Glare grades

To verify the validity of these assumptions and the associated model robustness with these parameters, the model was tested with different initial assumed delamination width. The results for the three Glare grades are shown in the first sub-section. In the second sub-section, the model is tested with Glare5.

6.8.a Size of the bridging elements

The following figures - Figure 6-14, Figure 6-15 and Figure 6-16 - present the effect of different bridging elements width on the fracture angles for Glare-2A, Glare 3 and Glare 4B respectively. The fracture angles were predicted with different elements width ranging from 0.001 to 0.1. The trend of the predicted fracture angles remains the same, but the magnitude of the predicted fracture angle changes. The increase in the bridging element width increases the predicted fracture angle magnitude. The element width show no convergence for the predicted fracture angle, but the bridging element width of 0.05 provides the highest accuracy with the experimental results. Interestingly, both Alderliesten [2] and Wilson [3] observed similar correlation for the in-axis fatigue crack growth prediction with respect to the bridging elements width.

This lack of convergence can be understood by observing the fibre failure in the experimental results of de Vries [274]. De Vries [274] results showed that fibres broke in bundles with varied width. These widths have no correlation with the fibre thickness or the elements width. Failure of the fibres affects the bridging stress at the crack tip. Furthermore, Rodi [4] in his sensitive study of the bridging stress with the element width showed that a reduced element width calculates higher stresses in the fibres. Higher stress in the fibres imply lower delamination and higher bridging stresses at the crack tip. The increased bridging stress affects the mixed-mode ratio by reducing the denominator in equation 6-27. Therefore, the fracture angles are overestimated with lower element width. He further mentioned that an optimum element width must be found through optimization procedure.

In the current research, the optimum width was found by predicting the fracture angle for various element widths, and selecting the length which had the best correlation with the experimental data.

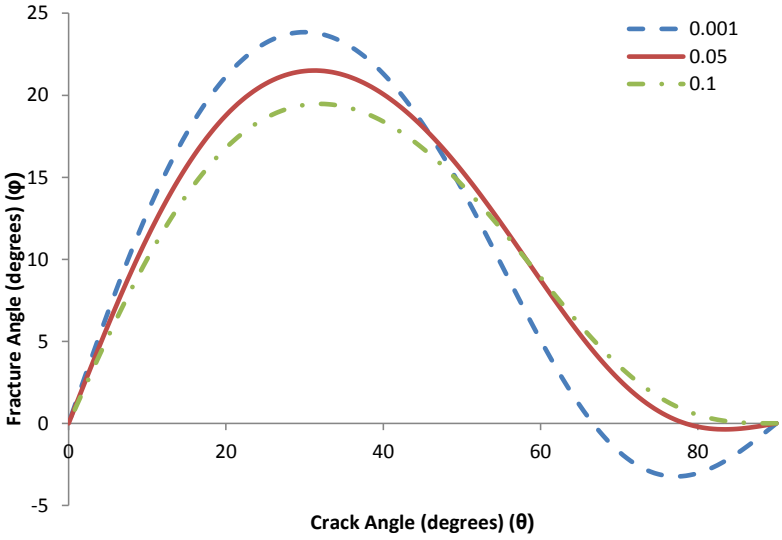

Figure 6-14. Fracture angle prediction with different initial maximum 1-D delamination width for Glare-2A

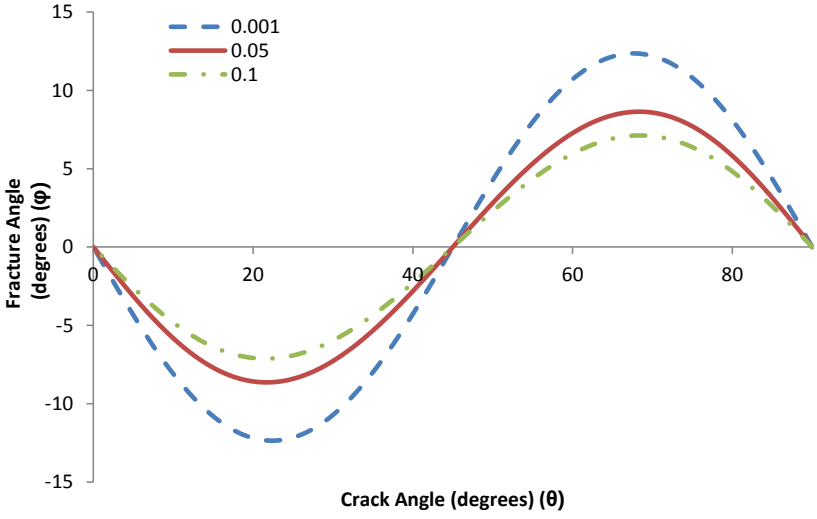

Figure 6-15. Fracture angle prediction with different initial maximum 1-D delamination width for Glare-3

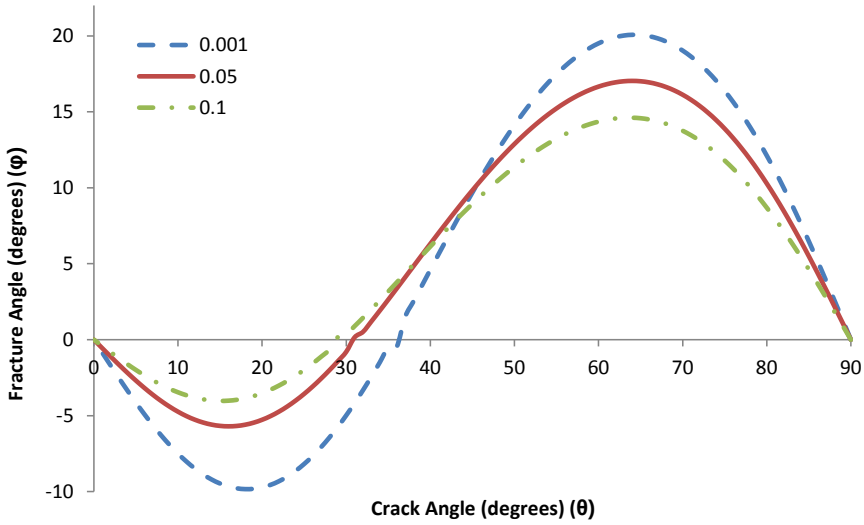

Figure 6-16. Fracture angle prediction with different initial maximum 1-D delamination width for Glare-4B

6.8.b Effect of delamination shapes on the crack paths

Delamination shapes influence the stress gradient for the bridging stress along the crack tip, and therefore, it is important to have the correct delamination shape in the prediction model. The shapes with sharper delamination profiles account for more bridging at the crack tip. The increased bridging overestimates the fracture angle because the denominator in M^e is reduced due to the excess bridging component. In the following figures, it is evident that delamination shapes with less sharper profiles - parabolic and elliptical delamination shapes [2] - at the crack tip have better correlation with the experimental results.

The shapes modelled are similar to Alderliesten [2], i.e. parabolic, elliptical, triangular and cosine. The elliptical and the parabolic delamination shape show the best correlations with the experimental results from the four shapes. Interestingly, Gonesh [7] results' show a parabolic delamination shape along the crack profile (inserted image in Figure 6-17 and Figure 6-18). In uniaxial Glare, i.e. Glare2A, the elliptical and parabolic delamination shape predict the trend of the fracture angle correctly in the ranges of 0-25° and the 55-90° fracture angle. While at 45° the value correlates better with the predicted fracture angle from triangular delamination shape. Gonesh [7] presented the result for Glare2A at 45° off-axis angle where the delamination shape is similar to a triangle at the tip of the initial saw-cut (inserted image in Figure 6-19). The results presented in this section show that the selection of the appropriate initial delamination shape is necessary to predict the fracture angle. This is most evident from the predicted fracture angles of Glare2A at different crack angles. Therefore, it is concluded that a correct initial delamination shape must be selected.

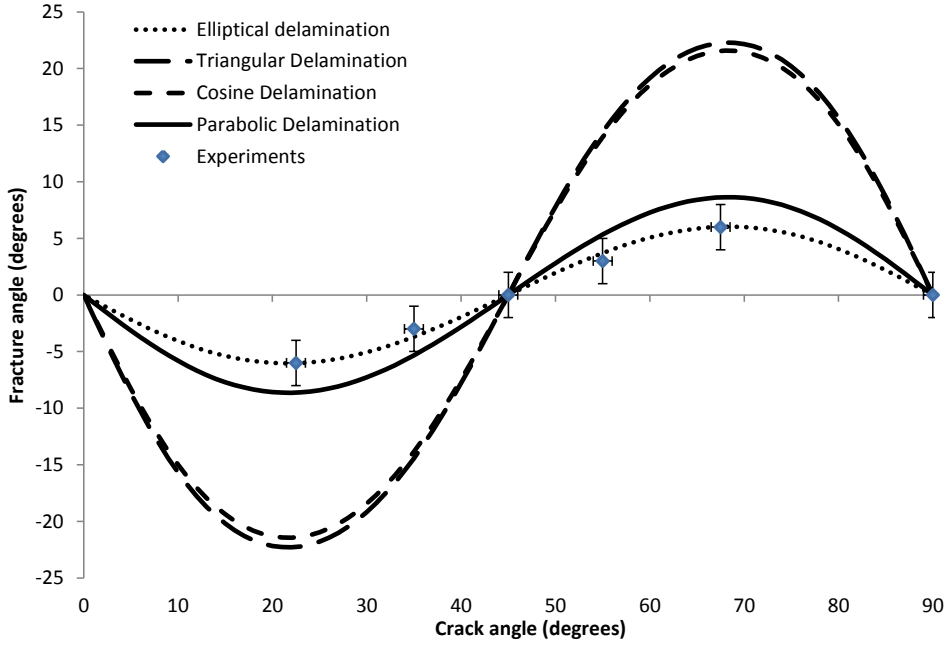

Figure 6-17. Effect of initial delamination shape on crack paths in Glare3

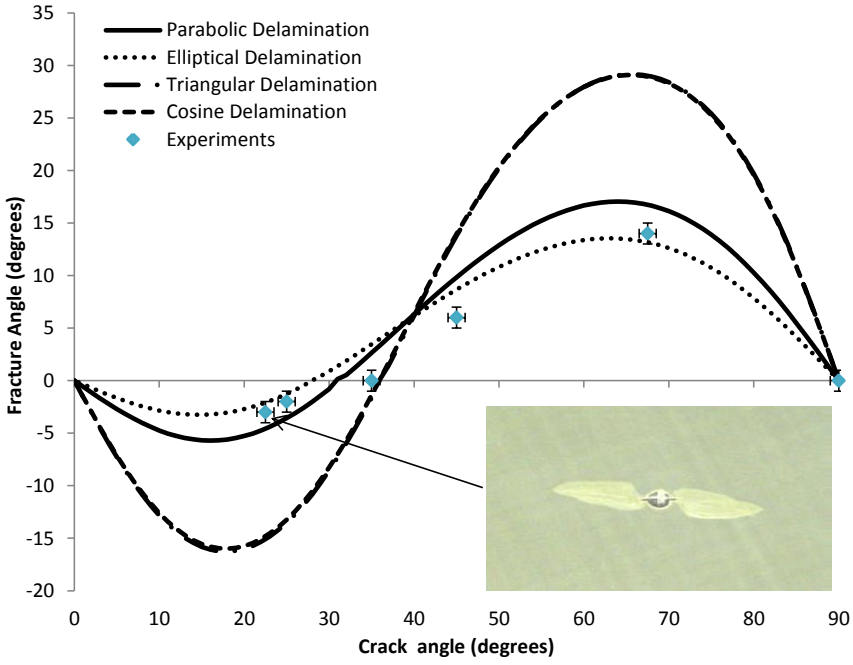

Figure 6-18. Effect of initial delamination shape on crack paths in Glare4B

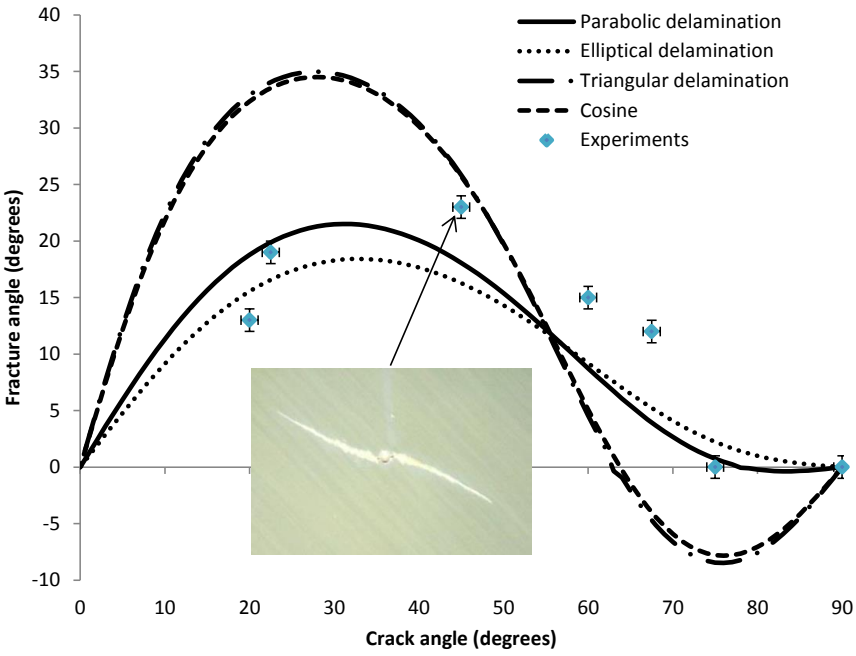

Figure 6-19. Effect of initial delamination shape on crack paths in Glare2A

6.8.c Other Glare grades

Alderliesten developed his model [2] using the principle of averaged fibre bridging effect. It implies that the bridging contribution of every fibre layer over the metal layers in the laminate can be modelled as one single fibre layer a single metal layer. This was applied to the uniaxial Glare (Glare-2A), symmetric biaxial grade of Glare (Glare-3) and asymmetric biaxial Glare (Glare-4B). The model predictions were compared with the results in Gonesh [6, 7]. To verify the validation for other Glare grades the model was used to predict the fracture angle for Glare5-4/3-0.4. The lay-up of Glare5-4/3-0.4 is defined below.

[2014-T3/0° glass/90° glass/90° glass/0° glass/2014-T3/0° glass/90° glass/90° glass/0° glass/2014-T3/0° glass/90° glass/90° glass/0° glass/2014-T3/0° glass/90° glass/90° glass/0° glass/2014-T3]

It is expected that due to the symmetrical laminate at 45° off-axis loading, the crack path will be zero degree similar to Glare-3 at 45° off-axis loading. Gonesh [6, 7] also presented the results for Glare-5 at 45° off-axis angle which was also predicted by the analytical model.

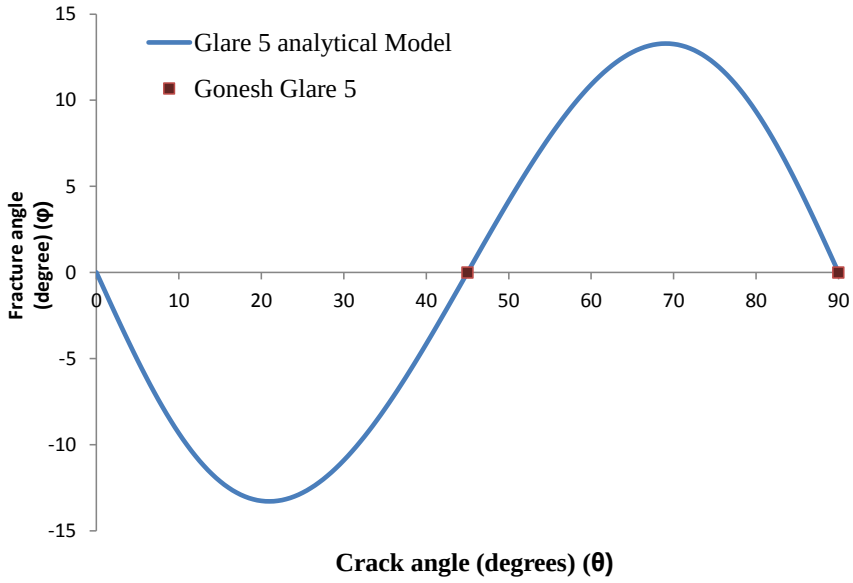

Figure 6-20. Fracture angle prediction for Glare5

6.9 Limitations

The crack path prediction model under off-axis loading for the FMLs in this research was developed for fatigue loading with the objective to extend FMLs application in aircraft structures. Therefore, the model has limitations for its application with respect to type of loading, and crack path behaviour. These are discussed in the following sub-sections individually.

6.9.a Quasi-static loading

The analytical model presented in this chapter incorporates the effects of fibre bridging. The pre-requisite for fibre-bridging that the fibres remain intact in order to carry stress over the crack is less likely to occur under quasi-static loading. This is because in quasi-static loading the loads borne are higher and closer to the failure strength of the fibres. Such high stress in the fibres causes failure of the fibres [13, 274], thus, rendering them incapable to carry the load over the crack. This leads to a different strain field at the crack tip compared to the strain field observed under fatigue loading.

Figure 6-2 summarizes the analytical model approach used in this research. Removing the bridging components from the damage directionality model under fatigue makes the boundary conditions similar to the quasi-static conditions, i.e. applied far-field load and a transverse component due to the fibre directions. This modified form of the analytical model is presented in the Chapter 7 and its predictions are compared with the experimental results obtained from Glare2S-3/2-0.3 under quasi-static loading.

6.9.b Edge-notched uniaxial Glare grade

Thibault-Liboiron *et al.* [11] observed crack deflection in edge-notched specimens. The fracture angles in double-edge-notched (DENT) specimens were different from the centrally notched (CN) specimens observed by Gonesh [6, 7]. The differences in the fracture angles in the experiments observed by the edge-notched specimens of Thibault-Liboiron *et al.* [11], and centrally notched specimens of Gonesh [6, 7] and the current research possibly occurs due to the edge effects on crack paths defined by Sanford [96]. The DENT specimen tested by Thibault-Liboiron *et al.* [11] is shown in Figure 6-21.

In the DENT specimens, the fibres in the wake of the notch – between the edge and the tip of the initial notch -, are not loaded as illustrated in Figure 6-21. This is different from the CN specimens tested in the current research work, and by Gonesh [6, 7] . The different loading of the fibres compared to the CN specimens produce a different bridging effect on the crack path. Consequently, the fracture angles observed in the two specimens – DENT and CN – specimens are different.

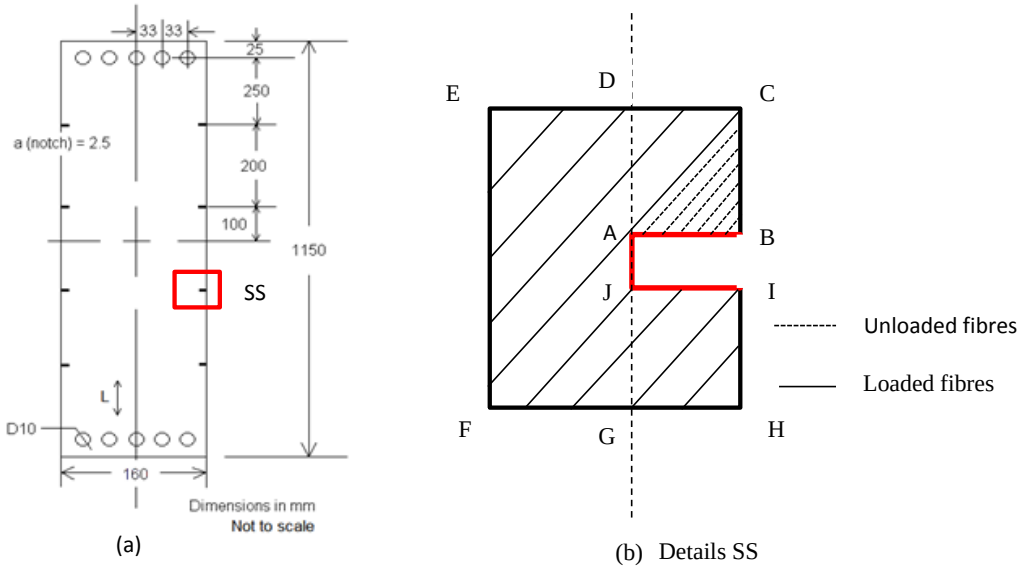

Figure 6-21. Image (a) shows the Double-edge notched Tension (DENT) specimen tested by Thibault-Liboiron *et al.* [11] and image (b) shows the details SS

Another difference between the two specimens is the trajectory of the paths after the initial deflection. In the CN specimens, it is observed that the cracks do not curve, while in the DENT specimens the curves continuously curve downwards. The downwards curvature of the specimen becomes more pronounced as the propagating crack length increases. The curving crack in the edge-notched specimens of monolithic metals was also mentioned by Leevers *et al.* [109, 111]. They attributed this to the in-plane bending effects introduced into the DENT specimens as the crack propagates farther from the edge.

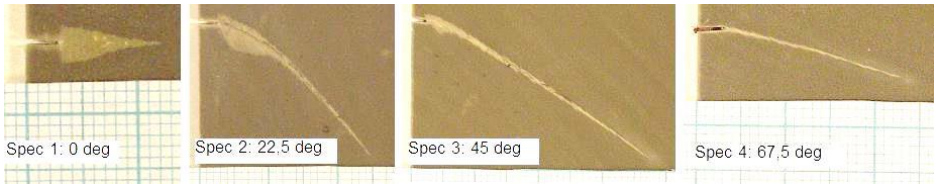

(a)

(b)

(c)

Figure 6-22. Delamination shapes for DENT specimens of (a) Glare2A, (b) Glare3, and (c) Glare4B tested by Thibault-Liboiron *et. al.* [11]

Additionally, it was observed that in the CN specimens delamination about the axis of the propagating crack remains equal in size shown in Figure 6-22. This is different from the delamination sizes in the DENT specimens where the delamination sizes are unequal about the propagating crack axis.

The analytical model developed in this research work was developed for centrally notched specimens, and did not consider the edge effects. Therefore, the analytical model's application remains limited to centrally notched specimens.

6.10 Conclusions

The analytical crack path model for predicting the fracture angle in FMLs under off-axis loading was presented in this chapter. It was concluded that the crack paths in FMLs under off-axis loading are influenced by both - laminate orthotropy, and fibre-bridging in the off-axis directions.

The analytical model developed predicts the trends for the fracture angles correctly in Glare2A, Glare3 and Glare4B. The analytical model shows an influence of the initial delamination profile on the predicted fracture angle. The less sharper delamination tip profile – parabolic and elliptical – best describe the trend in fracture angles, and also the magnitude of fracture angle which has least difference from the experimental results.

7 Chapter 7: Applicability of the developed analytical model to quasi-static model

7.1 Introduction

This chapter falsifies the hypothesis that only laminate orthotropy influences the crack paths in Fibre Metal Laminates (FML) under off-axis quasi-static loading. A brief review of the analytical and experimental studies on FMLs is presented followed by the presentation of an analytical model for damage directionality in fatigue loading modified for quasi-static loading. Thereafter, the experimental results are compared to the analytical results. It is demonstrated that laminate orthotropy alone is insufficient to explain crack paths in FMLs under quasi-static loading. A plausible approach using plastic deformation is also presented.

It is hypothesized that the laminate orthotropy alone influences the crack paths in quasi-static loading. To demonstrate this, the results for Glare2S under off-axis loading, and Glare4B [12] are compared with an analytical model for quasi-static loading. The quasi-static model is the fatigue model [275] developed in Chapter 6, but without the fibre-bridging components.

The chapter initially reviews the work done in FMLs under off-axis loading – both experimental and quasi-static. Thereafter, a quick overview of the fatigue model is presented. This overview is presented to highlight the differences between fatigue and quasi-static loading. Thereafter, the results from the tests performed in this research for quasi-static loading, and Tinga's results [12] are compared with the predictions from quasi-static model derived from the fatigue model. The lack of correlation between the results is shown and its possible causes are discussed.

7.2 Highlights from the literature

Tinga [12] performed residual strength tests on Glare4B-4/3-0.4 laminates for various off-axis angles. In his study, he also presented the obtained fracture angles as function of the off-axis angle. His results showed that as the residual strength decreased with the off-axis angle, while the fracture angle increased. Studies [6, 7, 275] presented experimental results on damage growth directionality under off-axis fatigue loading for centrally notched specimen, while Thibault-Liboiron [11] presented an experimental study for edge-notched specimen. Zaal [9, 15] had studied the damage directionality using the *T*-stress theory [20, 43, 46, 53] for predicting the damage directionality. However, Zaal's prediction with the *T*-stress theory [20] failed to explain the results from Gonesh [6, 7]. In the previous chapters the author explains the results of Gonesh [6, 7] using the fibre-bridging theory for fatigue loading and laminate orthotropy. Kawaii [10] explained the reduced fatigue life with the increasing off-axis angle in Glare3 but without explicitly addressing damage directionality.

7.3 A brief review of the analytical model

In the previous chapter the author identified both the fibre-bridging mechanism and the laminate orthogonality to induce mixed-mode at the crack tip under fatigue loading deflecting the crack path. The fibre-bridging mechanism is a unique mechanism for FMLs under fatigue loading. It is the phenomena of fibres carrying load over the crack in the metal layers. The load borne by the fibres is equivalent to a crack shielding effect. For fibre-bridging to be effective, the fibres must remain intact. It is safe to assume that fibres remain intact under fatigue loading because the applied loads are low. Figure 6-8 shows the schematics of the

analytical model developed for fatigue loading in which laminate orthotropy is marked as quasi-static loading.

For fatigue loading in FMLs under in-axis loading, the effective longitudinal Stress Intensity Factor (SIF) depends on two types of stresses – the far-field applied stress and the bridging stress under in-axis loading. The orientation of the fibres further induce two components of bridging – longitudinal and transverse bridging stress. Additionally, the off-axis fibres induce a clamping effect that induces shear at the crack tip. Therefore, under off-axis loading the effective SIFs in the longitudinal and transverse directions depend on the far-field applied stress, the clamping effect, and the fibre bridging components similar to in-axis loading

In the fatigue model, first the SIFs for the opening and shear mode are calculated for both clamping and fibre bridging. Subsequently, the SIF for the opening mode is linearly superimposed and similarly the shear mode SIF is superimposed. The mixed-mode ratio is calculated from the effective SIFs. Finally, the fracture angle is calculated from this obtained mixed-mode ratio. The structure of the computer programme implemented in MATLAB for the fatigue model is illustrated in Figure 6-8. In Figure 6-8, $\sigma_{br}(x,y)$ is the bridging stress component in the x and y directions respectively, K_{eff_I} is the effective SIF in the longitudinal direction, K_{eff_II} is the effective SIF in the laminate's transverse direction, M^e is the mixed-mode ratio (K_{eff_II} /K_{eff_I}) and G is the strain energy release rate. Various angles used in the analytical model are defined in Figure 7-1.

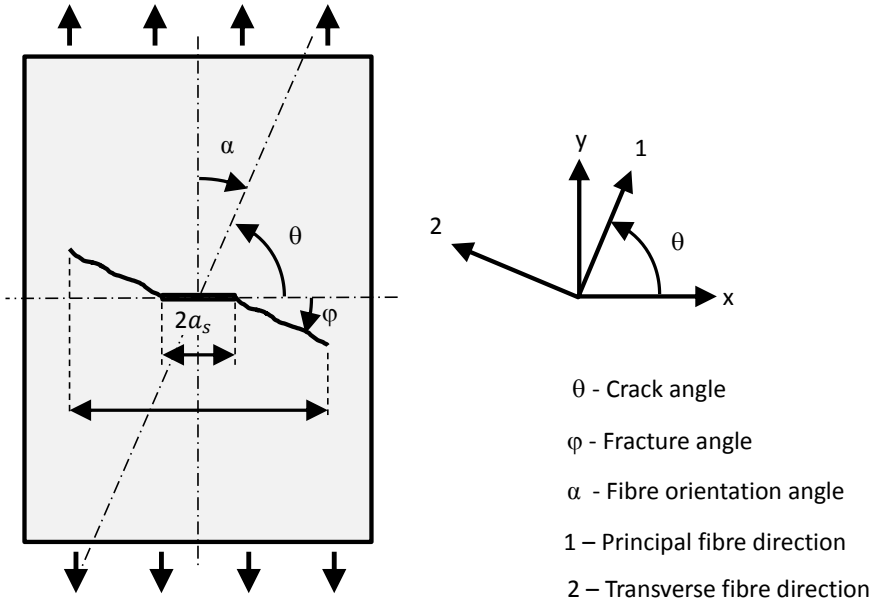

Figure 7-1. Illustrations for various angles in the laminate

The model for quasi-static loading can be derived by eliminating the fibre-bridging component from the fatigue model. Deleting fibre-bridging relates to the observation of fibre failure in the crack wake during quasi-static tests [12]. The procedure is explained.

When the off-axis fibres are not symmetric with respect to the loading axis, they cause an imbalance in the laminate orthotropy. This causes shear to be introduced into the laminate. This was explained by Herakovich [272] who states that orthotropic materials exhibit normal-shear coupling effects when the material is loaded in directions other than the principal material coordinates. This means that effectively, not only an axial load is applied to the specimen, but that with clamping also a transverse load is applied.

Herakovich further introduced two 'coefficients of mutual influence' to calculate this shear stress using the material properties. The first coefficient is used to calculate the effectively applied normal stress from the applied shear load, and the second coefficient is used to calculate the shear applied by application of a longitudinal load. Using the Classical Laminate Theory (CLT), he derived the following expression for the coefficient of mutual influence of the second kind (the coefficient relevant to our application):

$$\eta_{xy,x} = \frac{nm\left[m^2\left(2+2\nu_{12}-\frac{E_1}{G_{12}}\right)+n^2\left(-2\frac{E_1}{E_2}-2\nu_{12}+\frac{E_1}{G_{12}}\right)\right]}{\left[m^4+m^2n^2\left(-2\nu_{12}+\frac{E_1}{G_{12}}\right)+n^4\frac{E_1}{E_2}\right]} \quad \textbf{7-1}$$

where n is the cos(α), m is the sin(α) - (α is the fibre orientation angle), ν is the Poisson's ratio, E is the Young's modulus, and G is the shear modulus of the material.

In the current research, a more elaborate but mathematically simpler approach is used to incorporate this coupling effect. The shear strain in the entire laminate is calculated using the CLT with the following equation:

$$\begin{bmatrix}\varepsilon_{11}\\ \varepsilon_{22}\\ \varepsilon_{12}\end{bmatrix} = S\begin{bmatrix}\sigma_\infty\\ 0\\ 0\end{bmatrix}$$

where S is the compliance matrix, σ_∞ is the far-field stress caused by an applied load P. The obtained shear strain component in the strain vector is caused by the laminate orthotropy. To eliminate the effect of clamping, the equivalent stress (τ_{orth}) that causes the non-longitudinal strain in the strain vector is calculated with:

$$\begin{bmatrix}0\\ 0\\ \tau_{orth}\end{bmatrix} = C\begin{bmatrix}0\\ 0\\ \varepsilon_{12}\end{bmatrix}$$

where, C is the stiffness matrix and ε is the strain matrix. The correct stress applied to the laminate is the summation of the far-field stress σ_∞ and the equivalent stress that causes the transverse load due to clamping τ_{orth}. The effective SIFs in the longitudinal direction (K_{eff_I}) and the transverse direction (K_{eff_II}) due to the far-field load can be calculated using the following equations:

$$K_{eff\_I} = \sigma_\infty\sqrt{\pi a} \quad \textbf{7-2}$$

$$K_{eff\_II} = \tau_{orth}\sqrt{\pi a} \quad \textbf{7-3}$$

Where σ_{∞_I} and τ_{∞_II} are the longitudinal and shear stress obtained. Erdogan and Sih [19] developed the mixed-mode theory to find the plane of maximum tension which uses the following relation between K_{eff_I} and K_{eff_II} to calculate the fracture angle.

$$\cos\frac{\varphi}{2}\left[K_{eff\_I}\sin\varphi + K_{eff\_II}(2\cos\varphi - 1)\right] = 0 \qquad \textbf{7-4}$$

The predictions for the fracture angle from Equation 7-4 were compared with the experimental results obtained in the experiments for Glare2S and Tinga's results for Glare4B [12]. The test procedure for Glare2S is presented in the following section.

7.4 Tests

The cross-ply laminate Glare2S-4/3-0.3 (tested in this research) refers to respectively Glare grade, the lay-up (no. of metal layers and fibres) and, the aluminium layer thickness. The lay-up for this case is defined as [11]:

[2024-T3/+45° glass/+45° glass/2024-T3/+45° glass/+45° glass/2024-T3+45° glass/+45° glass/2024-T3]

Glare2S was considered as an unidirectional doubler material in high stressed corner locations – door and window cut-outs – where fibres are positioned under 45° angle with respect to the longitudinal directions. Keeping the rolling direction of aluminium in the longitudinal direction requires the Glare2S variant of Glare.

The specimen tested in this study is illustrated in Figure 7-2 and the test matrix is presented in Table 7-1. Two bolt rows were used to fasten the specimen to the clamping plates in order to limit the load on the bolt. The clamping plates were attached to a 250kN MTS machine. The load was applied with a displacement controlled method at a rate of 0.5mm/min. Fracture angles were measured with a protractor along the specimen surface. Similarly, Tinga [12] used two bolt rows to clamp specimens with load introduction plates, which had a pin joint with the machine as shown in Figure 7-3. He also used anti-buckling guides. Tinga's test matrix is presented in Table 7-2.

Table 7-1 Test Matrix

Specimen number	Glare grade	Off-axis angle (°)	Maximum load (kN)	No. of Specimens Tested	Fracture angle (°)
1	Glare2S-4/3-0.5	0			
2	Glare2S-4/3-0.5	15	170	2	18
3	Glare2S-4/3-0.5	22.5	145	2	20
4	Glare2S-4/3-0.5	30	120	2	25
5	Glare2S-4/3-0.5	45	90	2	33
6	Glare2S-4/3-0.5	67.5		2	37

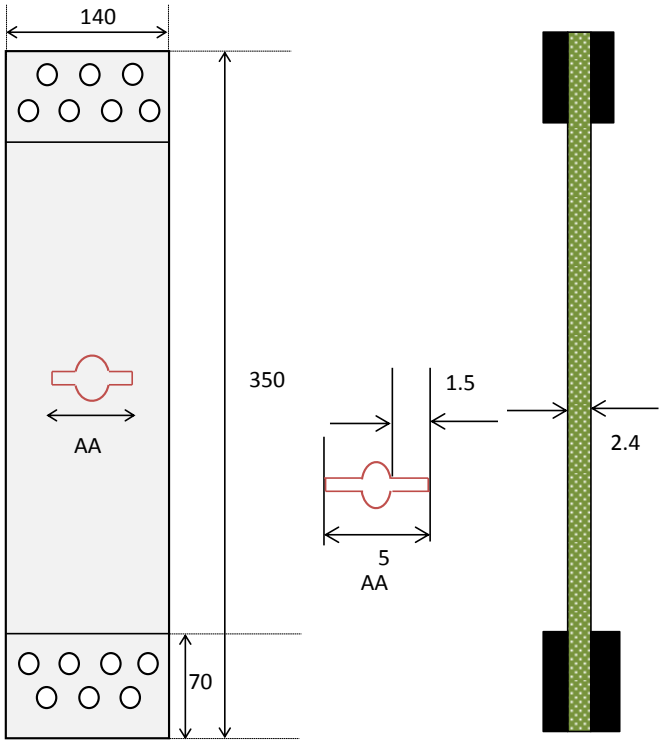

Figure 7-2. Specimen configuration (all dimensions in mm)

Table 7-2 Tinga's [12] test matrix

Specimen number	Glare grade	Off-axis angle (°)	Fracture angle (°)
1	Glare4B-4/3-0.4	15	8.8
2	Glare4B-4/3-0.4	30	20.4
3	Glare4B-4/3-0.4	45	33.8
4	Glare4B-4/3-0.4	60	-2.4
5	Glare4B-4/3-0.4	75	-1.1

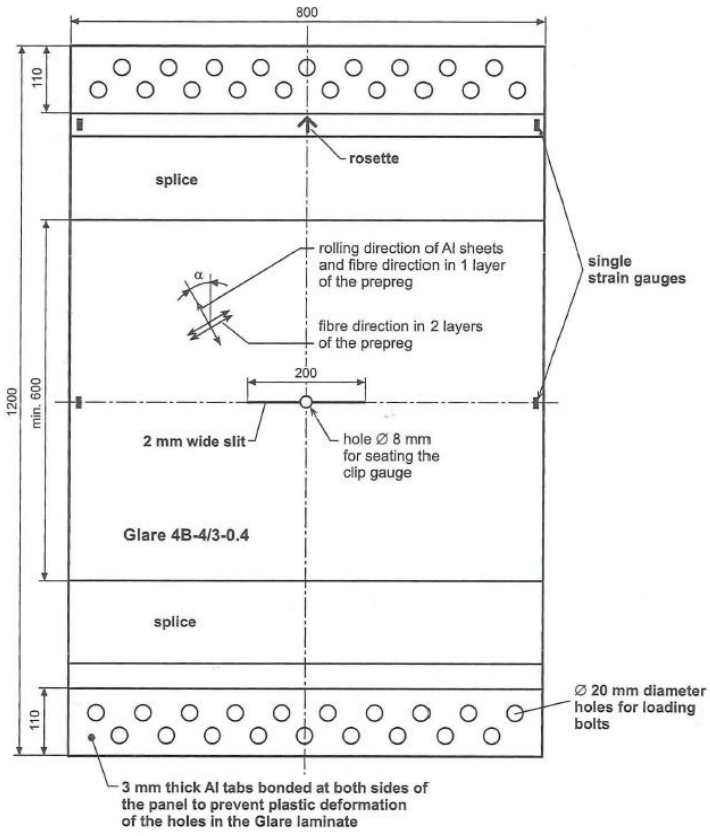

Figure 7-3. Glare4B specimen tested by Tinga [12]

7.5 Results

Figure 7-4 and Figure 7-5 compare the experimental results with the predictions from the two analytical models – fatigue model, and the quasi-static model. It is evident that the predictions from neither models correctly match the experimental results. The fatigue model fails to predict the results because the fibre-bridging mechanism – an important characteristic of fatigue in FMLs - does not occur under quasi-static loading. The quasi-static model also fails to correctly predict the results. These aspects are discussed in detail in the following section.

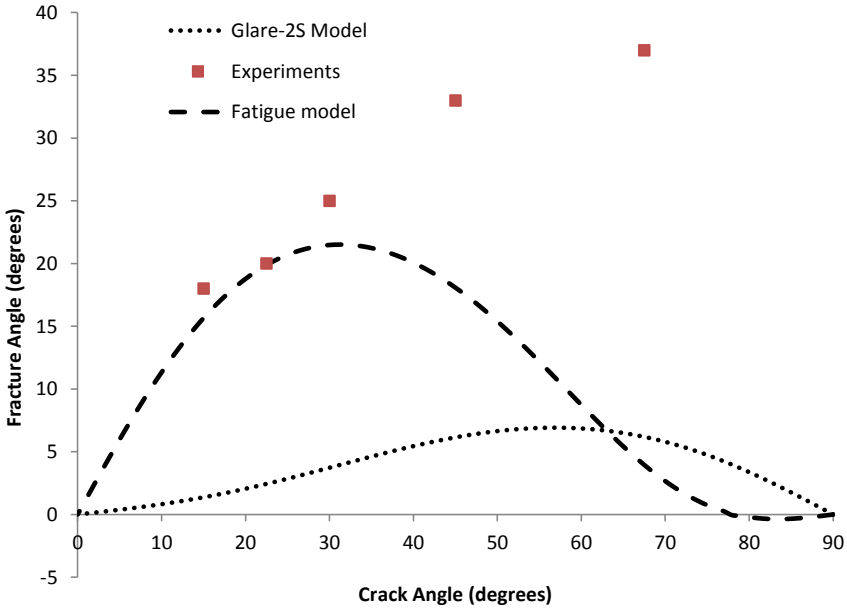

Figure 7-4. Experimental results of Glare2S in comparison with analytical model for fatigue with and without fibre-bridging

7.6 Discussion

During quasi-static loading, the fibres bear load that reach the ultimate strength of fibres which leads to fibre failure. The broken fibres cannot bridge the crack or provide crack closure, and hence, fibre-bridging won't influence the damage directionality in FMLs under off-axis loading. This is also observed in the results presented in Figure 7-4 and Figure 7-5 for Glare2A and Glare4B respectively. The fatigue model estimates the fracture angle observed in the experiments incorrectly. The absence of fibre-bridging implies that the mixed-mode ratio (M^e) as calculated in Chapter 6 is incorrect for quasi-static loading.

It could be argued that the fatigue model without the fibre-bridging components should predict the fracture angle correctly under quasi-static loading. To verify this, the fibre bridging components were eliminated from the fatigue model and the results are also presented in Figure 7-4 and Figure 7-5. The results from this model – laminate orthotropy – are also incorrect, and have a higher inaccuracy with the experimental results compared to the entire fatigue model. The fatigue model has a smaller deviation with the experimental results compared to the quasi-static model because of the effect of transverse component of fibre-bridging.

Additionally, both the models were developed using the Linear Elastic Fracture Mechanics (LEFM) principles. LEFM principles limit the strains to elastic strains, but under quasi-static

loading deformation can be plastic and hence, non-linear. Therefore, both models fail to predict the fracture angles under quasi-static loading correctly.

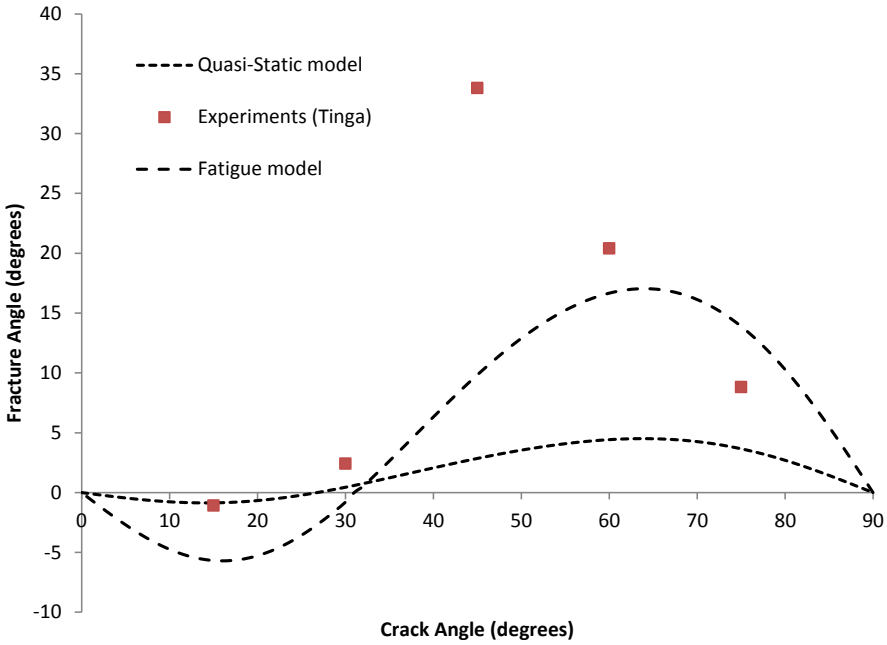

Figure 7-5. Experimental results of Glare4B in comparison with analytical model for fatigue with and without fibre-bridging

To develop a more accurate prediction model for fracture angles under quasi-static loading, the use of elasto-plastic mechanics could provide a better approach. To demonstrate this effect, the following section presents a similitude study of the plastic behaviour in FMLs, and the effect of change in plasticity on the fracture angles in FMLs under off-axis loading.

7.7 Possible Influence of plasticity on fracture angles

To understand the absence of correlation between the predictions with the quasi-static model and the experiments, illustrated in Figure 7-4 and Figure 7-5, the influence of plasticity has been evaluated. The quasi-static model assumes linear-elastic material behaviour captured with among others the elastic Young's modulus.

For fatigue crack growth this assumption of linear elastic response is deemed appropriate, because small scale yielding applies. However, in residual strength tests generally large scale yielding is observed, which invalidates this linear elastic assumption. Hence, the hypothesis here is that large scale plasticity changes the panel's stiffness, and as a consequence, the fracture angle. To test this hypothesis, the effect of plasticity on the effective axial stiffness is evaluated. This effect is simulated by reducing the Young's modulus of the material while

other material parameters remain constant. Only E has been reduced in this exercise. No changes were made to transverse or shear modulus.

The stress strain curve in Figure 7-6 illustrates that beyond the proportionality limit, the effective stiffness, i.e. the straight line between the origin O and the point A on the plastic portion of the stress strain curve, decreases. This effective stiffness at any point can be approximated to the slope of the curve from the point on the curve OABCDE to the origin O. As we move from the right to left on the horizontal axis we can observe that effective stiffness (slope of the curve) at point C is lower than at point A but higher than at point B. Further to the right, effective stiffness at D is lower than at point C but higher than at point E. In the prediction model this stiffness decrease is incorporated by changing the Young's modulus in axial direction in the input.

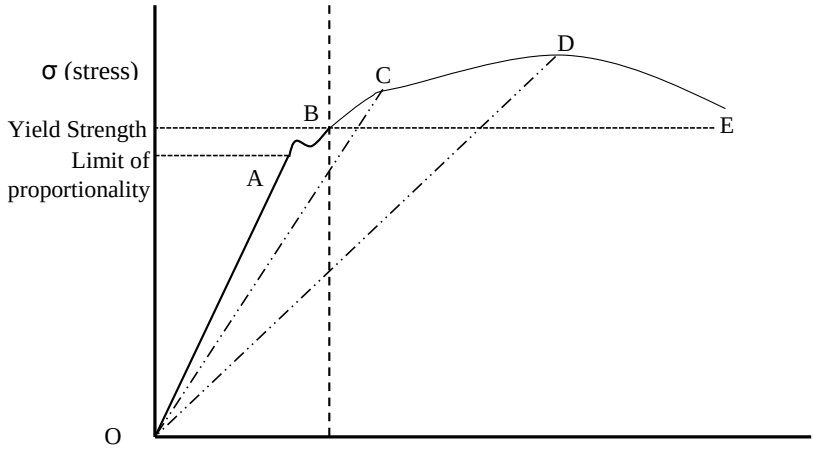

Figure 7-6. Illustrating the plastic deformation of a material

The results for various levels of reduced Young's moduli are illustrated in Figure 7-7. It illustrates that indeed reduction of the effective stiffness induced by large scale yielding, significantly increases the predicted fracture angles over the entire range of crack angles. The shape of the curves do not entirely match the experimental results, but this evaluation seems to confirm that plasticity is the major contributor to the absence of correlation between the initial quasi-static model and the experiments.

The waviness of the predicted curves, seems to suggest that a more detailed elastic plastic analysis is required. This detailed analysis must account for the shift in yield surfaces under off-axis loading angles to capture the effect of plastic deformation in the transverse and shear directions. However, this detailed analysis is beyond the scope of this research, and must be investigated independently.

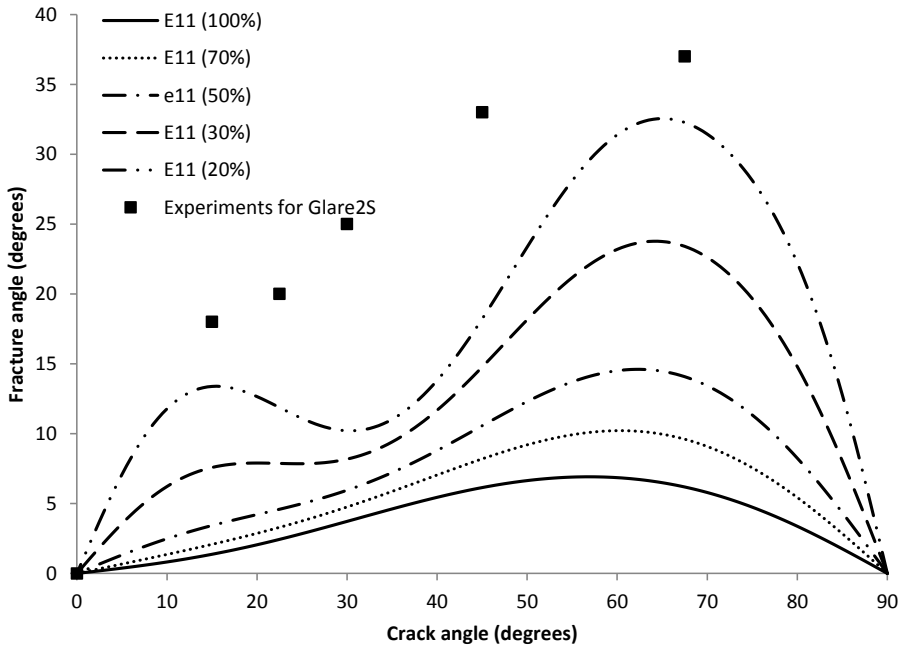

Figure 7-7. Comparing the change in fracture angle and Laminate's Young's modulus in Glare2S with the crack angle

7.8 Conclusion

The objective of the chapter was to verify the hypothesis whether the laminate orthotropy alone predicts the crack paths in FMLs under off-axis quasi-static loading. After the findings presented in this paper, it is concluded that the laminate orthotropy does not alone influence damage directionality in FMLs under off-axis quasi-static loading.

The analytical model developed for fatigue loading was applied without the fibre-bridging component also, i.e. it contained only the laminate orthotropy influence on the crack paths. The elimination of bridging resulted in a greater discrepancy with experimental results than the fracture angles predicted with the fatigue model. This illustrates that the amount of plasticity invalidates the assumption of small scale yielding in both models. The effect of reduced Young's modulli on the fracture angles was investigated to verify if plasticity did indeed affect fracture angles. The waviness observed in the predicted trend indicates proper yield zone models are required in consideration with classical laminate theories. As the objective of this chapter was to mainly highlight that the fatigue model cannot be used for predicting crack paths in FMLs under quasi-static off-axis loading. In support of this hypothesis a simulation was done by reducing Young's modulus of the laminate in the model. This was done so that plastic part of the stress-strain curve could be simulated in the model.

In doing so it was observed that the trend of the predicted curve started to change. As the plasticity was further increased in the model, the fit to the experimentally observed angles. A

good fit was observed at 20% of the original young's modulus, however, I would like to mention that this is unrealistic. But, it should also be noted that in reality fracture occurs non-linearly and in an exponential fashion. The exponential nature of the plastic curve could achieve a better fit at a higher young's modulus than 20% modulus as observed in this exercise.

It should also be noted that there could be other phenomena also that cause the crack paths under quasi-static loading to behave differently than under fatigue loading. However, as understanding the behaviour of crack paths under quasi-static loading is not the main objective of this thesis, therefore, the author has limited the discussion on those other phenomena in this thesis.

8 Chapter 8: Conclusions

8.1 Conclusions

The primary objective of the research was to develop understanding of the mechanisms affecting damage directionality of Fibre Metal Laminates (FMLs) under off-axis loading. Effect of laminate orthotropy under off-axis loading causes the principal axis of the laminate to be at an angle with respect to the loading axis. This causes the crack to deflect. Additionally, the effect of fibre-bridging in the transverse directions affects the strain field at the crack tip in the laminate. This creates a mixed-mode at the crack tip which causes the crack paths to deflect from their expected traverse path. Therefore, it was concluded that the damage directionality in FMLs is affected by both the laminate orthotropy and fibre-bridging in the off-axis direction.

T-stress crack path theory in its current form is unsuitable to predict crack paths in FMLs, and in metals. It was concluded that T-stress can be used as a constraint parameter for crack growth, however, its sign cannot be used to predict whether a crack would deflect or traverse straight.

The effect of the laminate orthotropy and fibre-bridging mechanisms was developed in an analytical model that predicts the crack path in FMLs under off-axis loading. These results were compared with experimental results conducted in this research and in previous studies. It was seen that the trend of fracture angles predicted from the implemented model matches the experimentally observed fracture angle. In terms of the values predicted there is a difference between the model and the experimental results. However, these errors are within 4° of the predicted value except for Glare2A under 67.5° off-axis angle where is differs by 7°. The cause of these errors were discussed in Section 5.6.

The observed fracture angles are generally small in biaxial Glare grades – Glare3B and Glare4B, and can be considered negligible by the manufacturers under fatigue loading. The added value from this thesis is that the manufacturers can ignore these minor deflections. For Glare2A, the deflections are larger and can become significant due to the change in the off-axis angle at the lower wing applications. Therefore, the understanding of the crack deflection mechanisms in FMLs under off-axis loading developed in this doctoral work should enable to make decisions about when crack deflections can be ignored and when they should not be ignored.

The analytical model was developed for fatigue loading, and its limitations in application to quasi-static loading were highlighted in Chapter 7 of this thesis. It was shown that laminate orthotropy does not alone influence the crack paths in FMLs under quasi-static loading. Under quasi-static loading plasticity develops in the laminate. Due to the plasticity, the stress-strain relationship becomes non-linear. Due to the non-linearity, the analytical model developed in this thesis using LEFM fails to predict the crack path in FMLs under quasi-static loading. To overcome this limitation, plasticity effects must be introduced into the developed analytical model. However, as understanding the behaviour of crack paths under quasi-static loading is not the main objective of this thesis, therefore, the author has limited the discussion on those other phenomena in this thesis.

8.2 Recommendations for future work

In the current study, the damage in FMLs was limited to the case of through-thickness cracks. In practice, cracks initiate from surface cracks, particularly, in aircraft structures. Understanding the surface crack behaviour under off-axis loading should provide knowledge for the application of this research to real application of FMLs. This research was developed with the principle of averaged fibre bridging effect, i.e. all metal layers and fibre layers were averaged as single layers of metals and fibres. However, with surface cracks, this principle may not be applicable. This is because in surface cracks, the crack at the surface of the laminate will only be bridged by the fibre layer adjacent to it, and not by entire prepreg between two metal layers in through thickness crack.

Furthermore, with the huge growth of investment in the predictive maintenance and Structural Health Monitoring (SHM) for aircraft maintenances, the developed analytical model can be used to monitor crack paths in real time operations. With SHM systems, crack growth in flight will be used as input data for the developed analytical model. The analytical model will be able to predict the direction of crack propagation during flight. Additional capabilities such as deviation between real data and predicted crack path could provide more functionalities and application to the maintenance as required by them.

An initial attempt has been made in Chapter 7 to investigate the difference between fatigue and quasi-static behaviour of FMLs under off-axis loading. It was shown that both fatigue and laminate orthotropy cannot predict the crack path observed under quasi-static loading. It was shown that under quasi-static loading plasticity has significant influence on the crack paths also. Therefore, it is recommended to make a detailed investigation on the quasi-static loading behaviour of FMLs under off-axis loading.

Bibliography

1. **Marissen, R. "Fatigue crack growth in ARALL, A hybrid aluminium-aramid composite material, crack growth mechanisms and quantitative predictions of the crack growth rate," *Department of Structural Integrity*. Vol. Doctor of Philosophy, Technische Universiteit, Delft, 1988.**
2. **Alderliesten, R. "Fatigue Crack Propagation and Delamination Growth in Glare," *Faculty of Aerospace Engineering*. Vol. Doctor of Philosophy, Technische Universiteit, Delft, 2005.**
3. **Wilson, G. S., Alderliesten, R. C., and Benedictus, R. "A generalized solution to the crack bridging problem of fiber metal laminates," *Engineering Fracture Mechanics*, No. 0.**
4. **Rodi, R. "The Residual Strength of Failure Sequence in Fibre Metal Laminates," *Department of Structural Integrity and Composites*. Vol. Doctor of Philosophy, Delft University of Technology, Delft, 2012.**
5. **Khan, S. U. "Fatigue crack and delamination growth in fibre metal laminates under variable amplitude loading," *Departmeft of Aerospace Materials and Manufacturing*. Vol. PhD thesis, Delft University of Technology, Delft, 2013.**
6. **Gonesh, K. "Test results and evaluation of crack propagation in off-axis Glare." Technische Universiteit, Delft, 2001.**
7. **Gonesh, K. "Additional test results and evaluation of crack propagation in off-axis Glare." Technische Universiteit, Delft, 2002.**
8. **Zaal, K. J. J. M. "The two-bay crack problem in fuselages built in GLARE and ARALL." Technische Universiteit, Delft, 1991.**
9. **Zaal, K. J. J. M. "An experimental study of the angled crack in GLARE 3." Technische Universiteit, Delft, 1993.**
10. **Kawai, M., and Arai, Y. "Off-axis notched strength of fiber–metal laminates and a formula for predicting anisotropic size effect," *Composites Part A: Applied Science and Manufacturing* Vol. 40, No. 12, 2009, pp. 1900-1910.**
11. **Thibault-Liboiron, K., Alederliesten, R.C., Benedictus, R., . "Off-axis crack propagation and delamination growth in FML's," *6th Canadian-International Composites Conference*. Winnipeg, Canada, 2007.**
12. **Tinga, T., Schra, L. "Off-axis residual strength of Glare laminates Part 1:Experimental results Glare4B-4/3-0.4." 2003.**
13. **R. Rodi, G. W., R.C. Alderliesten, R. Benedictus. "The effects of the fibre bridging on the entire strain field of fatigue cracks in fibre metal laminates."**
14. **Kawai, M., and Kato, K. "Effects of R-ratio on the off-axis fatigue behavior of unidirectional hybrid GFRP/Al laminates at room temperature," *International Journal of Fatigue* Vol. 28, No. 10, 2006, pp. 1226-1238.**
15. **Zaal, K. J. J. M. "A survey of crack path stability criteria and their application to crack flapping phenomena in stiffened strcutures." Technische Universiteit, Delft, 1992.**
16. **Greg Wilson, R. A., Riccardo Rodi, H.J.K. Lemmen. "Practical Applications of Improvements in FML crack bridging theory," *25th International Conference on Aeronautical Fatigue*. Rotterdam 2009.**
17. **Wilson, G., Alderliesten, R.C., Benedictus, R., . "A generlaized solution to the Crack Bridging Problem of Fiber Metal Laminates," Paper to be submitted.**
18. **Erdogan, F. "On the stress distribution on plates with collinear cuts under arbitrary load," *Fourth national conference on applied mechanics*. 1962, p. 547.**
19. **Erdogan, F., Sih, G.C. "On the crack extension in plates under plane loading and transverse shear," *Journal of Basic Engineering*, 1963, pp. 519 - 527.**
20. **Cotterell, B. "Notes on Paths and Stability of Cracks," *International Journal of Fracture Mechanics* Vol. 2, No. 3, 1966, pp. 526 - 533.**
21. **Sih, G. C. "Strain-energy-density factor applied to mixed mode crack problems," *International Journal of Fracture* Vol. 10, No. 3, 1974, pp. 305-321.**
22. **Broberg, K. B. "On crack paths," *Engineering Fracture Mechanics* Vol. 28, No. 5-6, 1987, pp. 663-679.**
23. **Vlot, A., Gunnink, J.W. *Fibre Metal Laminates an Introduction*. Dordrecht: Kluwer Academic Publishers, 2001.**
24. **Homan, J. J. "Fatigue initiation in fibre metal laminates," *International Journal of Fatigue* Vol. 28, No. 4, 2006, pp. 366-374.**
25. **Alderliesten, R. C. "Analytical prediction model for fatigue crack propagation and delamination growth in Glare," *International Journal of Fatigue* Vol. 29, 2007.**
26. **Schijve, J. *Fatigue of structure and materials*: Springer science+business media, 2003.**

27. **Guo, Y.-J., and Wu, X.-R. "Bridging stress distribution in center-cracked fiber reinforced metal laminates: modeling and experiment," *Engineering Fracture Mechanics* Vol. 63, No. 2, 1999, pp. 147-163.**
28. **Vasek, A., Polak, J., Kozak, V. "Fatigue crack initation in fibre-metal laminate GLARE2," *Material Science and Engineering*, 1997, pp. A234-A236.**
29. **Alderliesten, R. C. "Fatigue and damage tolerance of hybrid materials and structures - some myths, facts and fairy tales," *International conference on aeronautical fatigue, 2009*. Rotterdam, 2009.**
30. **Spronk, S. W. F., Şen, I., and Alderliesten, R. C. "Predicting fatigue crack initiation in fibre metal laminates based on metal fatigue test data," *International Journal of Fatigue* Vol. 70, No. 0, 2015, pp. 428-439.**
31. **Lekhnitskii, S. G., ed. *Theor of Elasticity of an Anisotropic Elastic Body*: Mir Publishers, 1964.**
32. **Guo, Y. J., and Wu, X. R. "A theoretical model for predicting fatigue crack and growth rates in fibre- reinforced metal laminates," *Fatigue & Fracture of Engineering Materials & Structures* Vol. 21, No. 9, 1998, pp. 1133-1145.**
33. **Swift, T. "Damage tolerance in pressurised fuselages," *14th Symposium of the ICAF, New Materials and Fatigue Resistant Aircraft Design*. Ottawa, Canada, 1987.**
34. **Swift, T. "The application of fracture mechanics in the development of the DC-10 fuselage," *Fracture Mechanics of Aircraft Structures, AGARD=AG-176*, 1974.**
35. **Petitt, R. G. "Crack turning in integrally stiffened aircraft structures." Vol. Doctor of Philosophy, Cornell University, New York, 2000.**
36. **Pettit, R. G., Chen, C. S., Ingraffea, A. R., and Hui, C. Y. "Process zone size effects on naturally curving cracks," *Engineering Fracture Mechanics* Vol. 68, No. 10, 2001, pp. 1181-1205.**
37. **Irwin, G. R. *"Fracture," in Handbuch der Physik VI*, 1958.**
38. **Irwin, G. R. "Analysis of stresses and strains near the end of a crack traversing a plate," *Journal of Applied Mechanics*, 1957, pp. 361-364.**
39. **Griffith, A. A. "The phenomenon of rupture and flow in solids," *Transaction of royal soceity*, 1921, pp. 163 - 198.**
40. **Irwin, G. R., Kies, J. "Fracturing and Fracture Mechanics," *Welding Journal - Research Supplement* Vol. 31, No. February, 1952, pp. 95s - 1002.**
41. **Tada, H., Paris, P.C., Irwin, G.R. "The Stress Analysis of Cracks Handbook." Third Edition ed., American Society of Mechanical Engineers, New York, 2000.**
42. **Westergaard. "Bearing pressure and cracks," *Journal of Applied Mechanics* Vol. 6, 1939, pp. A49-A53.**
43. **Williams, J., Ewing, P. D. "Fracture Under Complex Stress - Angled Crack Problem," *International Journal of Fracture Mechanics* Vol. 8, No. 4, 1972, pp. 441 - 446.**
44. **Sih, G. C. "On Cracks in Rectilinearly Anisotropic Bodies," *International Journal of Fracture Mechanics* Vol. 1, No. 3, 1965, pp. 189 - 203.**
45. **Finnie, I., and Saith, A. "A note on the angled crack problem and the directional stability of cracks," *International Journal of Fracture* Vol. 9, No. 4, 1973, pp. 484-486.**
46. **Ewing, P. D., and Williams, J. G. "Further observations on the angled crack problem," *International Journal of Fracture* Vol. 10, No. 1, 1974, pp. 135-135.**
47. **Ewing, P. D., Swedlow, J. L., and Williams, J. G. "Further results on the angled crack problem," *International Journal of Fracture* Vol. 12, No. 1, 1976, pp. 85-93.**
48. **Cotterell, B. "On brittle fracture paths," *international Journal of Fracture Mechanics* Vol. 1, No. 2, 1965, pp. 96-103.**
49. **Hussain, M. A., Pu. S. L., and Underwood, J. "Strain-Energy release rate for a crack under combined Mode I and Mode II," *ASTM*, 1974.**
50. **Wu, C. H. "Fracture Under Combined Loads by Maximum-Energy-Release-Rate Criterion," *Journal of Applied Mechanics* Vol. 45, No. 3, 1978, pp. 553-558.**
51. **Sih, G. C. "A special theory of crack propagation Mechanics of Fracture Initiation and Propagation." Vol. 11, Springer Netherlands, 1991, pp. 1-22.**
52. **Sih, G. C. "Some basic problems in fracture mechanics and new concepts," *Engineering Fracture Mechanics* Vol. 5, No. 2, 1973, pp. 365-377.**
53. **Cotterell, B., and Rice, J. R. "Slightly curved or kinked cracks," *International Journal of Fracture* Vol. 16, No. 2, 1980, pp. 155-169.**
54. **Sumi, Y., Nemat-Nasser, S., and Keer, L. M. "On crack path stability in a finite body," *Engineering Fracture Mechanics* Vol. 22, No. 5, 1985, pp. 759-771.**
55. **Streit, R., and Finnie, I. "An experimental investigation of crack-path directional stability," *Experimental Mechanics* Vol. 20, No. 1, 1980, pp. 17-23.**

56. **Goldstein, R., and Salganik, R. L. "Brittle-fracture of solids with arbitrary cracks," *International Journal of Fracture* Vol. 10, No. 4, 1974, pp. 507-523.**

57. **Sumi, Y., Nemat-Nasser, S., and Keer, L. M. "On crack branching and curving in a finite body," *International Journal of Fracture* Vol. 21, No. 1, 1983, pp. 67-79.**

58. **Theocaris, P. S., and Andrianopoulos, N. P. "The T-criterion applied to ductile fracture," *International Journal of Fracture* Vol. 20, No. 4, 1982, pp. R125-R130.**

59. **Nabil A.B, Y. "On the use of the T-criterion in fracture mechanics," *Engineering Fracture Mechanics* Vol. 22, No. 2, 1985, pp. 189-199.**

60. **Theocaris, P. S., and Philippidis, T. P. "Mixed-mode fracture mechanics of anisotropic plates by means of the T-criterion," *International Journal of Fracture* Vol. 52, No. 3, 1991, pp. 223-237.**

61. **Hayashi K., N. N. S. "Energy-release rate and crack kinking under combined loading," *Journal of Applied Mechanics* Vol. 48, 1981.**

62. **Gupta, G. D. "1976," *ASME* Strain-Energy release rate for Mixed Mode crack problem.**

63. **Wu, C. H. "Fracture under combined loads by maximum energy release rate criterion," *Journal of Elasticity* Vol. 8, 1978.**

64. **Nemat-Nasser, S. "The second law of thermodynamics and non-collinear crack growth," *Proceedings to Third Engineering Mechanics, Division Specialty Conference*. Unviersity of Texas at Austin, 1979, pp. 449 - 452.**

65. **Stamenkovic, D., Maksimovic, K., Nikolic-Stanojevic, V., Maksimovic, S., Stupar, S., and Vasovic, I. "Fatigue Life Estimation of Notched Structural Components," *Strojniski Vestnik-Journal of Mechanical Engineering* Vol. 56, No. 12, 2010, pp. 846-852.**

66. **Maksimovic, S., Maksimovic, K. "Improved computation method in residual life estimation of structural components, theoretical and applied mechanics," *Special issue of theoretical and applied mechanics* Vol. 40, 2012, pp. 223 - 246.**

67. **Azhdari, A., and Nemat-Nasser, S. "Energy-release rate and crack kinking in anisotropic brittle solids," *Journal of the Mechanics and Physics of Solids* Vol. 44, No. 6, 1996, pp. 929-951.**

68. **Sih, G. C., and Chen, E. P. "Dilatational and distortional behavior of cracks in magnetoelectroelastic materials," *Theoretical and Applied Fracture Mechanics* Vol. 40, No. 1, 2003, pp. 1-21.**

69. **Sih, G. C., and Chu, R. C. "Characterization of material inhomogeneity by stationary values of strain energy density," *Theoretical and Applied Fracture Mechanics* Vol. 5, No. 3, 1986, pp. 151-161.**

70. **Sih, G. C., and Chue, C. H. "Stability and integrity of mechanical joints in flight vehicles: Local and global energy density," *Theoretical and Applied Fracture Mechanics* Vol. 10, No. 2, 1988, pp. 135-149.**

71. **Theocaris, P. S., and Andrianopoulos, N. P. "Authors' closure on the discussion by G. C. Sih, E. T. Moyer Jr. and E. E. Gdoutos of "the mises elastic-plastic boundary as the core region in fracture criteria"," *Engineering Fracture Mechanics* Vol. 20, No. 4, 1984, pp. 691-694.**

72. **Theocaris, P. S., and Andrianopoulos, N. P. "The mises elastic-plastic boundary as the core region in fracture criteria," *Engineering Fracture Mechanics* Vol. 16, No. 3, 1982, pp. 425-432.**

73. **Benbow, J. J., and Roesler, F. C. "Experiments on controlled fractures," *Proceedings of the Physical Society of London Section B* Vol. 70, No. 2, 1957, pp. 201-&.**

74. **Rice, J. R. "Mechanics of crack tip formation and extension, Fatigue crack propgation," *ASTM*, 1967.**

75. **Roesler, F. C. "Brittel fractures near equilibrium," *Proceedings of the Physical Society of London Section B* Vol. 69, No. 10, 1956, pp. 981-&.**

76. **Li, X.-F., Liu, G.-L., and Lee, K. "Effects of T-stresses on fracture initiation for a closed crack in compression with frictional crack faces," *International Journal of Fracture* Vol. 160, No. 1, 2009, pp. 19-30.**

77. **A. R. Shahani, S. A. T. "Effect of T-stress on the fracture of a four point bend specimen," *Materials and Design* Vol. 30, 2009.**

78. **Leguillon, D., and Murer, S. "Crack deflection in a biaxial stress state," *International Journal of Fracture* Vol. 150, No. 1, 2008, pp. 75-90.**

79. **Jayadevan, K. R., Narasimhan, R., Ramamurthy, T. S., and Dattaguru, B. "A numerical study of T-stress in dynamically loaded fracture specimens," *International Journal of Solids and Structures* Vol. 38, No. 28-29, 2001, pp. 4987-5005.**

80. **Jayadevan, K. R., Narasimhan, R., Ramamurthy, T. S., and Dattaguru, B. "Effect of T-stress and loading rate on crack initiation in rate sensitive plastic materials," *International Journal of Solids and Structures* Vol. 39, No. 7, 2002, pp. 1757-1775.**

81. **Jayadevan, K. R., Narasimhan, R., Ramamurthy, T. S., and Dattaguru, B. "The effect of T-stress on plane strain dynamic crack growth in elastic-plastic materials," *Fatigue & Fracture of Engineering Materials & Structures* Vol. 26, No. 7, 2003, pp. 647-660.**

82. **Kawai, M., Hachinohe, A., Takumida, K., and Kawase, Y. "Off-axis fatigue behaviour and its damage mechanics modelling for unidirectional fibre–metal hybrid composite: GLARE 2," *Composites Part A: Applied Science and Manufacturing* Vol. 32, No. 1, 2001, pp. 13-23.**

83. **M. Gupta, R. C. A., R. Benedictus. "Understanding the role of T-stress in Linear Elastic Fracture Mechanics," *Engineering Fracture Mechanics*, 2013.**

84. **Hutchinson, J. W., Suo, Z. "Mixed mode cracking in layered materials," *Advances in Applied Mechanics* Vol. 29, 1992.**

85. **Melin, S. "The influence of the T-stress on the directional stability of cracks," *International Journal of Fracture* Vol. 114, No. 3, 2002, pp. 259-265.**

86. **Smith, D. J., Ayatollahi, M. R., and Pavier, M. J. "On the consequences of T-stress in elastic brittle fracture," *Proceedings of the Royal Society A: Mathematical, Physical and Engineering Science* Vol. 462, No. 2072, 2006, pp. 2415-2437.**

87. **Larsson, S. G., and Carlsson, A. J. "Influence of non-singular stress terms and specimen geometry on small-scale yielding at crack tips in elastic-plastic materials," *Journal of the Mechanics and Physics of Solids* Vol. 21, No. 4, 1973, pp. 263-277.**

88. **Zhou, R., Zhu, P., and Li, Z. "The Shielding Effect of the Plastic Zone at Mode-II Crack Tip," *International Journal of Fracture* Vol. 171, No. 2, 2011, pp. 195-200.**

89. **Sherry, A. H., France, C. C., and Goldthorpe, M. R. "Compendium of T-stress solutions for two and three dimensional cracked geometries," *Fatigue & Fracture of Engineering Materials & Structures* Vol. 18, No. 1, 1995, pp. 141-155.**

90. **Chen, Y. Z. "Integral equation methods for multiple crack problems and related topics," *Applied Mechanics Reviews* Vol. 60, No. 1-6, 2007, pp. 172-194.**

91. **Wells, A. A., Post, D. "The dynamic stress distribution surrounding a running crack - A photoelastic analysis," *Proceedings of the society for experimental stress analysis* Vol. 16, No. 1, 1958, pp. 93-96.**

92. **Williams, M. L. "Stress distribution at the base of a stationary crack," *Journal of Applied Mechanics*. 1957, pp. 109 - 114.**

93. **Pham, V. B., Bahr, H. A., Bahr, U., Fett, T., and Balke, H. "Crack paths and the problem of global directional stability," *International Journal of Fracture* Vol. 141, No. 3-4, 2006, pp. 513-534.**

94. **Ramesh, K. "Generalised Westergaard approach." Vol. 2012, Chennai, India, 2012.**

95. **Ramesh, K., Gupta, S., and Kelkar, A. A. "Evaluation of stress field parameters in fracture mechanics by photoelasticity—Revisited," *Engineering Fracture Mechanics* Vol. 56, No. 1, 1997, pp. 25-45.**

96. **Sanford, R. J. "A critical re-examination of the westergaard method for solving opening-mode crack problems," *Mechanics Research Communications* Vol. 6, No. 5, 1979, pp. 289-294.**

97. **Atluri, S. N., Kobayashi, A. S. "Mechanical response of materials," *Handbook On Experimental Mechanics*. Prentice-Hall, 1987.**

98. **Christopher, C. J., James, M. N., Patterson, E. A., and Tee, K. F. "A quantitative evaluation of fatigue crack shielding forces using photoelasticity," *Engineering Fracture Mechanics* Vol. 75, No. 14, 2008, pp. 4190-4199.**

99. **Han, J. J., and Chen, Y. H. "T-effect for the interaction problem of an interface macrocrack with a near-tip microvoid," *International Journal of Fracture* Vol. 102, No. 3, 2000, pp. 205-222.**

100. **Colombo, C., Du, Y., James, M. N., Patterson, E. A., and Vergani, L. "On crack tip shielding due to plasticity-induced closure during an overload," *Fatigue & Fracture of Engineering Materials & Structures* Vol. 33, No. 12, 2010, pp. 766-777.**

101. **Spaniel, M., Jurenka, J., and Kuzelka, J. "Verification of FE model of fatigue crack propagation under mixed mode conditions," *Meccanica* Vol. 44, No. 2, 2009, pp. 189-195.**

102. **Guernsey, R., and Gilman, J. "Photoelastic study of the stresses near a cleavage crack," *Experimental Mechanics* Vol. 1, No. 8, 1961, pp. 50-54.**

103. **Ayatollahi, M. R., and Safari, H. "Evaluation of crack tip constraint using photoelasticity," *International Journal of Pressure Vessels and Piping* Vol. 80, No. 9, 2003, pp. 665-670.**

104. **Ayatollahi, M. R., Smith, D. J., and Pavier, M. J. "Crack-tip constraint in mode II deformation," *International Journal of Fracture* Vol. 113, No. 2, 2002, pp. 153-173.**

105. **Zakeri, M., Ayatollahi, M. R., and Guagliano, M. "A Photoelastic Study of T-stress in Centrally Cracked Brazilian Disc Specimen Under Mode II Loading," *Strain* Vol. 47, No. 3, 2011, pp. 268-274.**

106. **Ayatollahi, M. R., and Zakeri, M. "T-Stress Effects on Isochromatic Fringe Patterns in Mode II," *International Journal of Fracture* Vol. 143, No. 2, 2007, pp. 189-194.**

107. **Zanaganeh M., T. M. A., Yates J R,. "T stress determination using thermoelastic stress analysis," *Journal of strain analysis for engineering* Vol. 43, 2008.**

108. **D. J. Smith, M. R. A., M. J. Pavier. "The role of T-stress in brittle fracture for linear elastic materials under mixed-mode loading," *Fatigue & Fracture of Engineering Materials & Structures*, 2001.**

109. **Leevers, P. S., Radon, J. C., and Culver, L. E. "Fracture trajectories in a biaxially stressed plate," *Journal of the Mechanics and Physics of Solids* Vol. 24, No. 6, 1976, pp. 381-395.**

110. **Leevers, P. S., Culver, L. E., and Radon, J. C. "Fatigue crack growth in PMMA and rigid PVC under biaxial stress," *Engineering Fracture Mechanics* Vol. 11, No. 3, 1979, pp. 487-498.**

111. **Leevers, P. S., and Radon, J. C. "Inherent stress biaxiality in various fracture specimen geometries," *International Journal of Fracture* Vol. 19, No. 4, 1982, pp. 311-325.**

112. **Llopart, L., Kurz, B., Wellhausen, C., Anglada, M., Drechsler, K., and Wolf, K. "Investigation of fatigue crack growth and crack turning on integral stiffened structures under mode I loading," *Engineering Fracture Mechanics* Vol. 73, No. 15, 2006, pp. 2139-2152.**

113. **Matvienko, Y. G. "Maximum Average Tangential Stress Criterion for Prediction of the Crack Path," *International Journal of Fracture* Vol. 176, No. 1, 2012, pp. 113-118.**

114. **Ki Ju, K. "Criteria for kinking out of interface crack," *Engineering Fracture Mechanics* Vol. 49, No. 4, 1994, pp. 587-598.**

115. **Hallback, N., Nilsson, F. "Mixed-mode I/II fracture behaviour of an aluminium alloy," *Journal of Mechanics of Physics and solids* Vol. 42, No. 9, 1994, pp. 1345-1374.**

116. **Joyce, J. A. "Experimental justification for proposed changes to the measurement of K-Ic using ASTM E 399," *Journal of Testing and Evaluation* Vol. 26, No. 5, 1998, pp. 455-462.**

117. **Yang, B., and Ravi-Chandar, K. "Evaluation of elastic T-stress by the stress difference method," *Engineering Fracture Mechanics* Vol. 64, No. 5, 1999, pp. 589-605.**

118. **Yang, B., and Ravi-Chandar, K. "Crack path instabilities in a quenched glass plate," *Journal of the Mechanics and Physics of Solids* Vol. 49, No. 1, 2001, pp. 91-130.**

119. **Shin, D. K., and Lee, J. J. "Fracture parameters of interfacial crack of bimaterial under the impact loading," *International Journal of Solids and Structures* Vol. 38, No. 30-31, 2001, pp. 5303-5322.**

120. **Yoneyama, S., Sakaue, K., Kikuta, H., and Takashi, M. "Instantaneous phase-stepping photoelasticity for the study of crack growth behaviour in a quenched thin glass plate," *Measurement Science & Technology* Vol. 17, No. 12, 2006, pp. 3309-3316.**

121. **Sakaue, K., Yoneyama, S., Kikuta, H., and Takashi, M. "Evaluating crack tip stress field in a thin glass plate under thermal load," *Engineering Fracture Mechanics* Vol. 75, No. 5, 2008, pp. 1015-1026.**

122. **Yoneyama, S., Sakaue, K., Kikuta, H., and Takashi, M. "Observation of stress field around an oscillating crack tip in a quenched thin glass plate," *Experimental Mechanics* Vol. 48, No. 3, 2008, pp. 367-374.**

123. **Guduru, V., Phan, A. V., and Tippur, H. V. "Transient analysis of the DSIFs and dynamic T-stress for particulate composite materials-Numerical vs. experimental results," *Engineering Analysis with Boundary Elements* Vol. 34, No. 11, 2010, pp. 963-970.**

124. **Xu, L. R., and Wang, P. "Dynamic fracture mechanics analysis of failure mode transitions along weakened interfaces in elastic solids," *Engineering Fracture Mechanics* Vol. 73, No. 12, 2006, pp. 1597-1614.**

125. **Ayatollahi, M. R., and Aliha, M. R. M. "Cracked Brazilian disc specimen subjected to mode II deformation," *Engineering Fracture Mechanics* Vol. 72, No. 4, 2005, pp. 493-503.**

126. **Ayatollahi, M. R., Asadkarami, A., and Zakeri, M. "Finite element evaluation of punch-type crack specimens," *International Journal of Pressure Vessels and Piping* Vol. 82, No. 9, 2005, pp. 722-728.**

127. **Ayatollahi, M. R., and Aliha, M. R. M. "On determination of mode II fracture toughness using semi-circular bend specimen," *International Journal of Solids and Structures* Vol. 43, No. 17, 2006, pp. 5217-5227.**

128. **Ayatollahi, M. R., Zakeri M. "T stress effects on isochromatic fringe patterns in Mode II," *International Journal of Fatigue* Vol. 143, 2007.**

129. **Ayatollahi, M. R., and Aliha, M. R. M. "Fracture toughness study for a brittle rock subjected to mixed mode I/II loading," *International Journal of Rock Mechanics and Mining Sciences* Vol. 44, No. 4, 2007, pp. 617-624.**

130. **Ayatollahi, M. R., and Aliha, M. R. M. "Wide range data for crack tip parameters in two disc-type specimens under mixed mode loading," *Computational Materials Science* Vol. 38, No. 4, 2007, pp. 660-670.**

131. **Ayatollahi, M. R., and Hashemi, R. "Mixed mode fracture in an inclined center crack repaired by composite patching," *Composite Structures* Vol. 81, No. 2, 2007, pp. 264-273.**

132. **Ayatollahi, M. R., and Hashemi, R. "Computation of stress intensity factors (K-I, K-II) and T-stress for cracks reinforced by composite patching," *Composite Structures* Vol. 78, No. 4, 2007, pp. 602-609.**

133. **Zakeri, M., Ayatollahi, M. R., and Nikoobin, A. "Photoelastic study of a center-cracked plate - The lateral load effects," *Computational Materials Science* Vol. 41, No. 2, 2007, pp. 168-176.**

134. **Aliha, M. R. M., and Ayatollahi, M. R. "On mixed-mode I/II crack growth in dental resin materials," *Scripta Materialia* Vol. 59, No. 2, 2008, pp. 258-261.**

135. **Ayatollahi, M. R., and Aliha, M. R. M. "Mixed mode fracture analysis of polycrystalline graphite - A modified MTS criterion," *Carbon* Vol. 46, No. 10, 2008, pp. 1302-1308.**

136. **Ayatollahi, M. R., and Aliha, M. R. M. "On the use of Brazilian disc specimen for calculating mixed mode I-II fracture toughness of rock materials," *Engineering Fracture Mechanics* Vol. 75, No. 16, 2008, pp. 4631-4641.**

137. **Ayatollahi, M. R., and Bagherifard, S. "Brittle fracture analysis of the offset-crack DCDC specimen," *Structural Engineering and Mechanics* Vol. 29, No. 3, 2008, pp. 301-310.**

138. **Aliha, M. R. M., and Ayatollahi, M. R. "Brittle fracture evaluation of a fine grain cement mortar in combined tensile-shear deformation," *Fatigue & Fracture of Engineering Materials & Structures* Vol. 32, No. 12, 2009, pp. 987-994.**

139. **Aliha, M. R. M., Ayatollahi, M. R., and Kharazi, B. "Mode II Brittle Fracture Assessment Using ASFPB Specimen," *International Journal of Fracture* Vol. 159, No. 2, 2009, pp. 241-246.**

140. **Ayatollahi, M. R., and Aliha, M. R. M. "Mixed mode fracture in soda lime glass analyzed by using the generalized MTS criterion," *International Journal of Solids and Structures* Vol. 46, No. 2, 2009, pp. 311-321.**

141. **Ayatollahi, M. R., and Aliha, M. R. M. "Analysis of a new specimen for mixed mode fracture tests on brittle materials," *Engineering Fracture Mechanics* Vol. 76, No. 11, 2009, pp. 1563-1573.**

142. **Ayatollahi, M. R., and Bagherifard, S. "Numerical analysis of an improved DCDC specimen for investigating mixed mode fracture in ceramic materials," *Computational Materials Science* Vol. 46, No. 1, 2009, pp. 180-185.**

143. **Mostafavi, M., Smith, D. J., and Pavier, M. J. "Quantification of constraint effects in fracture mechanism transition for cracked structures under mixed mode loading," *Fatigue & Fracture of Engineering Materials & Structures* Vol. 32, No. 1, 2009, pp. 5-17.**

144. **Aliha, M. R. M., and Ayatollahi, M. R. "Geometry effects on fracture behaviour of polymethyl methacrylate," *Materials Science and Engineering a-Structural Materials Properties Microstructure and Processing* Vol. 527, No. 3, 2010, pp. 526-530.**

145. **Ayatollahi, M. R., and Dehghany, M. "On T-Stresses Near V-Notches," *International Journal of Fracture* Vol. 165, No. 1, 2010, pp. 121-126.**

146. **Ayatollahi, M. R., and Sedighiani, K. "Crack tip plastic zone under Mode I, Mode II and mixed mode (I plus II) conditions," *Structural Engineering and Mechanics* Vol. 36, No. 5, 2010, pp. 575-598.**

147. **Ayatollahi, M. R., and Torabi, A. R. "Determination of mode II fracture toughness for U-shaped notches using Brazilian disc specimen," *International Journal of Solids and Structures* Vol. 47, No. 3-4, 2010, pp. 454-465.**

148. **Saghafi, H., Ayatollahi, M. R., and Sistaninia, M. "A modified MTS criterion (MMTS) for mixed-mode fracture toughness assessment of brittle materials," *Materials Science and Engineering a-Structural Materials Properties Microstructure and Processing* Vol. 527, No. 21-22, 2010, pp. 5624-5630.**

149. **Ayatollahi, M. R., and Aliha, M. R. M. "Fracture Analysis of Some Ceramics Under Mixed Mode Loading," *Journal of the American Ceramic Society* Vol. 94, No. 2, 2011, pp. 561-569.**

150. **Ayatollahi, M. R., Aliha, M. R. M., and Saghafi, H. "An improved semi-circular bend specimen for investigating mixed mode brittle fracture," *Engineering Fracture Mechanics* Vol. 78, No. 1, 2011, pp. 110-123.**

151. **Ayatollahi, M. R., Dehghany, M., and Nejati, M. "Fracture analysis of V-notched components - Effects of first non-singular stress term," *International Journal of Solids and Structures* Vol. 48, No. 10, 2011, pp. 1579-1589.**

152. **Ayatollahi, M. R., and Nejati, M. "Determination of NSIFs and coefficients of higher order terms for sharp notches using finite element method," *International Journal of Mechanical Sciences* Vol. 53, No. 3, 2011, pp. 164-177.**
153. **Ayatollahi, M. R., and Nejati, M. "An over-deterministic method for calculation of coefficients of crack tip asymptotic field from finite element analysis," *Fatigue & Fracture of Engineering Materials & Structures* Vol. 34, No. 3, 2011, pp. 159-176.**
154. **Aliha, M. R. M., and Ayatollahi, M. R. "Analysis of fracture initiation angle in some cracked ceramics using the generalized maximum tangential stress criterion," *International Journal of Solids and Structures* Vol. 49, No. 13, 2012, pp. 1877-1883.**
155. **Ayatollahi, M. R., and Sedighiani, K. "A T-stress controlled specimen for mixed mode fracture experiments on brittle materials," *European Journal of Mechanics a-Solids* Vol. 36, 2012, pp. 83-93.**
156. **Saghafi, H., and Monemian, S. "A New Fracture Toughness Test Covering Mixed-Mode Conditions and Positive and Negative T-Stresses," *International Journal of Fracture* Vol. 165, No. 1, 2010, pp. 135-138.**
157. **Ayatollahi, M. R., Pavier, M. J., and Smith, D. J. "Mode I cracks subjected to large T-stresses," *International Journal of Fracture* Vol. 117, No. 2, 2002, pp. 159-174.**
158. **Chao, Y. J., Liu, S., and Broviak, B. J. "Brittle fracture: Variation of fracture toughness with constraint and crack curving under mode I conditions," *Experimental Mechanics* Vol. 41, No. 3, 2001, pp. 232-241.**
159. **Abanto-Bueno, J., and Lambros, J. "Parameters controlling fracture resistance in functionally graded materials under mode I loading," *International Journal of Solids and Structures* Vol. 43, No. 13, 2006, pp. 3920-3939.**
160. **Kobayashi, T., Morita, S., and Toda, H. "Fracture toughness evaluation and specimen size effect," *Materials Transactions Jim* Vol. 42, No. 1, 2001, pp. 52-57.**
161. **Tronskar, J. P., Mannan, M. A., and Lai, M. O. "Accounting for constraint effects in fracture mechanics analysis of floating production, storage and off-loading vessels and ships," *Engineering Fracture Mechanics* Vol. 69, No. 11, 2002, pp. 1219-1248.**
162. **Moustabchir, H., Azari, Z., Hariri, S., and Dmytrakh, I. "Experimental and computed stress distribution ahead of a notch in a pressure vessel: Application of T-stress conception," *Computational Materials Science* Vol. 58, 2012, pp. 59-66.**
163. **Srinivas, M., Kamat, S. V., and Rao, P. R. "Influence of mixed mode I/III loading on fracture toughness of mild steel at various strain rates," *Materials Science and Technology* Vol. 20, No. 2, 2004, pp. 235-242.**
164. **Jernkvist, L. O. "Fracture of wood under mixed mode loading II. Experimental investigation of Picea abies," *Engineering Fracture Mechanics* Vol. 68, No. 5, 2001, pp. 565-576.**
165. **Hohe, J., Hebel, J., Friedmann, V., and Siegele, D. "Probabilistic failure assessment of ferritic steels using the master curve approach including constraint effects," *Engineering Fracture Mechanics* Vol. 74, No. 8, 2007, pp. 1274-1292.**
166. **Sumpter, J. D. G., and Hancock, J. W. "Shallo crack toughness of HY80 welds - an analysis basde on T-stresses," *International Journal of Pressure Vessels and Piping* Vol. 45, No. 2, 1991, pp. 207-221.**
167. **Chang, Y.-S., Kim, Y.-J., and Stumpfrock, L. "Development of cleavage fracture toughness locus considering constraint effects," *KSME International Journal* Vol. 18, No. 12, 2004, pp. 2158-2173.**
168. **Hebel, J., Hohe, J., Friedmann, V., and Siegele, D. "Experimental and numerical analysis of in-plane and out-of-plane crack tip constraint characterization by secondary fracture parameters," *International Journal of Fracture* Vol. 146, No. 3, 2007, pp. 173-188.**
169. **Roos, E., Stumpfrock, L., Schuler, X., and Eisele, U. "Fracture mechanics safety analysis of components based on fracture mechanics characteristics combined with multiaxiality of the stress state," *International Journal of Pressure Vessels and Piping* Vol. 82, No. 5, 2005, pp. 355-362.**
170. **Gao, X., Dodds, R. H., Tregoning, R. L., and Joyce, J. A. "Prediction of the T0 Shift between Specimens of Different Constraints Using the T-Stress Based T-Functions," *International Journal of Fracture* Vol. 104, No. 3, 2000, pp. 1-8.**
171. **Henry, B. S., Luxmoore, A. R., and Sumpter, J. D. G. "Elastic-plastic fracture mechanics assessment of low constraint aluminium test specimens," *International Journal of Fracture* Vol. 81, No. 3, 1996, pp. 217-234.**
172. **Henry, B. S., and Luxmoore, A. R. "Three-dimensional evaluation of the T-stress in centre cracked plates," *International Journal of Fracture* Vol. 70, No. 1, 1994, pp. 35-50.**

173. **Nilsson, K. F., Taylor, N., and Minnebo, P. "Analysis of fracture tests on large bend beams containing an embedded flaw," *International Journal of Pressure Vessels and Piping* Vol. 83, No. 1, 2006, pp. 72-83.**

174. **Wallin, K. "Quantifying T-stress controlled constraint by the master curve transition temperature T-0," *Engineering Fracture Mechanics* Vol. 68, No. 3, 2001, pp. 303-328.**

175. **Hallbäck, N., and Jönsson, N. "T-stress evaluations of mixed mode I/II fracture specimens and T-effects on mixed mode failure of aluminium," *International Journal of Fracture* Vol. 76, No. 2, 1995, pp. 141-168.**

176. **Wang, P., and Xu, L. R. "Dynamic interfacial debonding initiation induced by an incident crack," *International Journal of Solids and Structures* Vol. 43, No. 21, 2006, pp. 6535-6550.**

177. **Rice, J. R. "Limitations to the small scale yielding approximation for crack tip plasticity," *Journal of the Mechanics and Physics of Solids* Vol. 22, No. 1, 1974, pp. 17-26.**

178. **Ayatollahi, M. R., Pavier, M. J., and Smith, D. J. "Determination of T-stress from finite element analysis for mode I and mixed mode I/II loading," *International Journal of Fracture* Vol. 91, No. 3, 1998, pp. 283-298.**

179. **Wang, X. "Elastic T-stress for cracks in test specimens subjected to non-uniform stress distributions," *Engineering Fracture Mechanics* Vol. 69, 2002.**

180. **Tan, C. L., and Wang, X. "The use of quarter-point crack-tip elements for T-stress determination in boundary element method analysis," *Engineering Fracture Mechanics* Vol. 70, No. 15, 2003, pp. 2247-2252.**

181. **Parameswaran, V., and Sharma, S. "Estimation of fracture parameters and stress field for edge cracks in finite elastically graded plates using boundary collocation," *Acta Mechanica* Vol. 184, No. 1-4, 2006, pp. 159-170.**

182. **Pettit, R. G., Newman, J. C., and Domack, M. S. *Crack turning damage tolerance approach for integrally stiffened structure*. Sheffield: Engineering Materials Advisory Services Ltd, 1997.**

183. **Chen, C. S., Wawrzynek, P. A., and Ingraffea, A. R. "Prediction of residual strength and curvilinear crack growth in aircraft fuselages," *Aiaa Journal* Vol. 40, No. 8, 2002, pp. 1644-1652.**

184. **Becker, T. L., Cannon, R. M., and Ritchie, R. O. "Finite crack kinking and T-stresses in functionally graded materials," *International Journal of Solids and Structures* Vol. 38, No. 32-33, 2001, pp. 5545-5563.**

185. **Alani, A. M., and Hancock, J. W. "J-domination of short cracks in tension and bending," *Journal of the Mechanics and Physics of Solids* Vol. 39, No. 1, 1991, pp. 23-43.**

186. **Selvarathinam, A. S., and Goree, J. G. "T-stress based fracture model for cracks in isotropic materials," *Engineering Fracture Mechanics* Vol. 60, No. 5-6, 1998, pp. 543-561.**

187. **Zafosnik, B., Ren, Z., Flasker, J., and Mishuris, G. "Modelling of surface crack growth under lubricated rolling-sliding contact loading," *International Journal of Fracture* Vol. 134, No. 2, 2005, pp. 127-149.**

188. **Pehan, S., Kramberger, J., Flasker, J., and Zafosnik, B. "Investigation of crack propagation scatter in a gear tooth's root," *Engineering Fracture Mechanics* Vol. 75, No. 5, 2008, pp. 1266-1283.**

189. **Su, R. K. L., and Sun, H. Y. "A brief note on elastic T-stress for centred crack in anisotropic plate," *International Journal of Fracture* Vol. 131, No. 1, 2005, pp. 53-58.**

190. **Shim, D. J., Paulino, G. H., and Dodds, R. H. "A boundary layer framework considering material gradation effects," *Engineering Fracture Mechanics* Vol. 73, No. 5, 2006, pp. 593-615.**

191. **Shim, D. J., Paulino, G. H., and Dodds, R. H. "J resistance behavior in functionally graded materials using cohesive zone and modified boundary layer models," *International Journal of Fracture* Vol. 139, No. 1, 2006, pp. 91-117.**

192. **Kim, J. H., and Kc, A. "A generalized interaction integral method for the evaluation of the T-stress in orthotropic functionally graded materials under thermal loading," *Journal of Applied Mechanics-Transactions of the Asme* Vol. 75, No. 5, 2008.**

193. **Amit, K. C., and Kim, J. H. "Interaction integrals for thermal fracture of functionally graded materials," *Engineering Fracture Mechanics* Vol. 75, No. 8, 2008, pp. 2542-2565.**

194. **Zhang, S. C. "Stress intensity factors for spot welds joining sheets of unequal thickness," *International Journal of Fracture* Vol. 122, No. 1-2, 2003, pp. L119-L124.**

195. **Zhang, S. C. "T-stress and stress intensities for the interface cracks in some specimen-relevant geometries," *International Journal of Fracture* Vol. 111, No. 2, 2001, pp. L23-L28.**

196. **Radaj, D., and Zhang, S. "Stress intensity factors for spot welds between plates of unequal thickness," *Engineering Fracture Mechanics* Vol. 39, No. 2, 1991, pp. 391-413.**

197. **Lugo, M., and Daniewicz, S. R. "The influence of T-stress on plasticity induced crack closure under plane strain conditions," *International Journal of Fatigue* Vol. 33, No. 2, 2011, pp. 176-185.**

198. **Lee, H., and Kim, Y. J. "Interfacial crack-tip constraints and J-integrals in plastically mismatched bi-materials," *Engineering Fracture Mechanics* Vol. 68, No. 8, 2001, pp. 1013-1031.**

199. **Kim, J.-H., and Paulino, G. H. "T-stress, mixed-mode stress intensity factors, and crack initiation angles in functionally graded materials: a unified approach using the interaction integral method," *Computer Methods in Applied Mechanics and Engineering* Vol. 192, No. 11-12, 2003, pp. 1463-1494.**

200. **Chen, B., and Dillard, D. A. "Numerical analysis of directionally unstable crack propagation in adhesively bonded joints," *International Journal of Solids and Structures* Vol. 38, No. 38-39, 2001, pp. 6907-6924.**

201. **Chen, B., and Dillard, D. A. "The effect of the T-stress on crack path selection in adhesively bonded joints," *International Journal of Adhesion and Adhesives* Vol. 21, No. 5, 2001, pp. 357-368.**

202. **Chen, B., Dillard, D. A., Dillard, J. G., and Clark, R. L. "Crack path selection in adhesively-bonded joints: The role of material properties," *Journal of Adhesion* Vol. 75, No. 4, 2001, pp. 405-434.**

203. **Chen, B., Dillard, D. A., Dillard, J. G., and Clark, R. L. "Crack path selection in adhesively bonded joints: the roles of external loads and speciment geometry," *International Journal of Fracture* Vol. 114, No. 2, 2002, pp. 167-190.**

204. **Suo, Z., Bao, G., Fan, B., and Wang, T. C. "Orthotropy rescaling and implications for fracture in composites," *International Journal of Solids and Structures* Vol. 28, No. 2, 1991, pp. 235-248.**

205. **Wei, Y. "Constraint effects on the elastic-plastic fracture behaviour in strain gradient solids," *Fatigue & Fracture of Engineering Materials & Structures* Vol. 25, No. 5, 2002, pp. 433-444.**

206. **Wang, X. "Two-parameter characterization of elastic-plastic crack front fields: Surface cracked plates under uniaxial and biaxial bending," *Engineering Fracture Mechanics* Vol. 96, 2012, pp. 122-146.**

207. **Martin, J. T., and Lambert, S. B. "Analysis of constraint in single edge notch tension specimens using the T-stress," *International Journal of Pressure Vessels and Piping* Vol. 65, No. 1, 1996, pp. 13-19.**

208. **Andrews, R. M., and Garwood, S. J. "An analysis of fracture under biaxial loading using the non-singular T-stress," *Fatigue & Fracture of Engineering Materials & Structures* Vol. 24, No. 1, 2001, pp. 53-62.**

209. **Meliani, M. H., Azari, Z., Pluvinage, G., and Capelle, J. "Gouge assessment for pipes and associated transferability problem," *Engineering Failure Analysis* Vol. 17, No. 5, 2010, pp. 1117-1126.**

210. **Meliani, M. H., Matvienko, Y. G., and Pluvinage, G. "Two-parameter fracture criterion (K rho,c-Tef,c) based on notch fracture mechanics," *International Journal of Fracture* Vol. 167, No. 2, 2011, pp. 173-182.**

211. **Burstow, M. C., and Howard, I. C. "Predicting the effects of crack tip constraint on material resistance curves using ductile damage theory," *Fatigue & Fracture of Engineering Materials & Structures* Vol. 19, No. 4, 1996, pp. 461-474.**

212. **Burstow, M. C., Howard, I. C., and Ainsworth, R. A. "The effects of material strength mismatching on constraint at the limit load of welded three-point bend specimens," *International Journal of Fracture* Vol. 89, No. 2, 1998, pp. 117-142.**

213. **Burstow, M. C., Howard, I. C., and Ainsworth, R. A. "The influence of constraint on crack tip stress fields in strength mismatched welded joints," *Journal of the Mechanics and Physics of Solids* Vol. 46, No. 5, 1998, pp. 845-872.**

214. **Burstow, M. C., and Howard, I. C. "Damage mechanics models of ductile crack growth in welded specimens," *Fatigue & Fracture of Engineering Materials & Structures* Vol. 23, No. 8, 2000, pp. 691-708.**

215. **Karstensen A. D., N. A., Hancock J. W. "The constraint of elastic-plastic crack tip fields," *9th International conference in fracture (ICF9)*. Sydney, Australia, 1997.**

216. **Roy, Y. A., and Narasimhan, R. "Constraint effects on ductile fracture processes near a notch tip under mixed-mode loading," *Engineering Fracture Mechanics* Vol. 62, No. 6, 1999, pp. 511-534.**

217. **Roy, Y. A., and Narasimhan, R. "J-Dominance in mixed mode ductile fracture specimens," *International Journal of Fracture* Vol. 88, No. 3, 1998, pp. 259-279.**

218. **Kim, D. H., and Kang, K. J. "Two parameter approach for elastic-plastic fracture of short cracked specimens under mixed mode loading," *International Journal of Fracture* Vol. 116, No. 3, 2002, pp. 245-273.**

219. **Betegon, C., Hancock JW.,. "Two-parameter characterization of elastic-plastic crack-tip stress field," *Journal of Applied Mechanics* Vol. 58, No. 1, 1991.**

220. **Betegon, C., Belzunce, F. J., and Rodriguez, C. "A two parameter fracture criterion for high strength low carbon steel," *Acta Materialia* Vol. 44, No. 3, 1996, pp. 1055-1061.**
221. **Castro, J. T. P., Sousa R A., Lopes A A O. "Comparing improved crack tip plastic zone estimates considering corrections based on T-stress and on complete stress fields," 2011.**
222. **Sousa, R. A., Castro, J. T. P., Lopes, A. A. O., and Martha, L. F. "On improved crack tip plastic zone estimates based on T-stress and on complete stress fields," *Fatigue & Fracture of Engineering Materials & Structures*, 2012, pp. no-no.**
223. **Yeh, H.-Y., Ahmed, K.,. "Change of damage zone size by T-stress," *Journal of reinforced plastics and composites* Vol. 25, No. 6, 2006, p. 645.**
224. **Hello, G., Ben Tahar, M., and Roelandt, J.-M. "Analytical determination of coefficients in crack-tip stress expansions for a finite crack in an infinite plane medium," *International Journal of Solids and Structures* Vol. 49, No. 3–4, 2012, pp. 556-566.**
225. **Li Xian-Fang, X. L. R. "T-stresses across Static Crack Kinking," *Journal of Applied Mechanics* Vol. 74, 2007, pp. 181 - 190.**
226. **Li, D.-F., Li, C.-F., Qing, H., and Lu, J. "The elastic T-stress for slightly curved or kinked cracks," *International Journal of Solids and Structures* Vol. 47, No. 14-15, 2010, pp. 1753-1763.**
227. **Ma, S., Zhang, X. B., Recho, N., and Li, J. "The mixed-mode investigation of the fatigue crack in CTS metallic specimen," *International Journal of Fatigue* Vol. 28, No. 12, 2006, pp. 1780-1790.**
228. **Zappalorto, M., and Lazzarin, P. "On the intensity of linear elastic high order singularities ahead of cracks and re-entrant corners," *International Journal of Solids and Structures* Vol. 48, No. 6, 2011, pp. 953-961.**
229. **F. Berto, P. L. "On higher order terms in the crack tip stress field," *International Journal of Fracture and Micromechanics*, 2010.**
230. **Hello, G., Ben Tahar, M., and Roelandt, J. M. "Analytical determination of coefficients in crack-tip stress expansions for a finite crack in an infinite plane medium," *International Journal of Solids and Structures* Vol. 49, No. 3-4, 2012, pp. 556-566.**
231. **Leguillon, D. "Asymptotic and numerical analysis of a crack branching in non-isotropic materials," *European Journal of Mechanics and Solids* Vol. 12, No. 1, 1993, pp. 33 - 51.**
232. **Nazarali, Q., and Wang, X. "The effect of T-stress on crack-tip plastic zones under mixed-mode loading conditions," *Fatigue & Fracture of Engineering Materials & Structures*, 2011, pp. no-no.**
233. **Chen, Y. Z. "Stress analysis for an infinite strip weakned by periodic cracks," *Applied Mathematics and Mechanics-English Edition* Vol. 25, No. 11, 2004, pp. 1298-1303.**
234. **Eftis, J. "Load biaxiality and fracture - A 2-sided history of complementing errors," *Engineering Fracture Mechanics* Vol. 26, No. 4, 1987, pp. 567-592.**
235. **Berry, J. P. "Determination of fracture surface energues by cleavage technique," *Journal of Applied Physics* Vol. 34, No. 1, 1963, pp. 62-&.**
236. **Pook, L. P. *An alternative crack path stability parameter*. Sheffield: Engineering Materials Advisory Services Ltd, 1998.**
237. **Sobotka, J. C., and Dodds Jr, R. H. "T-stress effects on steady crack growth in a thin, ductile plate under small-scale yielding conditions: Three-dimensional modeling," *Engineering Fracture Mechanics* Vol. 78, No. 6, 2011, pp. 1182-1200.**
238. **Zhao, L. G., Tong, J., and Byrne, J. "Stress intensity factor K and the elastic T-stress for corner cracks," *International Journal of Fracture* Vol. 109, No. 2, 2001, pp. 209-225.**
239. **Nakamura, T., and Parks, D. M. "Determination of elastic T-stress along 3-dimensional crack frotns using an interaction integralL," *International Journal of Solids and Structures* Vol. 29, No. 13, 1992, pp. 1597-1611.**
240. **Meshii, T., Tanaka, T., and Lu, K. "T-Stress solutions for a semi-elliptical axial surface crack in a cylinder subjected to mode-I non-uniform stress distributions," *Engineering Fracture Mechanics* Vol. 77, No. 13, 2010, pp. 2467-2478.**
241. **Meshii, T., and Tanaka, T. "Experimental T-33-stress formulation of test specimen thickness effect on fracture toughness in the transition temperature region," *Engineering Fracture Mechanics* Vol. 77, No. 5, 2010, pp. 867-877.**
242. **Varias, A. G., and Massih, A. R. "Temperature and constraint effects on hydride fracture in zirconium alloys," *Engineering Fracture Mechanics* Vol. 65, No. 1, 2000, pp. 29-54.**
243. **Roychowdhury, S., Roy, Y. D., and Dodds, R. H. "Ductile tearing in thin aluminum panels: experiments and analyses using large-displacement, 3-D surface cohesive elements," *Engineering Fracture Mechanics* Vol. 69, No. 8, 2002, pp. 983-1002.**
244. **Patil, S. D., Narasimhan, R., and Mishra, R. K. "Effect of lattice orientation on crack tip constraint in ductile single crystals," *Fatigue & Fracture of Engineering Materials & Structures* Vol. 34, No. 8, 2011, pp. 604-618.**

245. **Patil, S. D., Narasimhan, R., and Mishra, R. K. "A numerical study of crack tip constraint in ductile single crystals," *Journal of the Mechanics and Physics of Solids* Vol. 56, No. 6, 2008, pp. 2265-2286.**

246. **Biswas, P., Narasimhan, R., and Tewari, A. "Influence of crack tip constraint on void growth in ductile FCC single crystals," *Materials Science and Engineering a-Structural Materials Properties Microstructure and Processing* Vol. 528, No. 3, 2011, pp. 823-831.**

247. **Biswas, P., and Narasimhan, R. "Effect of loading rate on crack tip fields in three point bend fracture specimen of FCC single crystal," *International Journal of Solids and Structures* Vol. 48, No. 16-17, 2011, pp. 2432-2445.**

248. **Eftis, J. "On the modified westergaard equations for certain plane crack problems."**

249. **Sugimura, Y., Lim, P. G., Shih, C. F., and Suresh, S. "Fracture normal to a bimaterial interface: Effects of plasticity on crack-tip shielding and amplification," *Acta Metallurgica et Materialia* Vol. 43, No. 3, 1995, pp. 1157-1169.**

250. **Du, Z. Z., and Hancock, J. W. "The effect of non-singular stresses on crack-tip constraint," *Journal of the Mechanics and Physics of Solids* Vol. 39, No. 4, 1991, pp. 555-567.**

251. **Tong, J. "T-stress and its implications for crack growth," *Engineering Fracture Mechanics* Vol. 69, 2002.**

252. **Hallback, N., and Nilsson, F. "Mixed-mode-I/II fracture behaviour of aluminium-alloy," *Journal of the Mechanics and Physics of Solids* Vol. 42, No. 9, 1994, pp. 1345-&.**

253. **Huajian, G., and Cheng-Hsin, C. "Slightly curved or kinked cracks in anisotropic elastic solids," *International Journal of Solids and Structures* Vol. 29, No. 8, 1992, pp. 947-972.**

254. **Kim, J.-H., and Paulino, G. "T-stress in orthotropic functionally graded materials: Lekhnitskii and Stroh formalisms," *International Journal of Fracture* Vol. 126, No. 4, 2004, pp. 345-384.**

255. **Ben-Aoun, Z. E. A., and Pan, J. "Influences of non-singular stresses on plane-stress near-tip fields for pressure-sensitive materials and applications to transformation toughened ceramics," *International Journal of Fracture* Vol. 77, No. 3, 1996, pp. 223-241.**

256. **Zhu, T., and Yang, W. "Crack kinking in a piezoelectric solid," *International Journal of Solids and Structures* Vol. 36, No. 33, 1999, pp. 5013-5027.**

257. **Li, X. F., and Lee, K. Y. "Crack growth in a piezoelectric material with a Griffith crack perpendicular to the poling axis," *Philosophical Magazine* Vol. 84, No. 18, 2004, pp. 1789-1820.**

258. **Li, X. F., and Lee, K. Y. "Fracture analysis of cracked piezoelectric materials," *International Journal of Solids and Structures* Vol. 41, No. 15, 2004, pp. 4137-4161.**

259. **Ma, H., and Wang, B. "T-stress in piezoelectric solid," *Applied Mathematics and Mechanics-English Edition* Vol. 25, No. 5, 2004, pp. 513-517.**

260. **Subramanya, H. Y., Viswanath, S., and Narasimhan, R. "Influence of crack tip constraint on void growth in pressure sensitive plastic solids - I: 2D analysis," *Engineering Fracture Mechanics* Vol. 75, No. 5, 2008, pp. 1045-1063.**

261. **Zhao, L. G., and Chen, Y. H. "Effect of the T-stress in microcrack shielding problems," *Journal of Applied Mechanics-Transactions of the Asme* Vol. 65, No. 1, 1998, pp. 71-75.**

262. **Zhao, L. G., and Chen, Y. H. "T-stress of an interface macrocrack induced by near tip subinterface microcracks," *International Journal of Fracture* Vol. 90, No. 3, 1998, pp. 275-285.**

263. **Sih, G. C., Paris, P. C., and Erdogan, F. "Crack-Tip, Stress-Intensity Factors for Plane Extension and Plate Bending Problems," *Journal of Applied Mechanics* Vol. 29, No. 2, 1962, pp. 306-312.**

264. **R. Rodi, G. W., R.C. Alderliesten, R. Benedictus. "The Effect of bridging fibres on the entire strain field in Fibre Metal Laminates," *17th ICCM International Conference on Composite Materials*. Edinburgh, United Kingdom, 2009.**

265. **M. Gupta, R. C. A., R. Benedictus. "A novel approach for estimation of crack paths in FMLs and hybrid structures," *Crack paths 2012*. Gaeta, Italy, 2012.**

266. **Gupta, M., Alderliesten, R. C., and Benedictus, R. "Crack paths in Fibre Metal Laminates: Role of fibre bridging," *Engineering Fracture Mechanics* Vol. 108, No. 0, 2013, pp. 183-194.**

267. **Cintron, R., Saouma, V. . "Strain Measurements with the Digital Image Correlation System Vic-2D." 2008.**

268. **"http://www.correlatedsolutions.com/vic-3d/." Vol. 2014.**

269. **Spronk, S. W. F. "Predicting fatigue crack initiation and propagation in Glare reinforced frames," *Structural integrity and composites*. Vol. Master of Science, Delft University of Technology, Delft, 2013.**

270. **Guo, Y.-J., and Wu, X.-R. "A phenomenological model for predicting crack growth in fiber-reinforced metal laminates under constant-amplitude loading," *Composites Science and Technology* Vol. 59, No. 12, 1999, pp. 1825-1831.**

271. **Houten, v. M. H. "Experimental fatigue and crack growth tests of Fibre Metal Laminate Structures under fatigue loading conditions - Results of the test campaign of the project SOV FML Toolbox II." 2013.**

272. **Herakovich, C. T., Aboudi, J., Lee, S. W., and Strauss, E. A. "Damage in composite laminates: Effects of transverse cracks," *Mechanics of Materials* Vol. 7, No. 2, 1988, pp. 91-107.**

273. **Alderliesten, R. C. *Fatigue and Fracture of Fibre Metal Laminates*. Dordrecht: Springer publications, 2016.**

274. **Vries, T. J. d. "Blunt and Sharp notch behaviour of Glare Laminates," *Faculty of Aerospace Engineering*. Vol. Ph. D, TU, Delft, Delft, 2001**

275. **Gupta, M., Alderliesten, R.C. , Benedictus, R. "The effect of laminate orthotropy and fibre-bridging on crack paths in Fibre Metal Laminates under off-axis loading (under review)," *Engineering Fracture Mechanics*. 2016.**

Appendix A: Algebraic solution to the Mixed-mode equation

Erdogan and Sih developed the equation for crack paths under mixed-mode loading as:

$$\cos\frac{\varphi}{2}\left[K_{eff\_I}\sin\varphi + K_{eff\_II}(3\cos\varphi - 1)\right] = 0 \qquad \textbf{0-1}$$

Where, K_{eff_I} is the stress intensity factor in opening mode, K_{eff_II} is the stress intensity factor in shear mode and φ is the fracture angle. Equation 1 has two solutions:

$$\cos\frac{\varphi}{2} = 0 \qquad \textbf{0-2}$$

And

$$\left[K_{eff\_I}\sin\varphi + K_{eff\_II}(3\cos\varphi - 1)\right] = 0 \qquad \textbf{0-3}$$

Equation 9-2 provides fracture angle as 180° which is the case of purely uniaxial loading. For the mixed-mode (M^e) loading, equation 9-3 must be solved. Deriving M^e from equation 9-3 leads to:

$$M^e = \frac{K_{eff\_I}}{K_{eff\_I}} = \frac{\sin\varphi}{(1-3\cos\varphi)} \qquad \textbf{0-4}$$

$$\Rightarrow\ (1 - 3\cos\varphi) = \frac{\sin\varphi}{M^e}$$

$$\Rightarrow\ (1 - 3\cos\varphi) = \beta^e\sin\varphi, \text{ where } \beta^e = \frac{1}{M^e}$$

$$(3\cos\varphi) = 1 - \beta^e\sin\varphi \ldots \text{ Squaring both sides}$$

$$\Rightarrow\ 9(\cos\varphi)^2 = 1 + 2\beta^e\sin\varphi - (\beta^e)^2(\sin\varphi)^2$$

$$\Rightarrow\ 9\{1 - (\sin\varphi)^2\} = 1 + 2\beta^e\sin\varphi - (\beta^e)^2(\sin\varphi)^2$$

$$\Rightarrow\ (\mathbf{9-1}) - \{\mathbf{9} + \boldsymbol{\beta^e}(\sin\boldsymbol{\varphi})^2\} - \mathbf{2}\boldsymbol{\beta^e}\sin\boldsymbol{\varphi} = 0$$

$$(\sin\boldsymbol{\varphi})^2(\boldsymbol{\beta^e} - \mathbf{9}) + \mathbf{2}\boldsymbol{\beta^e}\sin\boldsymbol{\varphi} - \mathbf{8} = \mathbf{0} \qquad \textbf{0-5}$$

Equation 9-5 is a quadratic equation where $\sin\varphi = x$. Solving for the roots of the equation will provide the fracture angle.

The solutions for the root of the equation is:

$$\boldsymbol{\varphi} = \sin^{-1}\left\{\frac{2\beta^e(+/-)\sqrt{(2\beta^e)^2(+/-)32\,\{9+\beta^e\}}}{2(9+\beta^e)}\right\} \qquad \textbf{0-6}$$

ACKNOWLEDGEMENTS

Rinze, I would like to thank you for providing me with an opportunity to complete a dream. It was my third attempt at PhD and would have also been my final attempt. Looking back to the 6 years I have spent in the group under your leadership, I realize I have learnt a lot of things. I am extremely grateful for all this, and hopefully, I have allayed your fears of hiring PhDs from the Indian sub-continent. Also, hopefully I have been able to make you divest your stocks from the stock exchange to sports betting. Jokes apart, I am grateful for your support throughout this PhD.

René, '*dank u wel'* for taking me under your supervision and guiding me through the topsy-turvy journey called doctoral research. Your supervision provided me with a real Dutch work experience, i.e. honesty, straightforwardness and absence of hierarchy. You backed your trust in me by providing me with absolute freedom to address my research problem with my own personality, i.e. random and unstructured thought-process. It was always a pleasure to meet you in the corridor and discuss things. Hopefully, someday I can mentor my team like the way you supervised me. And by the way to end our discussion on the impact of Artificial intelligence's role in our lives, *'I firmly believe that it will become intuitive in the next 20 years but by then we will call it Super Intelligence.'* Thank you once again.

Gemma, if I start to thank you for so many things you helped me with during my PhD, I might end up writing another 100 pages, so I am going to try and keep it very very short. To begin with, I was credited with the idea of starting the potluck and sports events. However, the truth is these events would never have occurred or being even half as much fun without your excitement, energy and planning experience. It is amazing how you can positively influence and stimulate the group with your energy. Your ability to read our minds – *even though we are from different cultures* – and provide us with solutions for our incumbent problems is something that I would like to learn from you. I am really grateful for everything you have helped me with during this research process.

Marianne, thanks for keeping your office door always open to me. I literally would walk in and spill my guts out with things that frustrated me. Your welcoming smile made it easy to do so.

Thanks to Berthil, Bob, Hans, Johan, Gert-Jan, Kees, Fred, Ad, Robert, Peter, and Rob Leonard for everything you taught me in the lab. In my interview with Rinze and Rene, I had categorically stated that I am not an experimental guy. However, now after so many years, it is because of you all I can say, *'I love to be in the lab: to observe experiments'.*

Thanks John-Alan and Niels for bearing with me in the office. It was extremely pleasant to discuss various tid-bits on various topics from history to politics. Without your knowledge, I would have miserably failed to understand, '*How things are done in Netherlands? – The efficiency versus the inclusive method.'* John-Alan, thanks for also updating the Dutch version of the summary of this thesis. Niels, thanks for also giving me initial feedbacks on The Fools Bookie and the initial Dutch version of the thesis' summary.

Captain Daniel Burger Dr., it was a pleasure to forge friendship with you. We have had amazingly insightful discussions on things in life from women to philosophy and god. Additionally, I would like to thank you for having the patience to listen my ideas about *T*-stress. Chirag, I really appreciate that you took time to read my chapters not once but many times, before they even became comprehensible for René. I do acknowledge the patience you have for listening to me and allowing me to barge into your office at my will.

It was also a grateful experience to have deep discussions with Calvin about general topics. Also, from 13th May, 2017 its most likely our ability to understand each other should become better. I will miss your polite yet dark sense of humour. Only you could have correlated sports with orgasm. Derek, I would love to thank you for the same, but unfortunately, we never had discussions – '*It was a monologue from your side*.'(*I know the phrase that has popped up in your mind at exactly this second– The pot calling the kettle black.*) I really did enjoy the talks, climbing and the running company, along with Greg, you provided.

Thomas, thanks for being a pain in the **** about the trivial things of life. Marijn for going out climbing so often and the drinks post climbing, and showing me how to be carefree and relaxing in life. Rotterdamse rugby club, thanks you for making me shed kilos and kilos, and also thanks to Aike, Karst, Kevin and Jasper for the company.

I have been writing for too long, and hence, I don't want to spend any more time on mentioning particular reasons for the others. Nevertheless, it was great to know you guys, and thanks for the good memories – Adrian Fernandez, Adrian Lara, Cornelis, Davide, Freek, Ilhan, Morteza, Freddy, Riccardo R. – for teaching me to test in the lab, Alfonso, Gustavo, Greg Rickerd, Greg Wilson, Nat, Natcha, Ping, Wandong, Jos – for the beers on the Dutch *eredivisie* -, Julian, Lucas, Ilias, Megan W., Nikos, Nicolas L., Nick E., Maria B., Maria S., Beatriz, Marcelo, Huajie, Lei, Fabricio, Michiel, Romina F., Renee - , Darwin – for reminding me the North Indian college humour after so many years, Roger – for the cricket discussion, Vincentius, Wouter Vogel – especially for the Ajax blogs, Pedro, Shafaat, Srikanth, Maruti, Zahid, Chunsen, Dimitrios, Andrey, Genevieve, Tian, Sofia, Julie, Irene, Eirini, Leila, Yao, Konstantin. More importantly, I would really like to take time to thank you all for always coming together on the beautiful ideas of the annual potluck, biannual sports day and other outings.

Nick, thanks for floating a company with me and believing in my informal data science ability. Also, warning me about the inopportune moments of not making jokes while entering formal meetings. But, be warned someday something inappropriate but extremely funny will blurt out from my mouth while we are closing a deal. Be prepared. Sonell, thanks for the company in the train rides to Rotterdam. Also, I appreciate you trying The Fools Bookie, and miserable losing money with it.

Daddy, thanks for always being supportive of my ideas, dreams and stubbornness to do things my way, and for inculcating a love for books in me. Mummy, thanks for being so caring, loving, and simple. Without your grooming and nurturing, it would have been extremely difficult to get through this difficult journey by myself. Bhaiya, thanks for all the gifts you buy me and backing me up. Rakhi, thanks for listening to me all your adult life and Palaksh, thanks for bringing joy to our lives.

LIST OF JOURNAL PUBLICATIONS

1. **M. Gupta,** R.C. Alderliesten, R. Benedictus, Applicability of a modified fatigue model to determine crack paths in Fibre Metal Laminates under quasi-static loading, ***To be re-submitted to Engineering Fracture Mechanics in October, 2017.***

2. V. Maretti, **M. Gupta,** R.C. Alderliesten, R. Benedictus, Understanding the directionality of surface cracks in Fibre Metal Laminates under off-axis loading, ***To be submitted to International Journal of Fatigue in April, 2017.***

3. **M. Gupta,** R.C. Alderliesten, R. Benedictus, The effect of laminate orthotropy and fibre-bridging on crack paths in Fibre Metal Laminates under off-axis loading, ***To be re-submitted,, 2017***

4. **M. Gupta,** R.C. Alderliesten, R. Benedictus, A review of *T*-stress and its effects in Fracture Mechanics, *Engineering Fracture Mechanics* Vol. 134, 2015, pp. 218-241

5. **M. Gupta,** R.C. Alderliesten, R. Benedictus, Crack paths in Fibre Metal Laminates: Role of fibre bridging, *Engineering Fracture Mechanics* Vol. 108, No. 0, 2013, pp. 183-194

CURRICULUM VITAE

Mayank Gupta was born in Etah on Sunday, the 25th August, 1985. His primary and secondary schooling was done in Dehradun from 1990 to 2001. Thereafter, he completed his senior secondary education in 2003 in Noida. In August, 2003 he started his Bachelor of Technology in Mechanical Engineering at Vellore Institute of Technology (VIT), Vellore in India. He wrote his Bachelor's thesis at ILK, TU-Dresden before embarking on his dual M.Sc. in Aeronautics engineering (with Erasmus Mundus scholarship) at Universita di Pisa, pisa, taly and Universidad Polytecnia de Madrid, Madrid, Spain. He wrote his Master;s thesis at Airbus Getafe. Thereafter, to pursue his PhD, he made first and second attempts at Universidad Polytecnica de Madrid and University of Ghent. However, unfortunate circumstances, and his won stubbornness led him to make a final attempt to obtain hi PhD at TU, Delft . Currently, he works at his own company (Jugaad BV) which is using causation with Big Data analytics to do predictive analytics. His free time is spent on solving 'The Gambler's Fallacy' problem with Big Data and hence, he spents most of his time watching or doing sports.

Robert Frost - The Road Not Taken

Two roads diverged in a yellow wood,
And sorry I could not travel both
And be one traveler, long I stood
And looked down one as far as I could
To where it bent in the undergrowth;

Then took the other, as just as fair,
And having perhaps the better claim,
Because it was grassy and wanted wear;
Though as for that the passing there
Had worn them really about the same,

And both that morning equally lay
In leaves no step had trodden black.
Oh, I kept the first for another day!
Yet knowing how way leads on to way,
I doubted if I should ever come back.

I shall be telling this with a sigh
Somewhere ages and ages hence:
Two roads diverged in a wood, and I—
I took the one less traveled by,
And that has made all the difference.

TU Delft

M2i materials innovation institute